Improving the localisation accuracy of AUVs operating in highly variable environmental conditions

by

Supun Anuradhitha Tilakeratne Randeni Pathiranachchilage

BEng (Hons) in Naval Architecture, University of Tasmania, 2013

A thesis submitted in fulfilment of the requirement for the degree of

Doctor of Philosophy

in

Maritime Engineering

National Centre for Maritime Engineering and Hydrodynamics,

Australian Maritime College (AMC), University of Tasmania.

November 2017

Abstract

The objective of this thesis is to contribute to Autonomous Underwater Vehicle (AUV) navigation by improving vehicle localisation accuracy when Doppler Velocity Log (DVL) bottom-tracking is unavailable. The Inertial Navigation System (INS) based localisation solution is prone to extreme uncertainties due to double integration of inherent errors within the INS acceleration measurements, unless the solution being externally aided (e.g. velocity measurements using the DVL bottom-track). As a solution for this, an improved model-aided INS localisation technique is introduced, which is complimented with the development of a novel model calibration and new water column velocity estimation method. The techniques established in this project are tested and validated using experimental data from a set of field manoeuvres using a *Gavia* class AUV and the performance is compared against other commonly used localisation methods.

A baseline mathematical model was developed in this work using system identification to predict the motion response of the AUV based on its control commands. However, such models are generally calibrated for low water column velocities and a standard vehicle configuration, and are limited in application for variations in environmental conditions. To address this limitation, a novel model calibration technique was established to field calibrate the parameters within the baseline model to the current operating condition and vehicle configuration. Model calibration improved the results of the baseline model up to 73% when operating in low energy environments and the AUV position can be computed within an uncertainty range of 1.5% of the distance travelled. In comparison, uncertainties of conventional non-bottom-tracking localisation techniques could be up to 10% in similar environmental conditions. A secondary approach is also presented to determine the hydrodynamic coefficients of the mathematical model using Computational Fluid Dynamics (CFD) simulations and captive model experiments when the AUV is operating in complex flow conditions.

A non-acoustic method was introduced to estimate the velocity of the water column using the motion response of the AUV. This method is capable of accurately estimating water column velocities in proximity to the AUV (i.e., the water column velocities at the same depth as the vehicle is), which is not typically resolved with existing methods such as acoustic Doppler current profilers. When the mathematical model-aided localisation solution is complimented

with water column velocity prediction method, the localisation error is limited to less than 6% of the distance travelled even in extremely high currents (i.e. >2 m s^{-1} in tested conditions). In such environmental conditions, the uncertainties of other commonly used non-bottom-tracking localisation methods, as tested against in this work, such as DVL water-track mode and unaided INS could be above 30%.

One of the key advantages of the proposed localisation technique is that it could be applied to any torpedo shaped AUV (for example, platforms such as *REMUS*, *Iver*, *Bluefin*, *Explorer*, etc.) of any configuration by simply conducting a set of established field manoeuvres to identify its mathematical model parameters. Further, additional sensors beyond a typical AUV navigational payload (i.e. global positioning, accelerometers and gyroscopes) are not required to implement this technique in an AUV. The localisation technique developed in this thesis is capable of improving the motion control and navigation solution of the AUV in the absence of DVL bottom-tracking, which is critical for the expansion of vehicle performance in extreme environmental conditions.

Declarations

Declaration of originality and authority of access

This thesis contains no material which has been accepted for a degree or diploma by the university or any other institution, except by way of background information and duly acknowledged in the thesis, and to the best of my knowledge and belief no material previously published or written by another person except where due acknowledgement is made in the text of the thesis, nor does the thesis contain any material that infringes copyright.

This thesis may be made available for loan and limited copying and communication in accordance with the Copyright Act 1968.

……..

Supun A. T. Randeni P.

Statement of published work contained in thesis

The publishers of the research articles comprising the Chapter 2 to Chapter 4 and Appendix A to Appendix C hold the copyright for that content, and access to the material should be sought from the respective journals and conference proceedings. Chapter 5 is submitted and under review at the time of writing, and may be made available for loan and limited copying and communication in accordance with the Copyright Act 1968.

Statement of co-authorship

The following researchers contributed to the publication of work undertaken as part of this thesis:

- Supun A. T. Randeni P., (**Candidate**) – Australian Maritime College, University of Tasmania, Launceston, Australia.
- Assistant Prof. Alexander L. Forrest, (**AF**) – Department of Civil and Environmental Engineering, University of California – Davis, Davis, California, USA and Australian Maritime College, University of Tasmania, Launceston, Australia.
- Dr. Zhi Q. Leong, (**ZL**) – Australian Maritime College, University of Tasmania, Launceston, Australia.
- Dr. Remo Cossu, (**RC**) – School of Civil Engineering, University of Queensland, Brisbane, Australia and Australian Maritime College, University of Tasmania, Launceston, Australia.
- Prof. Dev Ranmuthugala (**DR**) – Australian Maritime College, University of Tasmania, Launceston, Australia.
- Mr. Peter D. King, (**PD**) – Australian Maritime College, University of Tasmania, Launceston, Australia.
- Mr. Val Schmidt, (**VS**) – Centre for Coastal and Ocean Mapping, University of New Hampshire, Durham, New Hampshire, USA.
- Dr. Jonathan Duffy (**JD**) – Australian Maritime College, University of Tasmania, Launceston, Australia.
- Mr. Minh Tran (**MT**) – Australian Maritime College, University of Tasmania, Launceston, Australia.

- Dr. Hung D. Nguyen (**HN**) – Australian Maritime College, University of Tasmania, Launceston, Australia.
- Associate Prof. Jonathan Binns (**JB**) – Australian Maritime College, University of Tasmania, Launceston, Australia.
- Associate Prof. Shuhong Chai (**SC**) – Australian Maritime College, University of Tasmania, Launceston, Australia.

Chapter 2 – (Paper 1 – published in the Nonlinear Dynamics journal)

Parameter identification of a nonlinear model: replicating the motion response of an autonomous underwater vehicle for dynamic environments

Candidate was the primary author who conducted the design and analysis of the work while all co-authors assisted with refinements and presentation. Candidate, Assistant Prof. Forrest and Dr. Cossu were involved in the AUV deployment and data acquisition.

[Candidate: 75%, AF: 5%, RC: 5%, ZL: 5%, DR: 5%, VS: 5%]

Chapter 3 (Paper 2 – published in the Journal of Marine Science and Engineering)

Determining the Horizontal and Vertical Water Velocity Components of a Turbulent Water Column Using the Motion Response of an Autonomous Underwater Vehicle

Candidate was the primary author and he conducted the design of the technique and analysis together with Assistant Prof. Forrest and Dr Cossu. Co-authors assisted with refinements and presentation. Candidate, Assistant Prof. Forrest and Dr. Cossu were involved in the AUV deployment and data acquisition.

[Candidate: 70%, AF: 10%, RC: 10%, ZL: 5%, DR: 5%]

Chapter 4 (Paper 3 – published in the Marine Technology Society Journal)

Autonomous Underwater Vehicle motion response: A non-acoustic tool for blue water navigation

Candidate was the primary author and he conducted the design and analysis. Co-authors assisted with refinements and presentation. Candidate, Assistant Prof. Forrest and Dr. Cossu were involved in the AUV deployment and data acquisition.

[Candidate: 80%, AF: 5%, RC: 5%, ZL: 5%, PD: 2.5% DR: 2.5%]

Chapter 5 (Paper 4 – submitted for publication in the IEEE Journal of Oceanic Engineering)

Counteracting Autonomous Underwater Vehicle (AUV) localisation error as a precursor for blue water navigation

Candidate was the primary author and he conducted the design of the technique and analysis. Co-authors assisted with refinements and presentation. Candidate, Assistant Prof. Forrest and Dr. Cossu were involved in the AUV deployment and data acquisition.

[Candidate: 80%, AF: 5%, ZL: 5%, RC: 2.5%, DR: 2.5%, PD: 2.5%, VS: 2.5%]

Appendix A (Paper 5 – published in the proceedings of the 'MTS/IEEE Oceans 2015')

Estimating flow velocities of the water column using the motion response of an Autonomous Underwater Vehicle (AUV)

Candidate was the primary author and he conducted the design of the technique and analysis together with Assistant Prof. Forrest and Dr. Cossu. Co-authors assisted with refinements and presentation. Candidate, Assistant Prof. Forrest and Dr. Cossu were involved in the AUV deployment and data acquisition.

[Candidate: 75%, AF: 10%, RC: 10%, ZL: 2.5%, DR: 2.5%]

Appendix B (Paper 6 – published in the proceedings of the 'Third Vietnam Conference on Control and Automation')

Least Squares Optimisation Algorithm Based System Identification of an Autonomous Underwater Vehicle

Candidate was the second author of this publication. He assisted Mr Minh Tran to conduct the design and analysis of the work and was involved in the AUV deployments.

[MT: 75%, Candidate: 10%, HN: 5% JB: 5%, SC: 2.5%, AF: 2.5%]

Appendix C (Paper 7 – published in the Applied Ocean Research journal)

Numerical Investigation of the Hydrodynamic Interaction between Two Underwater Bodies in Relative Motion

Candidate was the primary author who conducted the experiments, numerical simulations and analysis of the work. Dr. Leong assisted with numerical simulations and all co-authors assisted with refinements and presentation.

[Candidate: 70%, ZL: 10%, DR: 10%, AF: 5%, JD: 5%]

We the undersigned agree with the above stated "proportion of work undertaken" for each of the above published (or submitted) peer-reviewed manuscripts contributing to this thesis

Signed:

…….....

Dr. Zhi Q. Leong
(Primary Supervisor)
Australian Maritime College,
University of Tasmania
28/11/2017

…….....

Assistant Prof. Alexander L. Forrest
(Co-supervisor)
Department of Civil and Environmental Engineering,
University of California – Davis.
28/11/2017

…….....

Dr. Remo Cossu
(Co-supervisor)
School of Civil Engineering,
University of Queensland.
28/11/2017

…….....

Prof. Dev Ranmuthugala
(Co-supervisor)
Australian Maritime College,
University of Tasmania
28/11/2017

…….....

Associate Prof. Michael Woodward
(Director)
National Centre for Maritime Engineering and Hydrodynamics, Australian Maritime College, University of Tasmania.
1/12/2017

Acknowledgements

Over the wonderful journey of my PhD, I have encountered many inspiring and helpful people from around the world and it is a great pleasure to thank them who made this thesis possible.

First and foremost I would like to thank my supervisors Assistant Prof. Alex Forrest, Dr. Zhi Leong, Dr. Remo Cossu and Prof. Dev Ranmuthugala for their unconditional support in all my endeavours. Throughout my PhD journey, they provided me encouragement, sound advices and also good company. Without them, this challenging journey would not be a success. Secondly I would like to thank Peter king, Nathan Kemp (currently at Blue Ocean Monitoring Pty. Ltd.), Isak Bowden-Floyd, Dr. Konrad Zurcher and Dr. Damien Guihen from the Autonomous Maritime Systems Laboratory at AMC, not only for their immense support for AUV deployments, but also for the moments we shared; talking about engineering, science and robotics. A special recognition must be made to Dr. Hordur Johannsson and Helgi Thorgilsson at Teledyne Gavia for their continued technical support and assistance throughout this project. I specially thank Val Schmidt from the Centre for Coastal & Ocean Mapping at University of New Hampshire for his directions. Similarly I thank Associate Prof. Karl Sammut, Dr. Andrew Lammas and their team at Flinders University for facilitating me to broaden my experience to autonomous surface vessels and for the adventures we shared in Singapore during Maritime RobotX Challenge 2014. I am grateful to Associate Prof. Art Trembanis for providing me the opportunity to validate my techniques using different vehicle platforms. I also thank his team including Carter DuVal, Kenny Haulsee and Stephanie Dohner at University of Delaware for their support during the AUV deployments and for the welcome I received in Delaware. I also acknowledge Korea Polar Research Institute with special thanks to Dr. Won Sang Lee, Dr. Sukyoung Yun and their team; and Fiona Elliott (National Institute of Water and Atmospheric Research), Lauren Roche (National Oceanic and Atmospheric Administration), Carson Witte and Una Miller (Columbia University) for our adventures in Antarctica. I warmly thank my colleagues at AMC who were not only co-workers, but also great friends who created a very memorable time at AMC.

I lovingly thank my brother and sister and their families for their unconditional love and support in ups and downs of my life. Last, but not least, I dedicate this thesis for my mom and dad. Without their endless love, support and encouragements this journey would not be a reality.

for my parents

Table of Contents

List of Figures

List of Tables

Abbreviations

2D	Two Dimensional
3D	Three dimensional
3-DOF	Three Degree-of-Freedom
6-DOF	Six Degree-of-Freedom
ADCP	Acoustic Doppler current profiler
ADV	Acoustic Doppler Velocimeter
AMC	Australian Maritime College
AUV	Autonomous Underwater Vehicle
BSLRSM	Baseline Reynolds Stress Model
CFD	Computational Fluid Dynamics
DVL	Doppler Velocity Log
EFD	Experimental Fluid Dynamics
GPS	Global Positioning System
HPMM	Horizontal Planer Motion Mechanism
IMU	Inertial Measurement Unit
INS	Inertial Navigation System
LBL	Long Base Line
MATLAB	Matrix Laboratory
MOOS-IvP	Mission Oriented Operating Suite – Interval Programming
OR	Outlier Rejection
PEM	Prediction Error Method
RANS	Reynolds Averaged Navier-Stokes
RLS	Recursive Least Squares
RMS	Root Mean Square
ROV	Remotely operated vehicle
RPM	Revolutions per Minute
SNAME	Society of Naval Architects and Marine Engineers
SSTCC	Shear Stress Transport with Curvature Correction
USBL	Ultra Short Base Line

Chapter 1: Thesis Introduction

1.1. Introduction

Interest in Autonomous Underwater Vehicles (AUVs) is growing for a wide range of scientific, commercial and military applications due their unique capabilities over surface vessels, and manned and tethered underwater vehicles (Stutters et al., 2008). Although the inception of AUV engineering occurred over a half-century ago, their systems are continuously improving to achieve better performance over a wide range of conditions (Griffiths, 2002). One of the major challenges is AUV localisation, which is complicated by wavelength attenuation of electromagnetic waves in water. This effectively limits radio communications and Global Positioning System (GPS) based localisation to surface operations. Furthermore, the high nonlinearity of the hydrodynamic forces and moments, and the unpredictability of the operating environmental conditions have added to the complexity of AUV manoeuvres and operations.

1.1.1. AUV localisation

Vehicle localisation is the foremost important element of the overall AUV autonomy. It is especially critical to accurately recognise the current position of the vehicle in three dimensional (3D) space for navigation (i.e., point to point guidance of the vehicle) as well as for motion control. Inaccurate localisation could result in the vehicle travelling away from the pre-planned mission route while assuming it is on the correct track, whereby resulting in an incorrectly geo-located dataset and a compromised mission. In the most severe examples of this, mission failure could result leading to a potentially damaged or lost AUV.

One of the traditional underwater localisation techniques is to triangulate the position of the vehicle using acoustic triangulation; i.e., using Long Base Line (LBL) systems or Ultra Short Base Line (USBL) systems (Vickery, 1998). Although LBL systems are one of the most accurate underwater localisation techniques, the range of an LBL beacon is limited; hence, an array of such devices is necessary for long range AUV operations. The requirement of surface vessel support and the deployment of moored equipment makes it a less preferred or unsuitable option for AUV localisation, specifically for deep water offshore operations (i.e., blue water operations). While USBL systems have seen increasing use in the last decade, they require a

dedicated supporting surface vessel shadowing the AUV for the entire duration of its mission, which is a major disadvantage.

Inertial Navigation System (INS) is one of the most commonly used methods for AUV localisation and navigation. The accelerometers and gyroscopic sensors of the Inertial Measurement Unit (IMU) within the INS measure the linear accelerations and angular rates of the AUV relative to the inertial space (Jalving et al., 2004). Subsequently, the measurements are integrated to determine the velocity, attitude and position of the vehicle. IMU measurements have uncertainties due to inherent errors of its sensors. Due to integration of these uncertainties, an unbounded drift will be accumulated with time in the position and velocity solutions unless true position and/or velocity measurements of the AUV are fed back into the INS position estimate through the use of a predictor-corrector model such as a Kalman filter (Medagoda et al., 2010). The vehicle velocity measurements from a bottom-tracking Doppler Velocity Log (DVL) are commonly used to aid the INS localisation solution in order to avoid the position drift.

1.1.2. Problem definition

The acoustic beams of DVLs are limited in terms of the frequency specific penetration through the water column; for example, a 300 kHz DVL has a maximum range of around 200 m and that of a 1200 kHz is around 15-25 m (Randeni et al., 2017a). Therefore, DVL aiding is unavailable when the vehicle-to-seabed-distance is larger than the range of the DVL. Blue water operations (i.e. starting in water depths exceeding the bottom-track penetration) often require the AUV to descend in the mid-water column without DVL bottom-track (Jalving et al., 2003). During such descents, the localisation error will increase rapidly if the INS is operating in its free inertial mode; i.e., unaided INS (see Figure 1.1). Once the AUV has dived down to the seabed and acquired the DVL bottom-lock, from that point onwards the accuracy of the INS localisation solution will be maintained. However, the positioning error that occurred during the descent will be introduced as a steady state offset error to the geo-location of the dataset for the entire mission (Randeni et al., 2016).

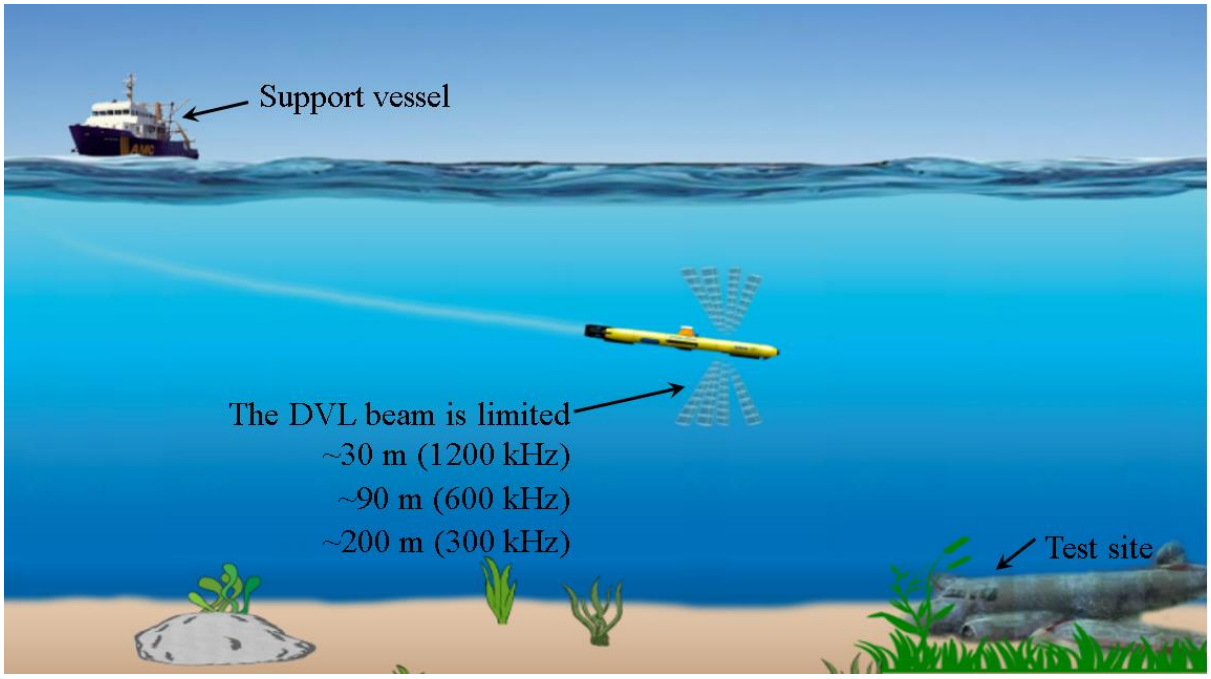

Figure 1.1 – An AUV descends to a test site in blue water where the altitude is larger than the maximum range of the DVL.

The traditional solution used by most currently operating AUVs is to track and measure the velocity of the vehicle relative to the water column; i.e., DVL water-track aided INS. This could provide a reasonably accurate localisation solution when the AUV is operating in environments with small underwater currents. However, the DVL water-track mode is unable to measure the velocity of the water column relative to the ground; therefore, the motion of the water column is often neglected. For this reason, the water-track mode of vehicles is prone to the velocity and position drifts due to the unaccounted movements of the water column in high energy environments with large underwater currents.

In addition to failure as a result of diving to depth, DVL bottom-track aiding could also be compromised when the AUV is travelling at a constant depth out of range of the bottom tracking mode. An example of this would be mid-water column surveys conducted at altitudes (i.e. depth above the seafloor) larger than the DVL range. DVLs are also prone to outages and instrument re-initialisations. In such cases, the INS will return to running in its free inertial mode. Finally, DVL bottom-track could be intermittently or completely unavailable when the AUV is flying over rough bathymetry due to uneven reflection of acoustic signals transmitted by the instrument (Hegrenaes and Berglund, 2009).

1.1.3. Model-aided INS localisation

The velocity of an AUV can be approximated with a dynamic motion response predicting mathematical model that represents the mass, hydrostatics and hydrodynamic properties of the AUV; i.e., known as a model-aided INS. One of the major advantages of model-aided localisation is that it does not require additional sensors beyond a typical AUV navigational payload and could be simply established with a modification to vehicle firmware. The velocity response predicting capability of such models depends on the accuracy of the parameters representing vehicle characteristics that typically vary with the vehicle configuration and ballast condition. However, previous model-aided INS systems were developed only for a given vehicle setting (Hegrenaes and Hallingstad, 2011, Hegrenaes et al., 2008, Jayasiri et al., 2016, Jayasiri et al., 2014, Yan et al., 2012). Commercial and scientific AUVs often change the configuration of the vehicle due to the addition and removal of payload sensors (Trembanis et al., 2012, Walker et al., 2013). Furthermore, the ballast condition of the AUV will vary with the salinity level of the operational environment. It is hypothesised in this work that a baseline mathematical model with parameters representing a particular vehicle setting may not adequately predict the motion of the vehicle with a different configuration.

Parameters within conventional AUV mathematical models represent the hydrodynamic, hydrostatic and mass properties of an AUV operating in calm water environments. That is, the model is unable to predict the external forces and moments acting on the vehicle such as those due to underwater currents and complex flow conditions (Randeni et al., 2015a). Therefore, the vehicle velocities predicted by a model are not absolute, but relative to the water column; i.e., equivalent to the velocities obtained from DVL water-tracking mode. In order to obtain the vehicle velocity relative to the ground, the motion of the water column needs to be compensated with the water column velocity measurements or predictions.

Yan et al. (2012) developed a model-aided INS using recursive identification for emergency navigation of AUVs when DVL malfunctions. However, this technique did not compensate for environmental forces such as underwater currents. Hegrenaes and Hallingstad (2011) introduced a model-aided INS, including a Kalman Filter based sea current estimation technique for a *HUGIN 4500* class AUV to be used when DVL aiding is unavailable. The velocities of the sea currents are calculated within the navigation system Kalman filter by using the model velocities that are relative to the water column and INS measurements relative to the inertial space. While this is an excellent example, the estimated sea currents could be less

accurate due to erroneous INS velocity measurements; since an outlier filtering technique is not utilised in this work. Furthermore, both of these techniques are not readily transferable to a different configuration of the AUV unless the parameter identification procedure is repeated. Finally, their performances were not evaluated for varying environmental conditions.

1.1.4. Objectives and research question

This project aims to improve the localisation accuracy of AUVs operating in low as well as high energy environments when direct DVL aiding is unavailable. An improved model-aided INS localisation technique is introduced by developing the dynamic motion response predicting mathematical model that can be field calibrated for different environmental conditions and vehicle configurations. The model-aided INS localisation technique is complimented with a novel, non-acoustic water column velocity estimation method, in order to counteract the position drift due to sea currents. Combining all of these elements, this project aims to resolve the following research question:

"How can INS localisation accuracy of an AUV operating without DVL bottom-track be improved for both low and high energy environments?"

Novel techniques established in this project were tested and validated with field experimental data from a *Gavia* class AUV.

1.2. Methodology

The methodology utilised to solve the research question of this project could be broken down into four main phases:

Phase 1: Conducting a study on existing AUV localisation techniques, focusing on previous work carried out to improve the INS localisation performance when DVL aiding is unavailable.

Phase 2: Establishing a methodology to determine an improved AUV motion response predicting mathematical model. This process involved:

- The introduction of a Recursive Least Squares (RLS) and Prediction Error Method (PEM) based system identification algorithms to obtain a baseline model; and

- Development of a model calibration method to field calibrate the baseline model for the current operating environment and vehicle configuration.

Phase 3: Developing a non-acoustic method to estimate the water column velocity components of a high energy environment using AUV motion response (referred to as the 'WVAM method'), and carrying out the following further evaluation:

- Investigation of the performance of the WVAM method as a function of the turbulence levels of the environment to verify whether the technique is able to predict underwater currents in a blue water environment;
- Examination of the feasibility of the WVAM method to be incorporated with a model-aided INS localisation solution for error counteraction; and,
- Upgrading the WVAM method to determine the water column velocity profile relative to the ground along the descend path of an AUV diving from the surface to the seabed.

Phase 4: Combining the model-aided INS localisation solutions with the WVAM method to improve the localisation accuracy of an AUV descending in blue water without DVL bottom-track.

1.3. Novel aspects

This project has provided original contributions to the state-of-art AUV technology in four main areas. The first is the methodology to determine an improved model-aided INS localisation technique that can be field calibrated for different environmental conditions and vehicle configurations. Previous studies have identified mathematical models for AUVs; however, they are limited for a given environmental setting and vehicle configuration (Hong et al., 2013, Marco et al., 2005, Yan et al., 2014). The novelty of this work is that the baseline model identified using complex identification manoeuvres conducted in a calm water environment can be calibrated to diverse operational environments and vehicle settings, online or offline, using the motion response data from a simple mission.

The non-acoustic technique introduced to determine the water column velocity components of a turbulent water column (i.e., the WVAM method) is the second novelty of this project. The key advantage of the WVAM method is that it provides velocity estimates within the blanking distance of the ADCP and the associated vehicle boundary layer, which

are usually unknown based on traditional methods. Previously, Hayes and Morison (2002) introduced a non-acoustic technique to determine the turbulent vertical water velocities, and fluxes of heat and salt by applying a Kalman filter to the AUV motion data. However, it cannot be readily adopted for commercial AUVs due to the modelling complexity and the requirement of the typically unavailable vehicle control law algorithm. Furthermore, this method was limited to the vertical water velocity, while the WVAM method estimates the water velocity components in the *x*, *y*, and *z* directions. Estimating horizontal water column velocities in proximity to the AUV (i.e., the water column velocities at the same depth as the vehicle is) is important for vehicle navigation and control system optimisation, and to fill the blanking distance gap within a water column velocity profile, which is important for flow field characterisation for environmental studies.

The third original contribution of this project is the technique introduced to determine the water column velocity profile relative to the bottom along the decent path when DVL bottom-track is unavailable, and utilising it to counteract the localisation error of an AUV diving in blue water. This technique included a novel Outlier Rejection (OR) filter that removes outliers present within the INS measurements, and a flow profile smoothening algorithm that applies a forward and backward correction, and a flow variation smoother to the water column velocity profile.

The final original contribution of this thesis is the numerical model developed using ANSYS CFX CFD package to simulate the pure sway motion of an AUV in proximity to a larger moving underwater vehicle, which was validated with captive model experiments (this work is presented in Appendix C). The pure sway motion can be used to accurately determine a number of hydrodynamic coefficients of an AUV mathematical model (Lewis, 1988). Furthermore, a simplified method is introduced to obtain the hydrodynamic coefficients of an AUV when operating close to a larger underwater body by transforming the single body hydrodynamic coefficients of the AUV using the steady-state interaction forces. This simplified method can be used to determine the variation of hydrodynamic coefficients with a lower CFD computational cost when the AUV is operating within an external pressure field. The purpose of this contribution within this thesis is to outline secondary methods that can be used to determine model parameters representing the hydrodynamic characteristics of an AUV in complex operational conditions.

1.4. Outline of thesis

This thesis follows a "chapterised thesis" structure, where Chapters 2 to 6 and Appendix A are comprised of scientific papers. The outline of the thesis structure is given below.

Chapter 1: Thesis introduction

Chapter 1 is the preface of this thesis that details the motives for the project, providing necessary background knowledge on AUVs and conventional AUV localisation techniques to date. Subsequently, the project objectives, methodology and the novel outcomes are defined. Chapter 1 also outlines the structure of the thesis, linking together the succeeding chapters that are comprised with academic papers.

Chapter 2: Replicating the motion response of an AUV for dynamic environments (published in the Nonlinear Dynamics journal)

Chapter 2 is motivated by the requirement of a mathematical model that can predict the motion response of an AUV based on its control commands, regardless of the operational environment. RLS and PEM based system identification algorithms are presented to determine the linear and nonlinear parameters of an AUV motion response predicting mathematical model. A baseline mathematical model that represents the dynamics of a *Gavia* class AUV in a calm water environment is developed. A novel technique is introduced to calibrate the parameters within the baseline model to provide the motion response in different environmental conditions by conducting a calibration mission in the new environment. These models are used to develop an improved model-aided localisation system for AUVs operating without DVL bottom-track in low energy environments.

Chapter 3: WVAM method – a non-acoustic technique to determine the velocity components of the water column (published in the Journal of Marine Science and Engineering)

Chapter 3 introduces the WVAM method to determine water column velocity components of a high energy environment using AUV motion response. The water column velocities are estimated by calculating the difference between the motion responses of the vehicle in the actual and calm water environment. The motion of the vehicle in the calm water environment is obtained by simulating the vehicle control commands executed during the field tests using the baseline mathematical model introduced in Chapter 2.

Chapter 4: Feasibility of WVAM method for AUV localisation error counteraction (published in the Marine Technology Society Journal)

Chapter 4 further compliments the WVAM method by analysing its feasibility to be incorporated with a model-aided INS localisation system. The study investigates and analyses the performance of the WVAM method as a function of the turbulence level of the environment by testing the method in an estuary that exhibits strong tidal currents (around 2.5 m s^{-1}). The performance of the WVAM method was compared with the vehicle on-board as well as stationary ADCPs in different water column conditions. This chapter discusses the necessary improvements required to incorporate the WVAM method within a model-aided INS.

Chapter 5: Counteracting AUV localisation error when operating beyond the range of bottom-tracking sonar (submitted for publication in the IEEE Journal of Oceanic Engineering)

Chapter 5 combines the work developed in previous chapters and presents an AUV localisation technique based on a mathematical model-aided INS for blue water operations conducted in high energy environments with strong non-uniform currents without DVL bottom-track. Inputs to the algorithm are vehicle control commands and unaided acceleration measurements from the INS. An Outlier Rejection (OR) filter is introduced to remove the outliers present within INS acceleration measurements prior to the data fusion with baseline model predicted velocities. The velocity profile of the water column relative to the ground along the descent path of the AUV is determined to avoid localisation drift resulting from underwater currents. The water column velocity profile is obtained with a flow velocity profile smoothing algorithm, which is an extension of the WVAM method.

The proposed technique is tested and validated for diving missions conducted at different water column conditions using a *Gavia*-class AUV. Its performance was evaluated by comparing with the localisation solutions from DVL bottom-track aided, DVL water-track aided, model-aided, and unaided INS systems.

Chapter 6: Summary, conclusions and future work

The closing chapter provides an overall summary of the project, bringing together the outcomes of the individual chapters. It also provides conclusions on the key findings and outcomes. Recommendations for future work is detailed in this section.

Appendix A: WVAM method in high energy environments (published in the Proceedings of the '*MTS/IEEE Oceans 2015*')

The purpose of the WVAM method is to predict the underwater currents acting on the vehicle in order to counteract the drift in the model-aided INS localisation solution of an AUV that operates in blue water. Water column velocity conditions in blue water environments are highly variable. Therefore, Appendix B investigates and analyses the performance of the WVAM method as a function of the turbulence level of the environment by testing the method in an estuary that exhibits strong tidal currents (around 2.5 m s^{-1}). The uncertainty of this method at different water column conditions was computed by comparing the velocity measurements from the WVAM method with those obtained from the AUV mounted ADCP.

Appendix B: Least squares based system identification algorithm to obtain a mathematical model of an AUV (published in the proceedings of the Third Vietnam Conference on Control and Automation)

Appendix B presents a secondary system identification technique based on Least Squares optimisation algorithm to determine the mathematical model of a *Gavia* class AUV. The purpose of the model is to accurately predict the system response over time starting from initial conditions. Appendix B is comprised of an article that provides an in detail explanation of the Least Squares optimisation algorithm as well as the formation of dynamic equations of motion.

Appendix C: Numerical Investigation of the Hydrodynamic Interaction between Two Underwater Bodies in Relative Motion – A secondary CFD based approach of determining the hydrodynamic coefficients of an AUV (published in the Applied Ocean Research journal)

Appendix C outlines a method that can be used to accurately determine the linear and nonlinear hydrodynamic coefficients of an AUV mathematical model. A CFD model was developed to simulate the pure sway motion of an AUV, which was in turn validated against towing tank experimental results. The main focus of the journal article presented in this subchapter is to investigate the hydrodynamic interaction between an AUV manoeuvring in close proximity to a larger moving underwater vehicle. The purpose of Appendix C is to outline secondary methods that can be used to determine model parameters representing the hydrodynamic characteristics of an AUV in complex operational conditions.

Chapter 2: Replicating the motion response of an AUV for dynamic environments

This chapter is based on the journal article '*Parameter identification of a nonlinear model: replicating the motion response of an autonomous underwater vehicle for dynamic environments*' that is published in the journal '*Nonlinear Dynamics*'. The citation for the article is:

Randeni SAT, Forrest AL, Cossu R, Leong ZQ, Ranmuthugala D, Schmidt V. Parameter identification of a nonlinear model: replicating the motion response of an autonomous underwater vehicle for dynamic environments. Non-linear Dynamics. 2017.

Abstract

This study presents a system identification algorithm to determine the linear and nonlinear parameters of an Autonomous Underwater Vehicle (AUV) motion response prediction mathematical model. The key objective of the model, which relies solely on propeller thrust, gyro measurements and parameters representing the vehicle hydrodynamic, hydrostatic and mass properties, is to calculate the linear velocities of the AUV in the x, y and z directions. Initially, a baseline mathematical model that represents the dynamics of a Gavia class AUV in a calm water environment was developed. Using a novel technique developed in this study, the parameters within the baseline model were calibrated to provide the motion response in different environmental conditions by conducting a calibration mission in the new environment. The accuracy of the velocity measurements from the calibrated model was substantially greater than those from the baseline model for the tested scenarios with a minimum velocity prediction improvement of 50%. The determined velocities will be used to aid the Inertial Navigation System (INS) position estimate using a Kalman Filter data fusion algorithm when external aiding is unavailable. When an INS is not externally aided or constrained by a mathematical model such as that presented here, the positioning uncertainty can be more than 4% of the distance travelled (assuming a forward speed of 1.6 m s^{-1}). The calibrated model is able to compute the position of the AUV within an uncertainty range of around 1.5% of the distance travelled, significantly improving the localisation accuracy.

2.1. Introduction

Autonomous Underwater Vehicles (AUVs) have evolved as specialised tools for challenging commercial, scientific, and military underwater applications such as subsea inspections (Mcleod et al., 2012), characterisation of the midwater column (Curtin et al., 1993) and security exercises in unstructured environments (Paull et al., 2014). Despite the developments of AUVs reaching back to the 1970s, the navigation and control subsystems of AUVs are continuously undergoing improvements (Hegrenaes and Berglund, 2009). In particular, one of the main challenges is accurate localisation and navigation in blue water (i.e., operating in regions out of range of bottom-track aided navigation), and to achieve the dynamic control stability of the vehicle that determines the data quality of AUV surveys (Paull et al., 2014).

Inertial Navigation Systems (INS) are one of the key methods to localise and navigate AUVs. An INS determines the position, velocity and orientation of the vehicle using data from Inertial Measurement Units (IMUs) relative to inertial space. Due to inherent errors, the INS localisation solution in its free inertial mode (i.e., unaided INS) rapidly drifts unless it is externally aided with vehicle's speed over the ground measurements from a bottom tracking Doppler Velocity Log (DVL) (Jalving et al., 2003, Medagoda et al., 2010). When DVL aiding is intermittently or completely unavailable (for example, due to instrument noise or as a result of the vehicle-to-seabed-distance being larger than the transmission range of acoustic frequency associated with the DVL), the vehicle velocities can be approximated with a mathematical model that characterises the hydrostatic and hydrodynamic properties of the AUV; i.e., a model-aided INS (Hegrenaes et al., 2008, Jayasiri et al., 2016). Although the localisation solution from a model-aided INS is not as accurate as a DVL aided INS, its accuracy is better than the unaided INS and the water-track mode of the DVL aided INS (Hegrenaes and Hallingstad, 2011).

The velocity response predicting capability of a mathematical model depends on the precision of the parameters representing hydrodynamic, hydrostatic, environmental and external forces, and the mass properties of the AUV, which typically vary with the operating environment and the vehicle configuration (i.e., the trim and ballast conditions). Therefore, a baseline mathematical model with parameters representing a calm water environment may not adequately predict the velocities of an AUV that operates in a dynamic environment in the

presence of high currents (Randeni et al., 2016). An improvement in the velocity prediction is essential to increase the AUV localisation accuracy from a model-aided INS.

A dynamically stable control system is essential for AUVs to undertake challenging tasks in complex flow conditions in high turbulent environments (Randeni et al., 2015a), in close proximity to the seabed (Ananthakrishnan, 1998), or to other moving underwater vehicles (Randeni et al., 2015b) and near the free surface (Polis et al., 2013). AUV control systems can be pre-optimised using a mathematical model that represents the dynamics of an AUV in its anticipated operating water column. With the availability of a mathematical model that updates in real time to characterise the operational environment, the control system optimisation can be conducted in real time or near real time (Hong et al., 2013).

Mathematical models can additionally be used to accurately predict the vehicle motion response which, in turn, is crucial for several other applications. For example, the velocity components of a turbulent water column can be determined through a non-acoustic technique using the AUV motion response; as previously described by the authors as the WVAM method in Randeni et al. (2015a). The WVAM method uses a mathematical model to calculate the flow velocities by comparing the actual motion response of the vehicle with the simulated response from a calm water based mathematical model. In addition, AUV simulators are used by vehicle developers and operators to test their mission plans and software modifications as well as to conduct trainings prior to field trials (Song et al., 2003). Such simulators need a mathematical model with precise representation of the vehicle characteristics to accurately simulate the dynamic motion response of the AUV.

The hydrodynamic forces acting on AUVs are highly nonlinear; hence, mathematical models should contain higher order hydrodynamic coefficients to represent these nonlinear characteristics. Previous works have introduced a number of methods to determine linear and nonlinear hydrodynamic coefficients of marine vehicles including the coupling effects between different motion modes; for example, captive model experiments (Randeni et al., 2015b, Dash et al., 2016), Computational Fluid Dynamics (CFD) simulation methods (Randeni et al., 2015b, Liang et al., 2016) and system identification using field data (Hong et al., 2013, Marco et al., 2005, Yan et al., 2014). Some of these efforts also account for environmental and external forces; although for underwater vehicles, these forces are generally based on wave and wind histogram data of a particular location (Fossen, 2011). However, previous data do not precisely reflect local variations of environmental condition; hence, may not replicate true external forces.

This paper presents a system identification algorithm to determine the linear and nonlinear parameters of an AUV mathematical model utilising the Recursive Least Squares (RLS) and the Prediction Error Method (PEM) optimisation techniques. The developed model accounts for the coupling effects influencing the surge, sway and heave velocities of the vehicle as well as the environmental and external forces. Utilising the model identification algorithms, the parameters of a *Gavia* class AUV mathematical model were estimated using motion response data from a complex identification manoeuvre conducted in a small, relatively calm lake (i.e. minimal surface mixing. A comparison is made between RLS and PEM, and the dependency of the parameters on the utilised dataset is also investigated. The identified model parameters are able to predict the motion response of the AUV in calm water condition and is referred to as the 'baseline' mathematical model hereafter. A novel technique is presented to field calibrate the baseline mathematical model to predict the vehicle motion response in diverse operational environments. The model calibration algorithm was extended to determine the AUV mathematical model in real time, processing a limited preceding data window for future goals such as real time control system optimisation. The following sections of this paper provide an overview of the field experimental setup (including the details of the utilised *Gavia* AUV and test site details), theory and justification of AUV dynamic modelling equations utilised in this study, and a brief description of the RLS and PEM techniques and the model simulation method. Baseline model estimation procedure and model calibration method are then explained together with a performance analysis. Finally, the real time model calibration is discussed, followed by a summary on possible future developments and conclusions.

2.2. Field experimental setup

2.2.1. Instrumentation

The system parameter identification algorithm was developed for a *Gavia*-class modular AUV (Thorgilsson, 2006) using the vehicle motion response data collected during various field trials. Due to the modularity of the vehicle, the component arrangement can be changed, which will alter the hydrostatic and hydrodynamic characteristics of the vehicle on any given deployment. The vehicle in the tested configuration (see Figure 2.1) consisted of a Nose Cone Module, Battery Module, Geoswath Interferometric Sonar Module, 1200 kHz Teledyne RDI Acoustic Doppler Current Profiler (ADCP) / DVL Module, Kearfott T24 INS (KI-4902S model) Module, Control Module, and a Propulsion Module. The vehicle had a length of 2.7 m, a diameter of 0.2 m, and a dry weight in air of approximately 70 kg. The propulsion module was

a three bladed ducted propeller system with four individually functioning control surfaces arranged in an 'X' configuration.

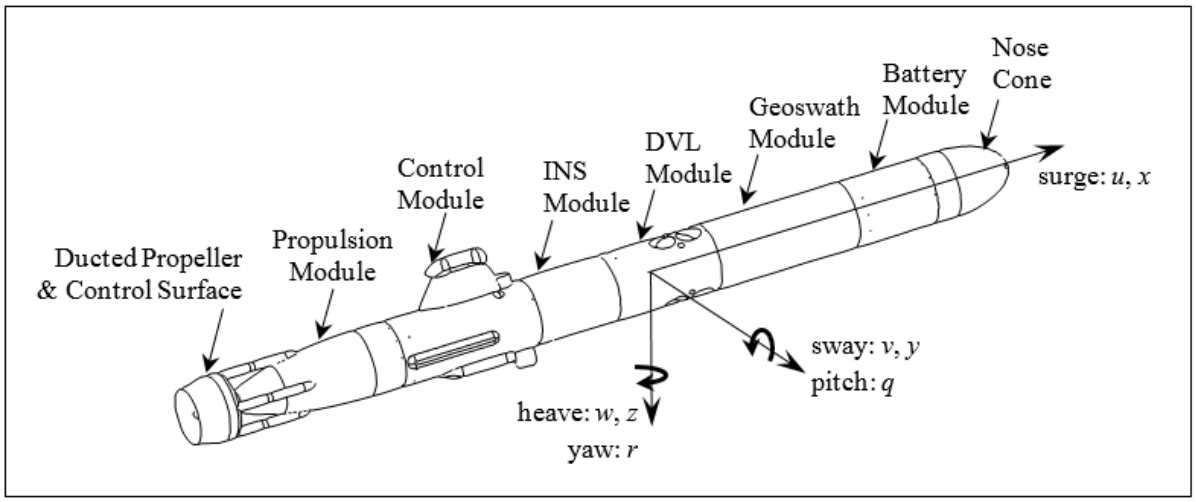

Figure 2.1 – Body-fixed frame of reference and the configuration of the utilised Gavia AUV. The origin is located at the centre of buoyancy of the vehicle. The vehicle had a length of 2.7 m, a diameter of 0.2 m, and a dry weight in air of approximately 70 kg

The DVL aided Kearfott T24 INS measured the accelerations in Six-Degree-of-Freedom (6-DOF) and orientation, to make estimates of the AUV's velocities and position. The heading and pitch angles of the vehicle were measured by the gyroscopic sensors, while the accelerations were determined through the use of accelerometers within the INS unit. The vehicle position estimate was corrected with the velocities over ground from the bottom tracking DVL (i.e., when the altitude of the AUV is below the range of the DVL acoustic beams) in order to avoid drifts in the derived localisation solution. The depth of the vehicle was obtained from the Keller Series 33Xe pressure sensor on-board the AUV. All sensor measurements were sampled at a frequency of 0.87 Hz and recorded in the vehicle log. The uncertainties of these instruments and the other sensors associated with the navigation unit are outlined in Table 2.1.

Table 2.1 – Specifications of Gavia AUV sensor packages. CEP for Circular Error Probable and TRMS for Time Mean Root Squared.

Sensor package	Measurements	Measurement accuracy
DVL bottom-track/GPS aided INS	Heading angle	±0.010° (RMS)
	Pitch angle	±0.005° (RMS)
	Position estimate	0.1% of the distance travelled (CEP)
	Velocity estimate (DVL aided)	0.001 m s^{-1} (RMS)
	Velocity estimate (GPS aided)	0.05 m s^{-1} (RMS)
DVL water-track aided INS	Position estimate	1852 m per 8 hours (TRMS)
		4.02% of the distance travelled*
	Velocity estimate	0.3 m s^{-1} (RMS)
1200 kHz Teledyne RDI DVL	Bottom tracking AUV velocity	±0.001 m s^{-1} (RMS) or 0.2% of the velocity
	Maximum bottom tracking range	30 m
Keller Series 33Xe pressure sensor	Vehicle depth	0.1% of the depth

*derived from the 1 nm per 8 hours uncertainty value for comparison, assuming an AUV forward speed of 1.6 m s^{-1}

2.2.2. Test site and experimental runs

The objectives of the field studies were to develop and to validate the parameter identification and calibration algorithms for different environments. Field studies were conducted in two locations: Lake Trevallyn in Tasmania, Australia (Figure 2.2a) and in Lake Ohau, South Island, New Zealand (Figure 2.2b).

During the Lake Trevallyn missions, the surface wave heights were less than 50 mm and the vehicle's ADCP recorded minor variations of the water column velocities, with averaged values of surge, sway and heave directions of 0.002 m s^{-1}, 0.002 m s^{-1} and 0.001 m s^{-1}

respectively. Due to these very small flow velocities, Lake Trevallyn can be classified as a calm water environment.

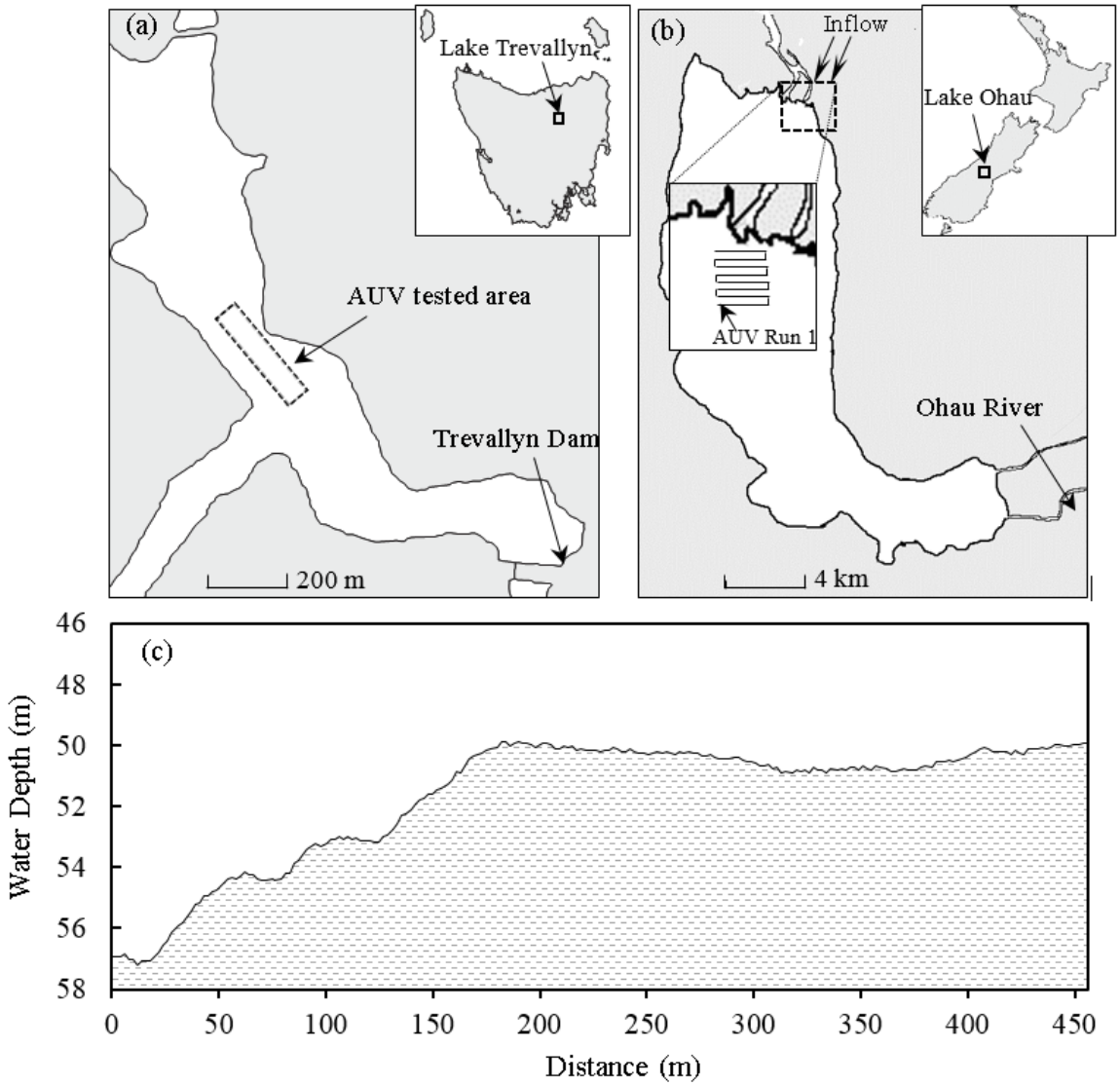

Figure 2.2 – AUV field deployments were conducted (a) in Lake Trevallyn, Tasmania, Australia and (b) Lake Ohau, South Island, New Zealand. Parameters of the mathematical model were determined from the manoeuvres conducted in Lake Trevallyn. The estimated models were verified with the vehicle motion response data from AUV deployments in Lake Ohau - eight AUV runs were conducted in a lawn-mover pattern (inset). (c) Bathymetry along the AUV Run 1, conducted in Lake Ohau, New Zealand

The Lake Ohau test site, on the other hand, reveals a more dynamic flow conditions due to its size and exposure to stronger external forces. The surface wave heights at time of conducting operations were around 0.3 m and the magnitudes of near surface water currents close to the inflow points of the Hopkins and Dobson Rivers measured from the vehicle ADCP

were around 0.15 m s^{-1} (Cossu et al., 2015). The test site at Lake Ohau had highly variable bathymetry; i.e., rough in proximity of the delta front as well as relatively flat lake floor in deeper parts of the lake (Figure 2.2c). For constant altitude AUV missions, the vehicle experienced highly fluctuating pitch angles (i.e., over ±10°) when flying above the region of variable bathymetry (i.e., up to 200 m from the starting position), while angles of less than ±2° were maintained above the flat terrain. For these reasons, the test site was decided to be a suitable stage to test the AUV mathematical models for different vehicle responses.

Lake Trevallyn field data were used to identify the baseline parameters of the mathematical model due to the lake's calm water condition with no external forcings. Two identification manoeuvres, named ID Manoeuvre 1 and ID Manoeuvre 2, were conducted to investigate the variation of the parameters on the utilised dataset. In order to successfully identify the model parameters, each manoevure consisted of three types of runs that stimulate the six motion modes (i.e., surge, sway, heave, roll, pitch and yaw). For example, in ID Manoeuvre 1, the AUV performed zig-zag runs in yaw (from 0 s to 260 s as in Figure 2.3) and pitch (from 260 s to 660 s as in Figure 2.3) planes by changing the coordinate way points and operating depths concurrently. From 660 s to 900 s, the propeller speed was increased in steps from 450 RPM to 975 RPM, covering the typical operational RPM range of the *Gavia* AUV. The pitch angle of the AUV unintentionally fluctuated while the horizontal heading angle was changed (Figure 2.3). Similarly, the horizontal heading oscillated while the depth changes were executed, stimulating coupling effects between the motion modes. Such unintentional fluctuations in pitch and yaw were low during the straight line runs. The propeller speed was varied to maintain a constant speed during the heading zig-zag runs. At three instances, the propeller RPM goes to negative values during the pitch zig-zag manoeuvres. This is due to activation of 'e-brake' as a result of the obstacle avoidance sonar detecting the sea bottom as an obstacle when the AUV is diving with a large pitch angle. However, this is not an issue for the system identification process as the time steps with negative propeller RPM values have been cut off during the identification procedure. Water depths in Lake Trevallyn vary between 10 – 15 m and the AUV missions were carried out between 2 – 8 m below the free surface to minimise the bias due to surface wave formation (Steel, 2010) and interaction with the lake bottom (Ananthakrishnan, 1998). Similarly, ID Manoeuvre 2 consisted of zig-zag runs in both pitch and yaw planes, and runs with different propeller speeds. The ID Manoeuvre 2 was carried out 6 – 12 m below the free surface.

In Lake Ohau, a lawn-mower pattern mission with eight transect lines was conducted. Each straight line run was carried out over the diverse bathymetry (i.e., the water depth was varying from around 50 – 60 m) maintaining a constant altitude of 8 m above the seabed. The first four lines (runs 1-4) of the lawn-mower pattern were used to calibrate the baseline model for the Lake Ohau water column condition utilising the model calibration method introduced in this work. The performance improvement of the calibrated model compared to the baseline model was analysed by testing the model with the last four lines (runs 5-8). Therefore, both calibration and performance analysis runs included smooth as well as rough bathymetric conditions.

Validation of the real time model estimation algorithm was conducted in Trevallyn as well as Ohau sites in order to establish its robustness in different field conditions. During all field tests, the vehicle altitude was within the range of the DVL acoustic beams, continuously aiding the INS solution. Hence, the motion response measurements used for model validations were maintained within the DVL aided INS uncertainty limits as given in Table 2.1.

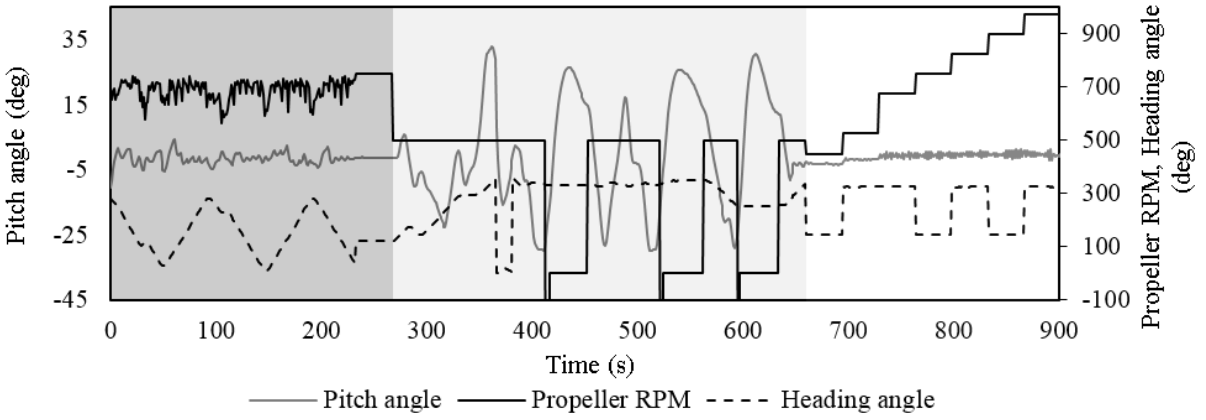

Figure 2.3 – Three types of manoeuvres were conducted in Lake Trevallyn site; i.e., zig-zag manoeuvres in yaw plane (section shaded in dark grey) and pitch plane (shaded in light grey), and step changes of propeller speed from 450RPM to 975RPM (no shading)

2.3. Dynamic modelling of the AUV

2.3.1. Notation

The mathematical formulae presented in this paper are based on the SNAME (1952) notation. Velocity, acceleration and position/Euler angle vectors are in the AUV's body fixed coordinate system (i.e., as shown in Figure 2.1) and relative to the ground unless it is stated otherwise.

2.3.2. AUV mathematical model

Manoeuvring equations of motion derived by considering the rigid-body kinetics, hydrodynamics, hydrostatics, environmental and other external forces acting on the AUV are generally used for vehicle modelling (Fossen, 2011, Newman, 1977, Fossen, 2002). In the work presented here, we used a basic mathematical model given in Equation (2.1) as specified for underwater vehicles by Fossen (2002); however, the hydrodynamic, environmental and control forces were modelled using a new mathematical model. One of the key advantages of this work is that the utilised mathematical model can be applied for any torpedo shaped AUV of any configuration.

$$\mathrm{M_{RB}}\dot{\bar{\nu}} + \mathrm{C_{RB}}(\bar{\nu})\bar{\nu} + \mathrm{M_A}\dot{\bar{\nu}} + \mathrm{C_A}(\bar{\nu})\bar{\nu} + \mathrm{D}(\bar{\nu})\bar{\nu} + \mathrm{g}(\eta) = \tau + \tau_{\mathrm{external}} \tag{2.1}$$

where, $\mathrm{M_{RB}}$ and $\mathrm{M_A}$ are the rigid body and added mass system inertia matrices, $\mathrm{C_{RB}}$ and $\mathrm{C_A}$ are the rigid body and added mass Coriolis-centripetal matrices, D is the hydrodynamic damping matrix, $\mathrm{g}(\eta)$ is the restoring gravitational/buoyancy force matrix, τ is the vector of propulsion and control surface forces, and τ_{external} represents the vector of environmental and external forces. The vector $\bar{\nu}$ denotes the velocity (i.e., $[u, v, w, p, q, r]^{\mathrm{T}}$ where u, v, w and p, q, r are the linear and angular velocities around the x, y and z axes), and η is the vector of position/Euler angles (i.e., $\eta = [x, y, z, \phi, \theta, \psi]$ where ϕ, θ and ψ are the roll, pitch and yaw angles respectively) as illustrated in Figure 2.1.

2.3.3. System inertia, Coriolis-centripetal and hydrostatic forces

Using the approach of Fossen (2002), Equations (2.2), (2.3) and (2.4) present the mathematical models in x, y and z directions of the AUV respectively. The left-hand sides of these equations represent the inertia, Coriolis-centripetal and hydrostatic force components along each direction. Inertial and Coriolis-centripetal forces contain both mass and added mass components that have a vital contribution in marine vehicle dynamics.

$$\left(m - X_{\dot{u}}\right)\dot{u} + mz_g\dot{q} - my_g\dot{r} - \left(W - B\right)\sin\left(\theta\right) - X_{prop} = \sum \mathrm{X} \tag{2.2}$$

$$\left(m - Y_{\dot{v}}\right)\dot{v} - mz_g\dot{p} + \left(mx_g - Y_{\dot{r}}\right)\dot{r} = \sum \mathrm{Y} \tag{2.3}$$

$$\left(m - Z_{\dot{w}}\right)\dot{w} - \left(mx_g - Z_{\dot{q}}\right)\dot{q} - \left(W - B\right) = \sum \mathrm{Z} \tag{2.4}$$

where the term m is the mass of the vehicle and x_g, y_g and z_g represent the position of the centre of gravity in x, y and z directions respectively from the centre of buoyancy of the vehicle. Further, W is the weight of the vehicle in air, B is the buoyancy force, θ is the pitch angle, and

X_{prop} is the thrust produced by the propeller. The right-hand side of these equations (i.e., $\sum \mathbf{X}$, $\sum \mathbf{Y}$ and $\sum \mathbf{Z}$) represent the summation of hydrodynamic damping, and environmental and external forces.

2.3.4. Hydrodynamic damping and external & environmental forces

Hydrodynamic damping of underwater vehicles is a result of several factors including: (1) the linear skin friction due to laminar boundary layer dynamics, (2) the nonlinear skin friction due to turbulent boundary layer dynamics, (3) the viscous damping force due to vortex shedding, (4) the form drag due to pressure variation across the body, and (5) the hydrodynamic lift forces due to cross flow drag and circulation of water around the hull (Fossen, 2011). Therefore, linear as well as higher order damping terms and relevant cross flow coupling terms are required to accurately model the flow around the vehicle (Abkowitz, 1964, Fossen, 2011). It is also important to model the vehicle dynamics with a minimum number of parameters because if the number of unknown parameters present in a model is large, the accuracy of the parameter estimation reduces (Ljung, 1999).

When using a mathematical model, an accurate description of environmental and external forces is required for calibration. In marine vehicle modelling, it is common to assume the principle of superposition when considering these highly nonlinear forces (Fossen, 2011). This principle suggests that the generalised environmental and external forces are added to the right-hand side of Equation (2.1); i.e., $\boldsymbol{\tau}_{\mathbf{external}}$.

2.3.4.1. Forces in x direction

In the current work, the hydrodynamic damping along the *x* direction is modelled using Equation (2.5).

$$\sum \mathrm{X} = X_{uuu}u^3 + X_{u|u|}u|u| + X_u u + X_{wq}wq + X_{vr}vr + X_{\psi|\psi|}\psi\,|\psi| + X_{\psi}\psi + X_{static} \tag{2.5}$$

where the notation of the hydrodynamic coefficients follow SNAME (1952). For example, X_u is the derivative of the surge force (X) with respect to the surge speed (u); i.e., $X_u = \partial X / \partial u$. $X_{\psi|\psi|}$ and X_{ψ} are the surge force coefficients due to underwater currents. X_{static} stands for variable independent static external forces along *x* direction.

This equation is comprised of damping terms up to the third order (i.e., X_u, $X_{u|u|}$ and X_{uuu}); hence, it includes laminar and turbulent skin friction damping components as well as viscous damping. The terms X_{wq} and X_{vr} represents the cross-coupled drag components; i.e., change in

the forward speed of the AUV resulting from heading and pitch variations. The external forces due to underwater currents depend on the heading of the vehicle. For example, if a steady underwater current is flowing from North to South, the external current force component acting on the vehicle when travelling with a heading angle of 0° would be different to a heading angle of 60°. Fossen (2011) models the forces due to underwater currents as a function of angle of attack of the AUV with the flow direction, which is also a function of the vehicle heading angle. Hence, in this work, external forces along the *x* direction due to current are modelled as functions of up to the second order of the vehicle heading (i.e., $X_{\psi|\psi|}$ and X_{ψ}). Other environmental and external forces (i.e., direction independent) acting along the *x* direction are assumed to be superimposed within the damping hydrodynamic parameters. This offers the ability to capture the external forces as functions of all the previously stated variables for different environmental conditions, maximising the accuracy of model calibration and minimising the number of data points required for the convergence. However, this has a disadvantage of not being able to obtain values for the pure hydrodynamic derivatives as environmental and external forces are incorporated in them. Any uncaptured steady external forces are included in the model as a variable independent constant X_{static}.

2.3.4.2. Forces in y direction

Similarly, the hydrodynamic damping forces and environmental/external forces acting along the *y* direction are modelled using Equation (2.6).

$$\sum \mathrm{Y} = Y_{v|v|} v|v| + Y_v v + Y_q q + Y_r r + Y_p p + Y_{\psi|\psi|} \psi\,|\psi| + Y_{\psi} \psi + Y_{static} \tag{2.6}$$

Nonlinear hydrodynamic damping along *y* direction was limited to the second order of the sway velocity (i.e., Y_v and $Y_{v|v|}$). The *Gavia* AUV is asymmetric about the *x*-*y* and *y*-*z* planes. Therefore, as the vehicle presents an angle of yaw to the flow (i.e., as the vehicle changes its horizontal heading angle), the AUV will start to roll and pitch, resulting in a change in the vehicle operating depth as the control system responds. Due to the asymmetry of the vehicle, this will occur in all directions. Therefore, the linear cross-coupled drag components due to roll, pitch and yaw motions (i.e., Y_p, Y_q and Y_r) were also included in Equation (2.6). Similar to the surge model, the sway force due to steady underwater currents is modelled as functions of up to the second order of the vehicle heading (i.e., $Y_{\psi|\psi|}$ and Y_{ψ}). The direction independent environmental/external forces acting along the sway direction are assumed to be superimposed within the hydrodynamic damping terms. Uncaptured steady external forces are incorporated as a variable independent constant Y_{static}.

2.3.4.3. Forces in z direction

Equation (2.7) describes the hydrodynamic damping and environmental/external force along the heave direction.

$$\sum \mathrm{Z} = Z_{w|w|} w|w| + Z_w w + Z_q q + Z_r r + Z_{static} \tag{2.7}$$

Similar to the sway force component, the nonlinear hydrodynamic damping in the *z* direction was limited to the second order of the heave velocity (i.e., Z_w and $Z_{w|w|}$). The cross-coupled damping terms due to pitch and yaw motions (i.e., Z_q and Z_r) were also included. The environmental/external forces acting along the heave direction were also assumed to be superimposed within the modelled hydrodynamic damping parameters. Uncaptured steady external forces are incorporated as a variable independent constant Z_{static}, which also represents any variations in the ballast condition from the baseline model. The heading direction dependent underwater currents along the vertical direction are neglected.

2.3.5. Final dynamic equations of motion and control forces

Equations (2.2) and (2.5) are combined and rearranged to determine the surge acceleration as shown in Equation (2.8).

$$\begin{aligned}\dot{u} = \frac{1}{\left(m - X_{\dot{u}}\right)}[&my_g\dot{r} - mz_g\dot{q} + (W - B)\sin(\theta) + X_{uuu}u^3 + X_{u|u|}u|u| + \\ &X_u u + X_{wq}wq + X_{vr}vr + X_{\psi|\psi|}\psi|\psi| + X_{\psi}\psi + X_{static} + X_{prop}]\end{aligned} \tag{2.8}$$

where, X_{prop} is the thrust produced by the propeller that is given by $X_n \times RPM^2$. *RPM* is the vehicle's propeller revolutions per minute and X_n is the thrust coefficient, which is 95×10^{-6} for the *Gavia* AUV according to the estimation by Thorgilsson (2006). The thrust coefficient is only valid for the propeller speed range from 450 RPM to 975 RPM.

The mass, added mass, buoyancy and the positions of the centre of gravity of the AUV varies with the vehicle configuration and the ballast condition. Therefore, these values are deployment dependent. Equation (2.8) is parameterised as shown in Equation (2.9) in order to superimpose these unknown properties inside the parameters to be identified, eliminating the requirement to measure those physical properties of the AUV. However, this has a disadvantage of not being able to obtain values for the pure hydrodynamic derivatives as other properties are overlayed within them.

$$\dot{u} - X_n \times RPM^2 = \alpha_1 \dot{r} + \alpha_2 \dot{q} + \alpha_3 \sin(\theta) + \alpha_4 u^3 + \alpha_5 u|u| + \alpha_6 u + \alpha_7 wq + \alpha_8 vr + \alpha_9 \psi|\psi| + \alpha_{10}\psi + \alpha_{11} \quad (2.9)$$

where, α_1, $\alpha_2 \ldots \alpha_{11}$ are the parameters to be estimated using the identification algorithm.

Similarly, Equations (2.3) and (2.6), and Equations (2.4) and (2.7) are combined, rearranged, and parameterised as shown in Equations (2.10) and (2.11) respectively.

$$\dot{v} = \beta_1 \dot{r} + \beta_2 \dot{p} + \beta_3 v|v| + \beta_4 v + \beta_5 p + \beta_6 q + \beta_7 r + \beta_8 \psi|\psi| + \beta_9 \psi + \beta_{10} \quad (2.10)$$

$$\dot{w} = \gamma_1 \dot{q} + \gamma_2 w|w| + \gamma_3 w + \gamma_4 q + \gamma_5 r + \gamma_6 \quad (2.11)$$

where, β_1, β_2 … β_{10} and γ_1, γ_2… γ_6 are the parameters to be estimated using the identification algorithm developed in this work.

Roll, pitch and heading angles of an AUV could be measured using the gyroscopic sensors inside the vehicle INS regardless of the availability of external velocity aiding from DVL. For this reason, it was determined that estimating Euler angles of the AUV were not required for this work. Hence, roll, pitch and yaw angular velocities and accelerations (i.e., *p*, *q*, *r*, $\dot{p}$, $\dot{q}$ and $\dot{r}$) were directly provided as inputs into the model. This provided the ability to limit the mathematical model to 3-DOF (i.e., linear motions along *x*, *y* and *z* directions), eliminating the requirement to model the rolling, pitching and yawing motions. This also had the added advantage of the actuator control surfaces in Equations (2.9), (2.10) and (2.11) not having to be modelled. Instead the actual turning behaviours of the vehicle (i.e., *p*, *q*, *r*, $\dot{p}$, $\dot{q}$ and $\dot{r}$) measured during the tests were provided as model inputs. The propulsion module utilised for this work had four independently operating control surfaces in a 'X' configuration. This arrangement concurrently generates moments around both *y* and *z* directions, incorporating complicated coupling effects between the control surfaces (Sun et al., 2013). As a result of the 3-DOF modelling used in this work, resolving the produced moments were not necessary.

2.4. Parameter identification and simulation model

2.4.1. Recursive Least Squares (RLS) identification

Recursive least squares based parameter identification was conducted using the Recursive Least Squares estimation block set of MATLAB's System Identification toolbox, which is based on the theoretical approach outlined in Ljung (1999). Equations (2.9), (2.10) and (11) are modified to the format given in Equation (2.12).

$$y_{(t)} = H_{(t)}\Theta_{(t)} \tag{2.12}$$

where $y_{(t)}$, $H_{(t)}$ and $\Theta_{(t)}$ are vectors as defined in Table 2.2 for surge, sway and heave models.

Table 2.2 – $y_{(t)}$, $H_{(t)}$ and $\Theta_{(t)}$ vectors of Equations (2.12) and (2.16) for *x*, *y* and *z* directions.

x direction	*y* direction	*z* direction
$y_{(t)} = \dot{u} - X_n \times RPM^2$	$y_{(t)} = \dot{v}$	$y_{(t)} = \dot{w}$
$H_{(t)} = \begin{bmatrix} \dot{r} & \dot{q} & \sin(\theta) & u^3 \\ u\lvert u\rvert & u & wq & vr & \varphi^2 & \varphi & 1 \end{bmatrix}$	$H_{(t)} = \begin{bmatrix} \dot{r} & \dot{p} & v\lvert v\rvert & v \\ p & q & r & \varphi^2 & \varphi & 1 \end{bmatrix}$	$H_{(t)} = \begin{bmatrix} \dot{q} & 1 & w\lvert w\rvert & w & q & r \end{bmatrix}$
$\Theta_{(t)} = \begin{bmatrix} \alpha_1 & \alpha_2 & \alpha_3 & \alpha_4 & \alpha_5 \\ \alpha_6 & \alpha_7 & \alpha_8 & \alpha_9 & \alpha_{10} & \alpha_{11} \end{bmatrix}$	$\Theta_{(t)} = \begin{bmatrix} \beta_1 & \beta_2 & \beta_3 & \beta_4 \\ \beta_5 & \beta_6 & \beta_7 & \beta_8 & \beta_9 & \beta_{10} \end{bmatrix}$	$\Theta_{(t)} = \begin{bmatrix} \gamma_1 & \gamma_2 & \gamma_3 & \gamma_4 & \gamma_5 & \gamma_6 \end{bmatrix}$

In the standard Least Squares Estimation method, the entire data set is processed concurrently to determine the parameter vectors; i.e., $\Theta_{(t)}$ in equations (2.12), by solving equation (2.13).

$$\Theta_{(t)} = \left[H_{(t)}{}^{T} H_{(t)}\right]^{-1} H_{(t)}{}^{T} y_{(t)} \tag{2.13}$$

While the AUV is under operation, new motion response data are continuously being measured and sampled at each time-step. If the standard Least Squares Estimation method is employed, it requires the identification algorithm to be re-run for the entire mission (i.e., for all the data from the initial time step to the current time step) with the arrival of each new measurement (Ljung, 1999). On the other hand, the RLS Estimation method, adds the subsequent measurements to the existing solution without requiring the algorithm to be rerun. Equation (2.14) shows how the estimated parameters are extended for the subsequent measurements (Ljung, 1999).

$$\Theta_{(t)} = \Theta_{(t-1)} + P_{(t)} H_{(t-1)} \varepsilon_{(t)} \tag{2.14}$$

where, t is the time-step and,

$\varepsilon_{(t)} = y_{(t)} - H_{(t)}\Theta_{(t-1)}$,

$P_{(t)} = \dfrac{\tilde{P}_{(t)}}{\lambda}$

$$\tilde{\mathrm{P}}_{(t)} = \mathrm{P}_{(t-1)} - \frac{\mathrm{P}_{(t-1)}\mathrm{H}_{(t-1)}\mathrm{H}_{(t-1)}{}^{\mathrm{T}}\mathrm{P}_{(t-1)}}{\lambda + \mathrm{H}_{(t-1)}{}^{\mathrm{T}}\mathrm{P}_{(t-1)}\mathrm{H}_{(t-1)}}$$

and where, λ is the forgetting factor.

$$\lambda = 1 - \frac{1}{T_0}$$

where, T_0 is the length of the preceding data set that will be processed during the identification process.

Thus, past measurement data can be removed with the arrival of new data and; therefore, successive measurements can have a higher weight in the estimation process. The maximum value of the forgetting factor is one, which corresponds to none of the past data being forgotten (i.e., the entire dataset from the beginning to the current time step will have an equal weight). The smaller the forgetting factor, the shorter the length of the utilised preceding data set. This is important when the variation of parameters has to be identified in real time in dynamic operational environments with varying environmental and external forcing.

The initial values of all the parameters were set to 1 in order to retain the assumption that the initial parameters of the AUV model are unknown to the user.

2.4.2. Prediction Error Method (PEM) identification

Prediction error estimation function of MATLAB System Identification toolbox was utilised for PEM based parameter identification. PEM identification is done by minimizing the difference between the predicted outputs $\hat{\mathbf{y}}_{(t)}$ (i.e., the outputs of Equations (2.9), (2.10) and (2.11) according to parameters $\boldsymbol{\Theta}_{(t)}$ that is being estimated recursively) and measured outputs $\mathbf{y}_{(t)}$ as given in Table 2.2.

$$\boldsymbol{\Theta}_{(t)} = \arg\min_{\boldsymbol{\Theta}} V\left(\boldsymbol{\Theta}_{(t)}\right) \tag{2.15}$$

where,

$$V\left(\boldsymbol{\Theta}_{(t)}\right) = \frac{1}{2N}\sum_{t=1}^{N}\left\| y_{(t)} - \hat{y}_{t|t-1\left(\boldsymbol{\Theta}_{(t-1)}\right)}\right\|^2$$

where, $\hat{y}_{t|t-1\left(\boldsymbol{\Theta}_{(t-1)}\right)}$ is the predicted linear acceleration output at *t*, using all the information until time *t*-1.

Similar to the RLS estimation, the initial values of all the parameters were set to 1. The computation of the minimizing argument is a complicated process with a substantial amount of calculations. A thorough discussion regarding this process is given in Ljung (1999).

2.4.3. Simulation model

The simulation model described in this section can be used to determine *u*, *v*, and *w* once the parameters (i.e., $\boldsymbol{\Theta}_{(t)}$) are completely estimated or the estimation is being carried out in real time. The acceleration vectors of the current time step in the *x*, *y* and *z* directions are calculated according to equations (2.9), (2.10) and (2.11) respectively using the controlling commands (i.e., the time stamps of propeller RPM, roll rate, roll acceleration, pitch rate, pitch acceleration, yaw rate and yaw acceleration) of the vehicle and the velocity vector from the previous time step (Figure 2.4). For real time conditions, the parameter vector will be updated at each time step, while for non-real time applications, it will remain constant. The calculated acceleration vector is then integrated with respect to the time in order to obtain the velocity vector (i.e., *u*, *v* and *w*) in the body-fixed reference frame. This process is repeated with a time-step of 0.0001 s for the entire mission time. The selected time-step is large enough to maintain a low computational time and small enough to converge the velocity solution between two control command sampling intervals (i.e., of 0.87 Hz).

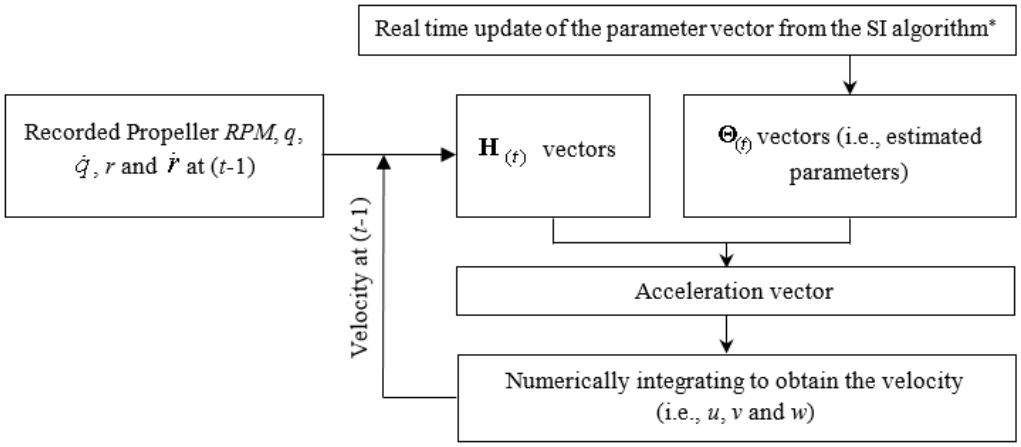

Figure 2.4 – Simulation model flowchart. The solution for the acceleration vector of the current time-step is determined using the control command vectors and velocity vectors from the previous time-step. The velocity vector is then calculated by integrating the acceleration vector with respect to time. *The parameter vector remains constant for non-real time identification

2.5. Baseline model identification and calibration

The primary application of mathematical model identification is to determine the unknown parameters of the AUV mathematical model in order to estimate the surge, sway and heave velocities of the vehicle when DVL velocity measurements are unavailable.

2.5.1. Baseline model identification

Baseline mathematical models that represent the dynamics of the *Gavia* AUV in a calm water environment was first determined using the RLS and PEM system identification algorithms. Since external and environmental forces caused by currents, turbidity, pressure fluctuations, etc. are neglected in the baseline model, the surge and sway force parameters due to steady underwater currents (i.e., α_9, α_{10}, β_8 and β_9) and uncaptured steady external forces (i.e., α_{11} and β_{10}) were removed from Equations (2.9) and (2.10). However, minor external/environmental forces might be incorporated within the remaining parameters of the model. The parameter representing the steady external forces along z direction (i.e., γ_6) was not removed from Equation (2.11) as it also represents the (B-W) term as shown in Equation (2.4). For the RLS method, a forgetting factor of one was utilised in order to process the entire length of the data set with an equal weight (i.e., no forgetting) and determine the parameter vectors (i.e., $\boldsymbol{\Theta}_{(t)}$) by solving equations (2.13) and (2.14). To establish baseline conditions, the identification algorithm was run using Lake Trevallyn field manoeuvres (i.e., ID Manoeuvres 1 and 2).

Parameter identification was conducted with both RLS and PEM techniques to determine the most effective estimation method for the mathematical model defined in this work. In order to investigate parameter estimation using a dataset with dissimilar inputs and outputs, each identification technique (i.e., RLS and PEM) was repeated for the two identification manoeuvres (i.e., for ID Manoeuvres 1 and 2). At the end of each identification process, parameter values had converged within 5% of the mean values. These baseline parameters for the vehicle (as configured) are presented below in Table 2.3.

Table 2.3 – Numerical values of the *Gavia* AUV's baseline parameters determined from RLS and PEM techniques using ID Manoeuvres 1 and 2. Note that the values of the parameters are not pure hydrodynamic, hydrostatic and mass coefficients as the environmental and external forces are overlayed within them.

Parameter	RLS (ID Manoeuvre 1)	RLS (ID Manoeuvre 2)	PEM (ID Manoeuvre 1)	PEM (ID Manoeuvre 2)
$\alpha_1 = \frac{my_g}{(m - X_{\dot{u}})}$	0.5294	0.3502	0.5279	0.4448
$\alpha_2 = \frac{-mz_g}{(m - X_{\dot{u}})}$	0.0909	0.0550	0.0959	0.3102
$\alpha_3 = \frac{(W - B)\sin(\theta)}{(m - X_{\dot{u}})}$	-2.5098	-2.8987	-2.4622	-2.1622
$\alpha_4 = \frac{X_{uuu}}{(m - X_{\dot{u}})}$	-8.5937	-7.4594	-8.6492	-7.4957
$\alpha_5 = \frac{X_{u\|u\|}}{(m - X_{\dot{u}})}$	-22.3129	-18.2884	-22.4870	18.2994
$\alpha_6 = \frac{X_u}{(m - X_{\dot{u}})}$	-32.7171	-29.7355	-32.8517	-29.5699
$\alpha_7 = \frac{X_{wq}}{(m - X_{\dot{u}})}$	-7.1061	-16.1337	-7.0680	-13.1852
$\alpha_8 = \frac{X_{vr}}{(m - X_{\dot{u}})}$	-13.5405	-12.7996	-13.5564	-12.8060
$\alpha_9 = \frac{X_{\psi\|\psi\|}}{(m - X_{\dot{u}})}$	-	-	-	-
$\alpha 10 = \frac{X_{\psi}}{(m - X_{\dot{u}})}$	-	-	-	-
$\alpha_{11} = \frac{X_{static}}{(m - X_{\dot{u}})}$	-	-	-	-
$\beta_1 = \frac{(Y_{\dot{r}} - mx_g)}{(m - Y_{\dot{v}})}$	0.0133	0.0135	0.0133	0.0133
$\beta_2 = \frac{mz_g}{(m - Y_{\dot{v}})}$	0.0029	0.0031	0.0029	0.0029
$\beta_3 = \frac{Y_{v\|v\|}}{(m - Y_{\dot{v}})}$	0.0444	0.0173	0.0480	0.0094
$\beta_4 = \frac{Y_v}{(m - Y_{\dot{v}})}$	-0.0364	-0.0722	-0.0367	-0.0552
$\beta_5 = \frac{Y_p}{(m - Y_{\dot{v}})}$	0.0005	0.0004	0.0005	0.0004
$\beta_6 = \frac{Y_q}{(m - Y_{\dot{v}})}$	-0.0001	0.0003	0.0000	0.0001
$\beta_7 = \frac{Y_r}{(m - Y_{\dot{v}})}$	0.0008	0.0016	0.0007	0.0013
$\beta_8 = \frac{Y_{\psi\|\psi\|}}{(m - Y_{\dot{v}})}$	-	-	-	-
$\beta_9 = \frac{Y_{\psi}}{(m - Y_{\dot{v}})}$	-	-	-	-

$\beta_{10} = \frac{Y_{static}}{(m - Y_{\dot{v}})}$	-	-	-	-
$\gamma_1 = \frac{(Z_{\dot{q}} - mx_g)}{(m - Z_{\dot{w}})}$	-0.0059	-0.0062	-0.0058	-0.0061
$\gamma_2 = \frac{Z_{w\|w\|}}{(m - Z_{\dot{w}})}$	-0.0138	-0.0186	-0.0094	-0.0038
$\gamma_3 = \frac{Z_w}{(m - Z_{\dot{w}})}$	-0.0347	-0.9837	-0.0372	-0.7185
$\gamma_4 = \frac{Z_q}{(m - Z_{\dot{w}})}$	-0.0011	0.0044	-0.0010	-0.0083
$\gamma_5 = \frac{Z_r}{(m - Z_{\dot{w}})}$	0.0001	-0.0032	0.0001	-0.0028
$\gamma_6 = \frac{(W - B) + Z_{static}}{(m - Z_{\dot{w}})}$	0.0016	0.0020	0.0015	0.0020

2.5.2. Model calibration

The baseline mathematical model may be unable to predict the vehicle motion response in operational environments different from the baseline environment. For example, if the vehicle is operating in a highly turbulent waters, the baseline model will be unable to predict the AUV's actual velocities over ground. Similarly, variations in the vehicle setting due to different ballast and trim conditions, addition of new payloads, and change in module configuration will change the hydrostatic and hydrodynamic forces acting on the AUV and hence, the mathematical model representing it. Therefore, any deviation from the baseline vehicle condition requires alteration of the mathematical model to obtain an accurate motion response. A model calibrating algorithm was introduced to overcome this by adjusting the baseline model for the new vehicle operational environments and configurations by carrying out a calibration mission.

For model calibration, the RLS algorithm was run for Equation (2.16) instead of for Equation (2.12). That is, in Equation (2.16), $\mathbf{y}_{(t)}$ and $\mathbf{\Theta}_{(t)}$ of Equation (2.13) will be replaced by the terms $(\mathbf{y}_{(t)} - \mathbf{F})$ and $\mathbf{\Theta}_{(t),\text{alteration}}$ respectively.

$$\mathrm{y}_{(t)} - \mathrm{F} = \mathrm{H}_{(t)} \Theta_{(t),\text{alteration}} \tag{2.16}$$

where, $\mathrm{y}_{(t)}$ and $\mathrm{H}_{(t)}$ are as defined in Table 2.2 for surge, sway and heave models, while F reflects the right-hand-side in equations (2.9), (2.10) and (2.11) respectively. The baseline model was used to obtain the solutions for F. The terms in $\Theta_{(t),\text{alteration}}$ represents the corrections required for the initial parameters in the baseline model.

In this investigation, the baseline model identified with the RLS method using ID Manoeuvre 1 was calibrated to predict the vehicle motion response in the environmental conditions in Lake Ohau. The same *Gavia* AUV with the identical module configuration as in the Lake Trevallyn tests was used for Lake Ohau mission. Therefore, the mass and hydrostatic vehicle properties were unaffected, and the corresponding parameters were not calibrated. Thus α_1, α_2, α_3, β_1, β_2 and γ_1 parameters and corresponding motion variable elements were removed from $\boldsymbol{\Theta}_{(t),\text{alteration}}$ and $\mathbf{H}_{(t)}$ vector respectively. Surge and sway force parameters due to steady underwater currents (i.e., α_9, α_{10}, β_8 and β_9) and external forces (i.e., α_{11} and β_{10}), which were neglected in the baseline model, were included for the model calibration as the objective is to capture the effect of environmental forces. At the end of the calibration run, the calibrated parameters were obtained by adding the required corrections to the original baseline parameters according to Equation (2.17).

$$\boldsymbol{\Theta}_{(t),\text{calibrated}} = \boldsymbol{\Theta}_{(t)} + \boldsymbol{\Theta}_{(t),\text{alteration}} \tag{2.17}$$

where, $\boldsymbol{\Theta}_{(t),\text{calibrated}}$ is the final set of calibrated parameters.

2.5.3. Performance analysis & discussion

Performances of the determined baseline models were examined by applying the identified parameter vectors (i.e., $\boldsymbol{\Theta}_{(t)}$) into the simulation model and simulating a set of pitch and yaw plane zig-zag manoeuvres conducted in Lake Trevallyn (i.e., under the same environmental and vehicle conditions). The AUV runs used for model estimations were not used for this validation process to have an unbiased validation.

Simulated vehicle velocities from baseline models were compared against actual measurements from the DVL aided INS. Baseline models included those identified using RLS and PEM techniques, with each technique processed twice using field data from ID Manoeuvres 1 and 2. Figure 2.5a, 2.5b and 2.5c compare the experimental and model predicted velocities in surge, sway and heave directions respectively (i.e., *u*, *v* and *w*). The uncertainties in surge velocity predictions from all models increase with time due to accumulation of acceleration prediction error during the integration to determine the velocity. Conversely, the error propagations in sway and heave velocities are negligibly smaller due to error counteraction during the velocity fluctuations. Table 2.4 presents the Root Mean Squared (RMS) errors (Devore, 2011b) of baseline models in comparison to actual measurements from the DVL bottom-track aided INS. Good correlations were observed from all models with RMS

errors less than 0.13 m s^{-1}, 0.03 m s^{-1} and 0.03 m s^{-1} for *u*, *v* and *w*. In comparison, as given in Table 2.1, the RMS uncertainty of surge, sway and heave velocity estimations from a DVL water-track aided INS is 0.3 m s^{-1}, GPS aided INS is 0.05 m s^{-1} and DVL bottom-track aided INS is 0.001 m s^{-1} (Alameda Jr, 2002, Kearfott Corporation, 2016).

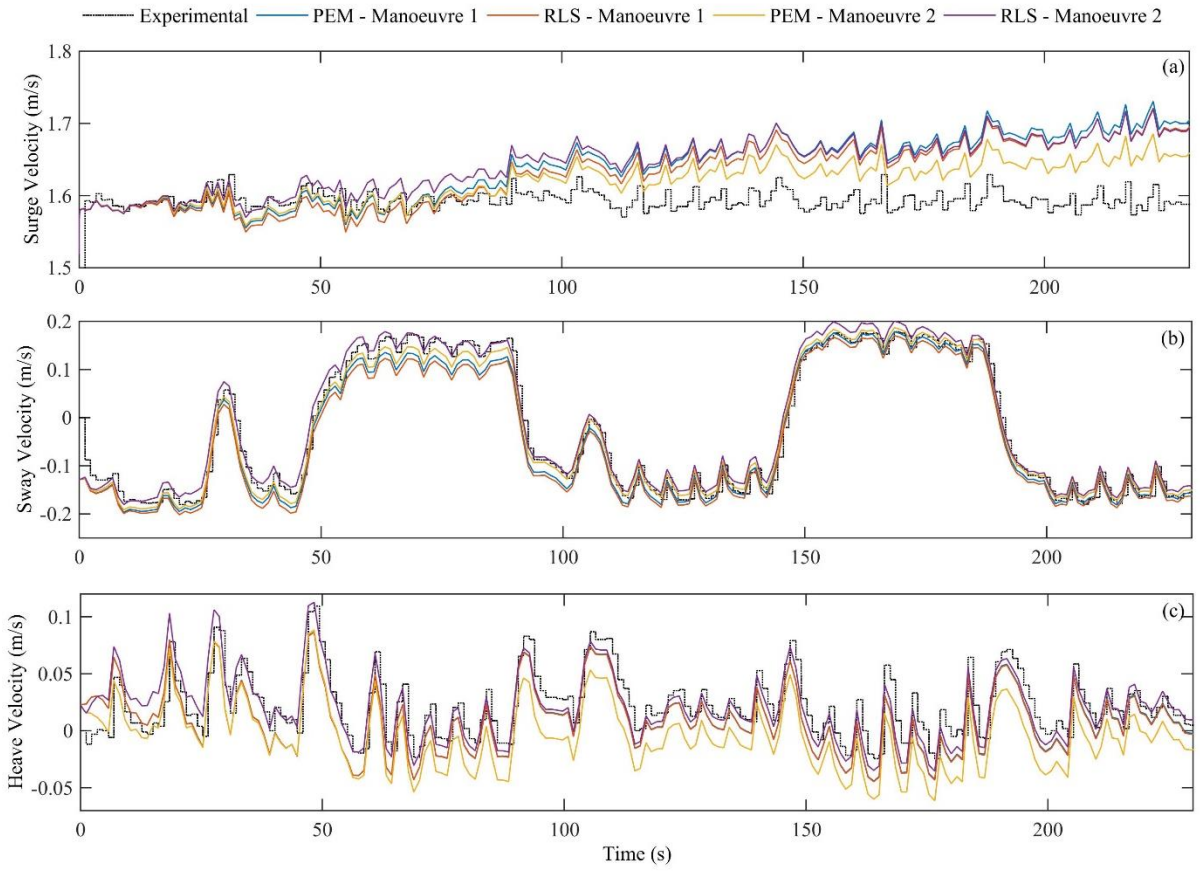

Figure 2.5 – Comparison between the baseline models and experimental velocities of the AUV in (a) *x*, (b) *y* and (c) *z* directions for the Lake Trevallyn field tests

The difference between velocity prediction uncertainties of the models identified using RLS and PEM are negligibly small (see Table 2.4). That is, both identification algorithms are equally capable of estimating the parameters of the model defined by Equations (2.9), (2.10) and (2.11). The initial parameter values were set to 1 in both techniques in order to preserve the assumption that the initial guesses of the parameters are unknown. Dependency of the parameters estimation accuracy on the initial values was evaluated by repeating the RLS and PEM estimation algorithms with initial values being set to previously identified parameters. Negligibly small variations of the parameter values were observed (i.e., less than 0.5%). Therefore, the estimated parameters are independent of the initial values. This is likely to be as

a result of the utilised identification manoeuvres that stimulate the vehicle dynamics in all motion modes.

Table 2.4 – Accuracies of the vehicle velocity predictions from the four baseline models (i.e., models identified with RLS and PEM techniques, with each technique processed twice utilising ID Manoeuvres 1 and 2) compared to velocity measurements from the DVL aided INS.

Identification technique	Manoeuvre	RMS error compared to actual measurements (m s^{-1})		
		Surge velocity	Sway velocity	Heave velocity
RLS	ID Manoeuvre 1	0.13	0.03	0.02
	ID Manoeuvre 2	0.13	0.02	0.02
PEM	ID Manoeuvre 1	0.13	0.03	0.02
	ID Manoeuvre 2	0.12	0.02	0.03

The parameter estimation was repeated for both ID Manoeuvres 1 and 2 to investigate the variation of the estimated parameters with the utilised dataset. As seen from Figure 2.5, models obtained by processing both datasets perform well with a maximum RMS difference of 0.01 m s^{-1} (see Table 2.4). The RLS and PEM algorithms were able to process an 862-second long dataset with computation times of 12 s and 10 s utilising an Intel Core i7-4470 3.40 GHz central processing unit. That is, the measurement data can be processed in rates of 74 Hz and 62 Hz respectively. Real time measurement sampling rate of the AUV is around 25 Hz. Therefore, either of the two algorithms are deemed to be feasible for real time or near real time estimation.

Given that all four baseline models are equally capable, the model parameters obtained from RLS technique by processing ID Manoeuvre 1 was utilised for the discussion hereinafter. The baseline model-aided INS solution was obtained by fusing the vehicle velocities from the RLS baseline model with unaided INS acceleration measurements. A Kalman filter based data fusion algorithm developed according to Farrell (2008) was utilised for INS aiding. The baseline model-aided INS was tested for the lawn mower pattern run in Lake Ohau (AUV Runs 5 – 8) to investigate the performance in different environments (recall Figure 2.2b). Figure 2.6a, 2.6b and 2.6c compare *u*, *v* and *w* velocities of the vehicle from baseline model-aided INS against those measured by the AUV's DVL aided INS. The sudden peaks and dips at the time periods of 300s, 650s and 1050s were a result of the 180˚ heading turns of the vehicle at the end of each straight line run. The RMS errors between the baseline model-aided INS and

experimentally measured DVL aided INS were 0.15 m s^{-1}, 0.02 m s^{-1} and 0.02 m s^{-1} for *u*, *v* and *w* respectively. The AUV's on board ADCP measured an averaged background water current magnitude of around 0.1 m s^{-1} in the Lake Ohau test site. According to the WVAM method (Randeni et al., 2015a), the difference between the actual vehicle velocities and those simulated by a baseline model that represents a calm environment provides the velocities of the water column around the AUV. Although, this difference is reduced when the baseline model is fused with actual vehicle acceleration measurements from the INS. The observed difference between the actual and baseline model-aided INS results is due to the water currents in Lake Ohau.

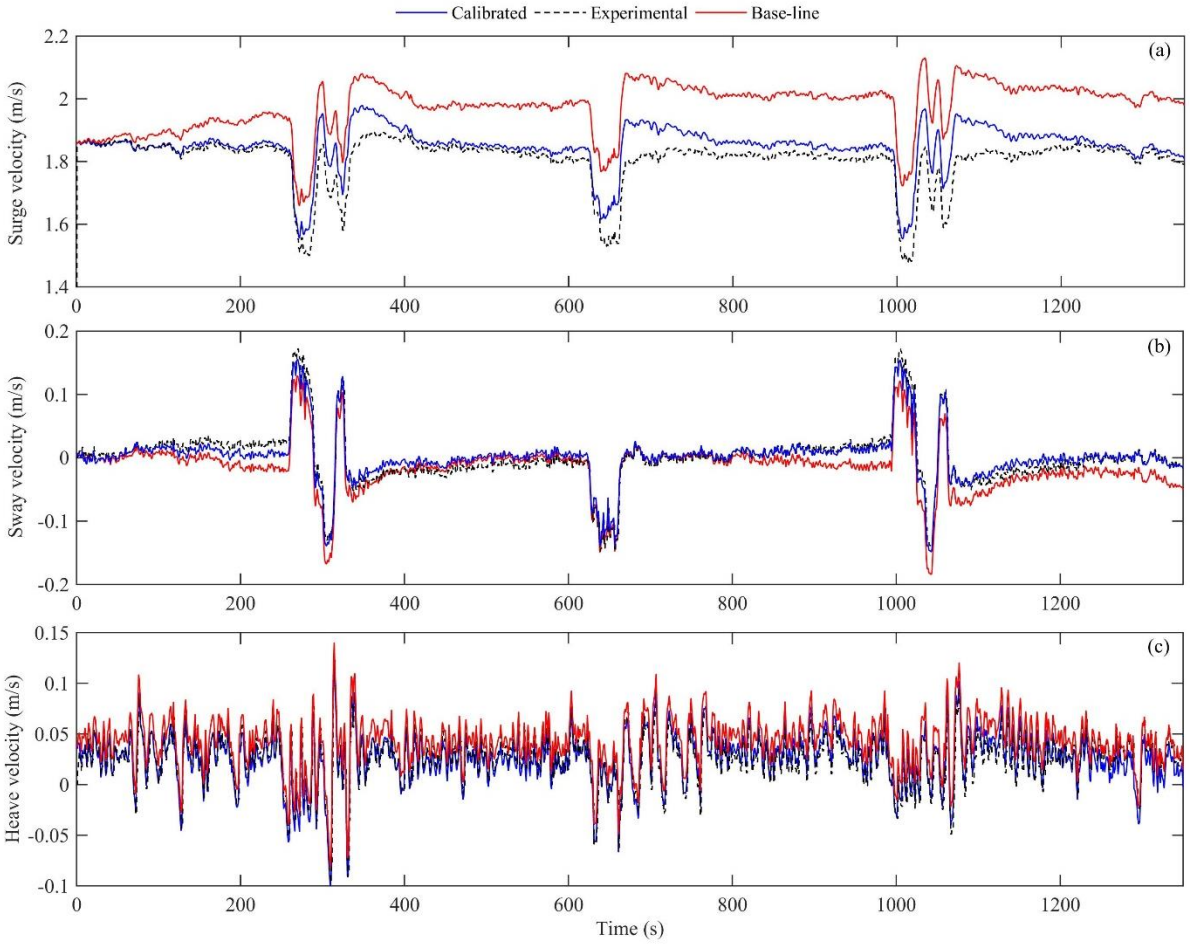

Figure 2.6 – Comparison of the baseline and calibrated model-aided INS velocities in (a) *x*, (b) *y* and (c) *z* directions against those from the DVL aided INS for the Lake Ohau runs 2 and 3

The baseline model was calibrated by running the calibration algorithm for AUV Runs 1 – 4 in Lake Ohau. The solid blue lines in Figure 2.6 show the velocity from the calibrated model-aided INS for AUV Runs 5 – 8. A significant improvement is that RMS errors compared to actual measurements have reduced to 0.04 m s^{-1}, 0.01 m s^{-1} and 0.01 m s^{-1} for respective

velocities in surge, sway and heave directions. That is an improvement of 73%, 50% and 50% in each of the three directions, respectively. Table 2.5 presents the numerical values of the baseline model parameters (i.e., from RLS method with ID Manoeuvre 1) and those of the model calibrated for the Lake Ohau environmental condition.

Table 2.5 – Numerical values of the *Gavia* AUV's baseline model (i.e., from RLS method with ID Manoeuvre 1) parameters and those of the model calibrated for Lake Ohau.

Parameter	Baseline model	Calibrated model
$\alpha_1 = \frac{my_g}{(m - X_{\dot{u}})}$	0.5294	0.5294
$\alpha_2 = \frac{-mz_g}{(m - X_{\dot{u}})}$	0.0909	0.0909
$\alpha_3 = \frac{(W - B)\sin(\theta)}{(m - X_{\dot{u}})}$	-2.5098	-2.5098
$\alpha_4 = \frac{X_{uuu}}{(m - X_{\dot{u}})}$	-8.5937	-8.4707
$\alpha_5 = \frac{X_{u\|u\|}}{(m - X_{\dot{u}})}$	-22.3129	-22.1499
$\alpha_6 = \frac{X_u}{(m - X_{\dot{u}})}$	-32.7171	-31.7411
$\alpha_7 = \frac{X_{wq}}{(m - X_{\dot{u}})}$	-7.1061	-6.7996
$\alpha_8 = \frac{X_{vr}}{(m - X_{\dot{u}})}$	-13.5405	-12.7575
$\alpha_9 = \frac{X_{\psi\|\psi\|}}{(m - X_{\dot{u}})}$	-	0.0001
$\alpha 10 = \frac{X_{\psi}}{(m - X_{\dot{u}})}$	-	-1.0225
$\alpha_{11} = \frac{X_{static}}{(m - X_{\dot{u}})}$	-	-1.8920
$\beta_1 = \frac{(Y_{\dot{r}} - mx_g)}{(m - Y_{\dot{v}})}$	0.0133	0.0133
$\beta_2 = \frac{mz_g}{(m - Y_{\dot{v}})}$	0.0029	0.0029
$\beta_3 = \frac{Y_{v\|v\|}}{(m - Y_{\dot{v}})}$	0.0444	0.0415
$\beta_4 = \frac{Y_v}{(m - Y_{\dot{v}})}$	-0.0364	-0.0603
$\beta_5 = \frac{Y_p}{(m - Y_{\dot{v}})}$	0.0005	0.0007
$\beta_6 = \frac{Y_q}{(m - Y_{\dot{v}})}$	-0.0001	0.0001
$\beta_7 = \frac{Y_r}{(m - Y_{\dot{v}})}$	0.0008	0.0009

$\beta_8 = \frac{Y_{\psi\|\psi\|}}{(m - Y_{\dot{v}})}$	-	0.0000
$\beta_9 = \frac{Y_{\psi}}{(m - Y_{\dot{v}})}$	-	-0.6001
$\beta_{10} = \frac{Y_{static}}{(m - Y_{\dot{v}})}$	-	1.0064
$\gamma_1 = \frac{(Z_{\dot{q}} - mx_g)}{(m - Z_{\dot{w}})}$	-0.0059	-0.0059
$\gamma_2 = \frac{Z_{w\|w\|}}{(m - Z_{\dot{w}})}$	-0.0138	-0.0283
$\gamma_3 = \frac{Z_{w}}{(m - Z_{\dot{w}})}$	-0.0347	-0.0390
$\gamma_4 = \frac{Z_{q}}{(m - Z_{\dot{w}})}$	-0.0011	-0.0103
$\gamma_5 = \frac{Z_{r}}{(m - Z_{\dot{w}})}$	0.0001	-0.0001
$\gamma_6 = \frac{(W - B) + Z_{static}}{(m - Z_{\dot{w}})}$	0.0016	0.0003

The baseline model-aided INS surge velocity prediction diverges with time compared to DVL aided INS solution due to accumulation of error. However, the surge velocity is accurately estimated by the calibrated model-aided INS for the entire duration of the mission. Out of the three, the heave velocity component delivered the most accurate replication of the actual velocity of the AUV. Although, the velocity prediction in *z* direction is not critical for localisation as the vehicle depth and depth rates can be accurately measured with the pressure sensor, it can be used as a backup for emergency situations.

There is an uneven divergence between the actual and calibrated sway velocities (Figure 2.6b). Consistently, this difference is observed at one side of the four lawn mower pattern straight lines; i.e., at the right-hand side of the bathymetry shown in Figure 2.2c. This could be due to strong underwater currents of around 0.15 m s^{-1} present near the inflow point caused by the Hopkins and Dobson Rivers (Cossu et al., 2015). This discrepancy gets larger as the distance gets smaller. Therefore, a water column velocity measurement method could be integrated together with the model predicted vehicle velocities in order to improve the accuracy of the localisation solution of the AUV when DVL aiding is unavailable for longer time intervals (Hegrenaes and Hallingstad, 2011, Randeni et al., 2016).

Figure 2.7a compares the 2-dimensional (2D) localisation solutions computed using the measured vehicle velocities (i.e., the actual vehicle path) and those estimated using the baseline model for the pitch and yaw plane zig-zag manoeuvres conducted in Lake Trevallyn site. Note that the AUV paths are plotted in a local coordinate system. The baseline model predicted

localisation solution was within the 1.5% of the distance travelled uncertainty range. Therefore, the estimated baseline model is deemed accurate to predict the vehicle position with an uncertainty margin of 1.5% of the distance travelled when the AUV is operating under similar environmental forcings.

Figure 2.7b compares the 2D localisation solutions of the AUV for Lake Ohau Runs 5 – 8 computed using the measured DVL aided INS velocities and those from the baseline and calibrated model-aided INSs. The baseline model-aided INS over predicts the surge velocity of the AUV by approximately 0.15 m s^{-1}, resulting in a deviated vehicle position derivation compared to the actual path. However, this position error is counteracted during the opposite directions runs of the lawn mower pattern mission. The over prediction of the surge velocity is significantly reduced in the calibrated model providing a more accurate localisation solution.

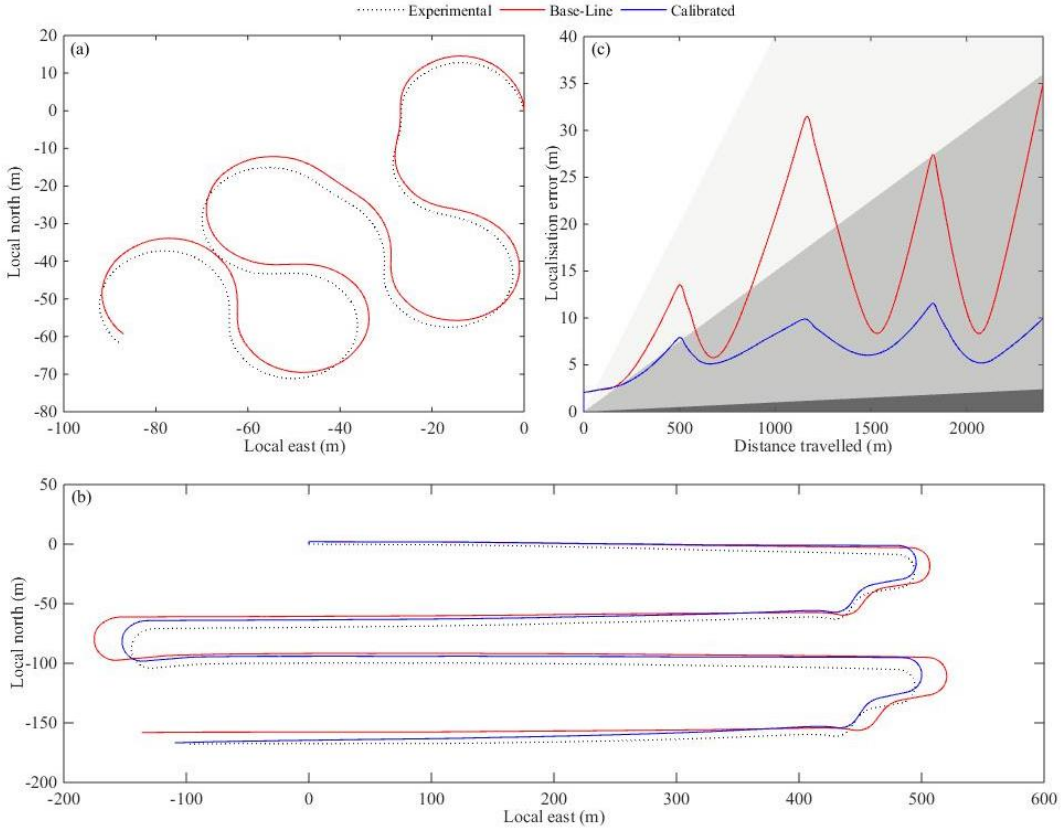

Figure 2.7 – (a) two dimensional AUV paths of Lake Trevallyn manoeuvres derived from the actual vehicle velocities (i.e., experimental), and baseline model predicted velocities plotted in a local coordinate system. (b) actual and model predicted (i.e., baseline model and calibrated model) localisation solutions of Lake Ohau Runs 5 – 8. (c) comparison of the localisation errors (i.e., the difference between the actual and model predicted vehicle positions) from baseline and calibrated models. Dark grey area indicates the 0.1% of the distance travelled localisation error level (i.e., positioning uncertainty of a typical DVL bottom-track aided INS) while grey and light

grey regions show that of 1.5% and 4.0% (i.e., the localisation error level of an DVL water-track-aided INS)

Figure 2.7c plots the localisation errors (i.e., the difference between the DVL aided and model-aided INS vehicle positions) for baseline and calibrated models against the AUV's travel distance for the Lake Ohau mission. The fluctuations in the localisation errors are due to the error counteraction during the opposite direction runs. Three different uncertainty margins are indicated by grey shaded areas with dark grey representing the localisation error level of 0.1% of the distance travelled. Grey and light grey zones show respective error levels of 1.5% and 4.0% of the distance travelled. The localisation solution from the baseline model-aided INS was outside of the 1.5% band but, was generally within the 1.8% of the distance travelled margin. The positioning uncertainty is generally within 1.5% level when the model is calibrated to the operational environment.

The localisation accuracy of the *Gavia* AUV with Kearfott T24 INS when DVL aiding is available is within 0.1% of the distance travelled; i.e., region shaded in dark grey (Hiller et al., 2011). However, according to the published specifications, the DVL water-track-aided Kearfott T24 INS (i.e., when DVL bottom-track is unavailable) has a time root mean squared localisation uncertainty of 1852 m (i.e., 1 nm) per 8 hours (Kearfott Corporation, 2016). Assuming a forward speed of 1.6 m s^{-1}, this yields a positioning error of around 4.0% of the distance travelled (i.e., region shaded in light grey). A calibrated model-aided INS could limit the positioning uncertainty to around 1.5% of the distance travelled for a typical AUV mission.

2.6. Real time model identification

2.6.1. Real time parameter calibration

In highly dynamic environments, the parameters of the mathematical model fluctuate with time due to environmental and external forcing. The objective of the real time model calibration algorithm is to generate a mathematical model that continuously updates to provide the vehicle motion response in the present operational environment; especially in highly dynamic environments. The procedure outlined in Section 2.5.2 was employed for real time parameter calibration. However, in order to identify the variation of parameters in a dynamic environment, data from preceding measurements have to be forgotten/discarded as new data arrives and the successive measurements should contain a higher weighting in the estimation process. Therefore, the performance of the real time calibration model for different data

processing set lengths were investigated by testing for forgetting factors of 1.00, 0.95 and 0.90; i.e., an infinite length, a time period of 20 s and 10 s, respectively.

2.6.2. Performance analysis & discussion

In order to verify whether the mathematical model provided by the real time model calibration method precisely represents the hydrodynamic characteristics of the AUV, the real time algorithm was tested using a horizontal heading angle zig-zag manoeuvre conducted in Lake Trevallyn (i.e., the first 260 s of the ID Manoeuvre 1 shown in Figure 2.3) and a straight line run conducted in Lake Ohau (i.e., AUV Run 1 shown in Figure 2.2b). Parameters that are being updated in real time were used in the simulation model to determine the vehicle linear accelerations along surge, sway and heave directions and were compared against those measured by the vehicle INS. The maximum discrepancy between the two was observed in the surge acceleration.

Table 2.6 presents the averaged difference between the actual and simulated accelerations for forgetting factors of 1.00, 0.95 and 0.90. The accuracy of the real time model is comparatively lower when the forgetting factor was set to 1 in order to disable the forgetting effect and to process the entire data series from the first to the last measurement. On the other hand, the averaged percentage differences for the Lake Trevallyn and Lake Ohau runs for the forgetting factors of both 0.90 and 0.95 were less than 1%. Thus, the accuracies of the mathematical models identified using the real time algorithm increased after enabling the forgetting effect. It can be concluded that the smaller the forgetting factor is (i.e., the shorter the length of the data series being processed) the higher the accuracy is. However, the numerical values of all parameters converged within 5% of the mean values for all the tested forgetting factors.

Table 2.6 – The variation of the averaged difference between the actual and simulated accelerations with the forgetting factor for Lake Trevallyn and Ohau runs.

Forgetting factor	Averaged difference between actual and simulation accelerations ($m\ s^{-2}$)					
	Lake Trevallyn test			Lake Ohau test		
	Surge	Sway	Heave	Surge	Sway	Heave
0.90	1.49×10^{-8}	2.59×10^{-7}	9.19×10^{-9}	3.14×10^{-8}	1.59×10^{-8}	2.11×10^{-8}

0.95	1.84×10^{-7}	1.93×10^{-6}	1.13×10^{-7}	3.55×10^{-8}	3.67×10^{-7}	4.83×10^{-8}
1.00	1.37	4.60×10^{-3}	3.81×10^{-3}	4.18×10^{-3}	1.55×10^{-3}	1.61×10^{-3}

2.7. Limitations and future work

The model identification algorithms presented in this article utilise the roll, pitch and yaw rates and accelerations as the control command inputs instead of the control surface angles to create a simplified 3-DOF model of the vehicle. Although the use of this model presents a major limitation for using on AUVs without accurate sensors to measure vehicle orientations, it would be widely applicable for most commercially available AUVs on the market today.

Although the calibration method can be utilised to adjust a baseline model of an AUV for different configurations, this was not experimentally verified in this work. Authors expect to investigate this by testing the algorithm for different configurations of the *Gavia* AUV. Furthermore, it is anticipated to link the model predicted vehicle velocities with the non-acoustic water column velocity estimation method (i.e., the WVAM method) previously developed by the authors (Randeni et al., 2016) in order to accurately estimate the vehicle velocities over ground for INS aiding.

One of the key advantages of the mathematical model identification and calibration algorithms is that they could be applied to any torpedo shaped AUV (e.g. *REMUS*, *Iver*, *Bluefin*, *Explorer*, etc.) in any configuration. Authors have utilised this algorithm to successfully identify the mathematical models of an *Iver III* AUV and a *Gavia* AUV with different module configurations.

2.8. Conclusions

This study presents a system identification algorithm to determine the linear and nonlinear parameters of an AUV mathematical model utilising the RLS and PEM optimisation methods. A baseline model that represents the dynamics of the *Gavia* AUV in a calm water environment was developed. The estimated baseline model accurately predicted the vehicle velocities in three dimensions when the vehicle and environmental conditions are similar to those represented by the baseline model. Model accuracy decreases when the operational environment is different. A novel technique was developed in this study to calibrate the parameters within the baseline model to different environmental conditions by conducting a calibration mission in the new environment. The accuracy of the velocity measurements from

the calibrated model was substantially greater than those from the baseline model for the tested scenarios with a minimum velocity prediction improvement of 50%. The calibrated model is able to compute the position of the AUV within an uncertainty range of 1.5% of the distance travelled. It is hypothesised that this uncertainty could be further reduced by incorporating the model predicted vehicle speeds obtained through a water column velocity estimation method. In comparison, the uncertainty of a DVL aided INS is around 0.1% of the distance travelled and that of a DVL water-track aided INS is around 4% (assuming a forward speed of 1.6 m s^{-1}).

The algorithm was extended to real time parameter calibration and the extended algorithm was tested at two field sites with different environmental conditions; i.e., in a quiescent lake with relatively flat seabed, and in a more dynamic water column with rough and unstructured bathymetry. The performance of the real time calibration model for different processing data set lengths were investigated by testing for forgetting factors of 1.00, 0.95 and 0.90. The smaller the forgetting factor is (i.e., the shorter the length of the data series being processed) the higher is the accuracy.

The long term objective of this work is to predict the three dimensional velocity vector of the AUV in order to localise the vehicle when velocity over ground measurements from the DVL are unavailable for INS aiding.

Chapter 3: WVAM method – a non-acoustic technique to determine the velocity components of the water column

---

Chapter 3 is based on the journal article '*Determining the Horizontal and Vertical Water Velocity Components of a Turbulent Water Column Using the Motion Response of an Autonomous Underwater Vehicle*' published in the '*Journal of Marine Science and Engineering*'. The citation for the article is:

Randeni, S. A. T., Forrest, A. L., Cossu, R., Leong, Z. Q., & Ranmuthugala, D. (2017). Determining the Horizontal and Vertical Water Velocity Components of a Turbulent Water Column Using the Motion Response of an Autonomous Underwater Vehicle. Journal of Marine Science and Engineering, 5(3), 25.

Abstract

This work introduces a new method to calculate the water velocity components of a turbulent water column in the *x*, *y*, and *z* directions using the Autonomous Underwater Vehicle (AUV) motion response (referred to as the 'WVAM method'). The water column velocities were determined by calculating the difference between the motion responses of the vehicle in calm and turbulent water environments. The velocity components obtained using the WVAM method showed good agreement with measurements from an acoustic Doppler current profiler (ADCP) mounted to the AUV. The standard deviation between the two datasets were below 0.09 m s^{-1} for the velocity components in the *x*, *y*, and *z* directions, and were within the uncertainty margin of the ADCP measurements. With the WVAM method, it is possible to estimate the velocity components within close proximity to the AUV. This region encompasses the vehicle boundary layer and the ADCP blanking distance, which is not typically resolved. Estimating vertical and horizontal velocities around the boundary layer of the AUV is important for vehicle navigation and control system optimisation, and to fill the blanking distance gap within a water column velocity profile, which is important for flow field characterisation. The results show that it is possible to estimate the flow field in the vicinity of AUVs and other self-propelled vehicles.

3.1. Introduction

Measuring water column velocities is an essential component of physical oceanographic surveys but is also important for many applications, such as determining sediment transport (Hughes et al., 1997) and assessing the turbulent flux in the surface mixed layer (Hayes and Morison, 2002). Conventionally, broadband Acoustic Doppler Current Profilers (ADCPs) are used to measure water column velocity profiles using the Doppler frequency shift of a sound wave transmitted by the device resulting from particles in the water column moving with the fluid (Simpson, 2001). Stationary ADCPs can be used to determine flow profiles at a fixed location. The spatial and temporal distributions of velocity fields can be potentially determined with an array of such devices; however, the associated costs may restrict the number of sensors, limiting the spatial resolution of the measured velocity profiles.

An alternative is to install similar instrumentation on mobile platforms to map the three dimensional water velocity components with a higher spatial resolution, although it is difficult to capture time series information with these vehicles (Sprintall et al., 2012). At larger water depths, subsea mobile platforms, such as Autonomous Underwater Vehicles (AUVs), provide increased potential for such surveys that are logistically not possible using surface-borne techniques. AUVs are more reliable to undertake missions in areas logistically difficult or inaccessible for surface vessels and other types of underwater vehicles such as Remotely-Operated Vehicles (ROVs) and manned submersibles. For this reason, combined with the relative stability of the vessel and being decoupled from surface noise and reflectance, AUV mounted ADCPs have been frequently used to measure water column velocities (Fong and Jones, 2006, Kimura et al., 2016).

Acoustic Doppler current profilers have a blanking distance in proximity to the device whose size depends on the frequency of the instrument in which the flow velocity data is not resolved (Simpson, 2001). Larger AUVs tend to have low frequency ADCPs to obtain a larger range; however, it also increases the size of the blanking distance. For example, 150 kHz ADCPs have a maximum range of around 200 m and a blanking distance of around 2–3 m, while the maximum range and blanking distance of 1200 kHz ADCPs are around 20 m and 0.5–1 m respectively. Gandhi et al. (2008) utilised a power-law relation to interpolate the water velocity profile for the blanking distance near the sensor when determining discharge measurements in small hydropower stations in order to reduce the error due to the blanking distance. However, such interpolations are invalid in unstructured flow fields.

Previously, Hayes and Morison (2002) introduced a new technique to determine the turbulent vertical water velocities, and fluxes of heat and salt using the AUV motion data. A horizontal profile of vertical water velocity was obtained by applying a Kalman filter to the AUV motion data. However, it cannot be readily adopted for commercial AUVs due to the modelling complexity and the requirement of the typically unavailable vehicle control law algorithm. Frajka-Williams et al. (2011) developed a technique to estimate vertical water velocities from Seaglider autonomous underwater gliders, produced by Kongsberg Maritime AS, Kongsberg, Norway, using the difference between a predicted glider flight speed in still water and the observed glider vertical velocity from pressure. Rudnick et al. (2013) determined the vertical water velocity from Spray gliders using two methods; first, using a model approach similar to the Frajka-Williams et al. (2011). The second approach was to high-pass the measured vertical velocity of the vehicle under the assumption that changes in glider flights are low frequency compared to the water velocities. All three of these methods were limited to the vertical water velocity.

This study introduces a method to calculate the water velocity components in the *x*, *y*, and *z* directions of a turbulent water column using the AUV motion response (hereinafter referred to as the 'WVAM method'). The WVAM method determines the fine scale variations of water velocities (with a smallest measurable length scale of around 2.7 m in the current vehicle configuration) by comparing the motion response of the vehicle when operating within turbulent and calm water environments respectively. The key advantage of the WVAM method is that it provides velocity estimates within the blanking distance of the ADCP and the associated vehicle boundary layer which are usually unknown based on previous methods. The following sections of the article provide an overview of the experimental tools, test field details and novel methodologies employed for this work. Subsequently, the assessment and discussion of the validation and verification of the WVAM method are presented. Potential applications of the WVAM method and possible future developments are discussed in the Recommendations section of this chapter (i.e., Section 3.5).

3.2. Materials and Procedures

3.2.1. Instrumentation

A Gavia-class modular AUV (Forrest et al., 2012) built by Teledyne Gavia ehf., Kópavogur, Iceland was used to test and validate the proposed WVAM method. As configured

for testing, this vehicle consists of a nose cone module, battery module, GeoSwath Plus Kongsberg Maritime AS (Kongsberg, Norway) interferometric sonar module, 1200 kHz Teledyne RD Instruments (San Diego, USA) ADCP/Doppler Velocity Log (DVL) module, Kearfott (New Jersey, USA) T24 inertial navigation system (INS) module, control module, and a propulsion module (Figure 3.1). The overall length of the vehicle was 2.7 m, the diameter was 0.2 m, and the dry weight in air was approximately 70 kg. The Kearfott T24 INS, aided with velocity over ground measurements obtained from the DVL bottom-tracking mode, was utilised by the AUV to determine position of the AUV and vehicle velocities in six-degree-of-freedom (6-DOF). The depth of the vehicle was obtained from the Keller (Winterthur, Switzerland) Series 33Xe pressure sensor on-board the AUV. These sensor measurements were recorded in the vehicle log at a frequency of 0.87 Hz.

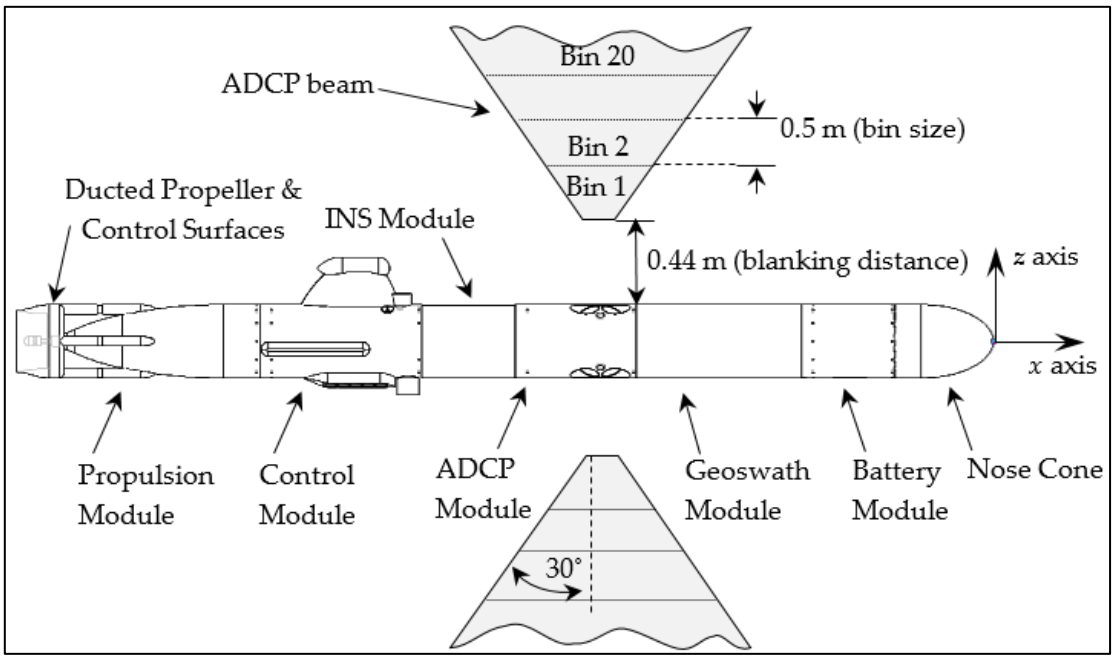

Figure 3.1 – Configuration of the utilised Gavia AUV with the ADCP beam geometry as indicated.

AUVs are preprogramed to follow a pre-set mission route with a given surge speed. When an AUV is operating in an environment with highly-fluctuating water velocities (e.g., in a turbulent water column), the forces induced by these velocities can interrupt the control stability and change the vehicle speed, depth, pitch, and yaw angles (i.e., motion response of the AUV) from the pre-set values. In order to compensate for such changes in performance, the vehicle's dynamic control system adjusts the revolution speed of the propeller and the angles of the four control surfaces located at the stern of the propulsion module. According to

these adjustments, the motion response of the AUV will change and the AUV will target the initially-prescribed mission track (Kim and Ura, 2003) unless the propeller and the control surfaces are unable to cope with the external forces.

The ADCP module of the AUV included two 1200 kHz Teledyne RD Instruments ADCPs/DVLs arranged in upward- and downward-looking configurations. While the upward-looking transducers were configured so that the instrument only collected water column velocity data relative to the AUV, the downward-looking set had a dual purpose: (i) water column data collection (i.e., ADCP mode), and (ii) estimation of the velocity of the vehicle relative to the ground as an input into the navigation solution of the vehicle (i.e., DVL mode). At every sampling time-step, the instrument's mode of operation switched between the ADCP and DVL. The ADCPs were programmed to profile approximately 10 m of water column in 0.5 m range bins so that the three directional water velocity components relative to the AUV in the body-fixed coordinate system are measured in each bin. During post processing, water velocity components relative to the AUV were converted to the Earth-relative velocities by using the vehicle's Earth-referenced velocity measurements from the DVL aided INS. However, the water velocity measurements remained in the body-fixed coordinate system.

In front of the ADCP transducers (both above and below) there was a blanking distance of 0.44 m (shown in Figure 3.1). This blanking distance (i.e., a vertical extent away from the vehicle where no velocity measurements are made) exists as transducers are required to recover electronically from the transmit pulse and to prepare to receive the return signal (Simpson, 2001). An ADCP requires only three transducer beams to acquire the three dimensional water velocity components. The fourth redundant transducer evaluates the quality of the velocity measurements by comparing two estimations of the vertical water velocity. The difference between the two is called the error velocity (Lu and Lueck, 1999).

3.2.2. Site Description

The objective of this study was to derive the WVAM method that calculates the velocity components of a water column by comparing the motion response of the vehicle when operating within a turbulent environment and a simulated calm water environment. The determined velocities are validated with the velocity measurements from the on-board ADCP. Field tests were carried out at two locations in Tasmania, Australia—in Lake Trevallyn (a low energy system with average flows at <0.05 m s^{-1}) to develop the calm water based simulation

model and in the Tamar estuary (a high energy system with peak flows at 2.5 m s^{-1}) to test the WVAM method (Figure 3.2a).

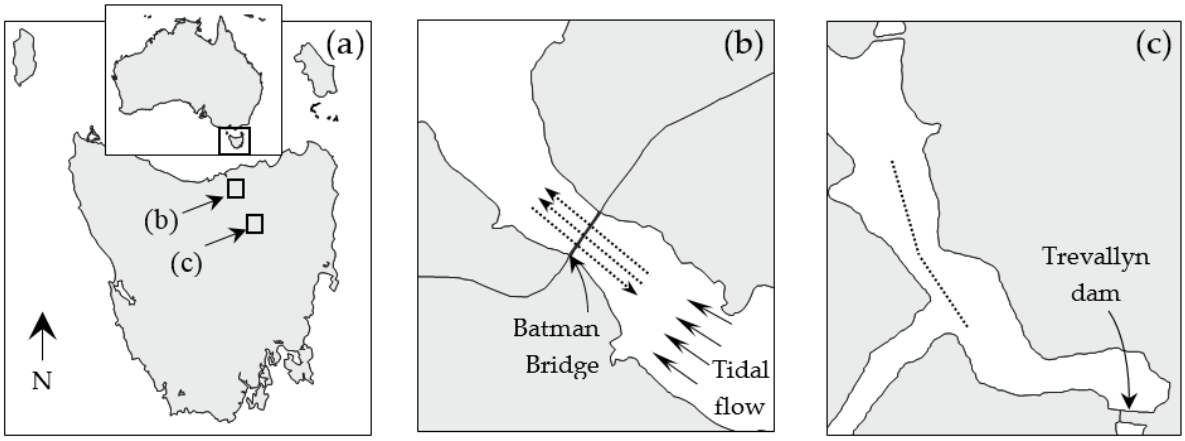

Figure 3.2 – (a) The two experimental field sites in Tasmania, Australia (inset). (b) The Batman Bridge site with the direction of dominant tidal current flow as shown with solid straight-line arrows. AUV tracks are illustrated with dotted arrows. (c) The Lake Trevallyn site with low turbulence conditions. AUV missions were conducted along the dotted line.

The main field study was conducted in the Tamar estuary near the Batman Bridge (Figure 3.2b) on 14 June 2014. The width of the estuary narrows down to less than 300 m near the Batman Bridge, which causes highly turbulent flow conditions along the main channel axis, as shown in Figure 3.2b. In addition, varying bathymetry of the estuary (i.e., the 35 m depth at the north-west end of the test location reduces to 15 m near the bridge and increases again to 30 m at the opposite end) induces further constraints to the tidal flow. As a result of the narrowing and resulting flow constriction, this section of the estuary usually exhibits strong tidal currents (with maximum flow of >2.5 m s^{-1}) and water level fluctuations of around 3m (Green et al., 2016). Three straight-line AUV runs were conducted along, and against, the tidal flow direction (see Figure 3.2b), maintaining a constant altitude of 10m above the bottom, and a propeller speed of 700 Revolutions Per Min (RPM). These missions were used to determine the water column velocities using the WVAM method.

A series of manoeuvres was conducted in Lake Trevallyn, Tasmania (Figure 3.2c) between 30 October and 14 November 2013 to derive the hydrodynamic coefficients of the AUV using a system identification approach. The manoeuvres included straight-line runs conducted for five different propeller speeds (i.e., 525 RPM, 600 RPM, 675 RPM, 750 RPM, and 825 RPM) and a zig-zag manoeuvre in yaw and pitch planes by changing the coordinate waypoints and operating depths concurrently. The manoeuvres were designed to simulate the

vehicle dynamics in vertical as well as the horizontal planes, which is critical for accurate estimation of simulation model parameters. The water depth of the test site was greater than 6 m and surface wave heights were below 50 mm. The AUV missions were carried out between 2 and 4 m below the free surface to minimise the surface wave formation and the interaction effects with the lake bottom (Ananthakrishnan and Zhang, 1998, Steel, 2010). During the manoeuvres, the vehicle's ADCP recorded minor variations of the water column velocities with averaged values in the surge, sway, and heave directions of less than 0.05 m s^{-1}. These minor water velocities indicate a calm water environment. The AUV missions were conducted along the dotted line shown in Figure 3.2c.

3.2.3. WVAM Method

The mathematical formulae presented in this paper are based on the SNAME (1952) notation. Force/moment, velocity, acceleration and position/Euler angle vectors are in the AUV's body fixed coordinate system (i.e., as shown in Table 3.1 and Figure 3.4) and are relative to the ground unless stated otherwise. The origin of the body-fixed reference frame was at the centre of buoyancy of the vehicle, which is located at the ADCP module as shown in Figure 3.4.

Table 3.1 – The 6-DOF notation system.

Degree-of-Freedom	Forces & Moments	Linear & Angular Velocity	Position & Euler Angles
Motions in the x-direction (surge)	X	u	x
Motions in the y-direction (sway)	Y	v	y
Motions in the z-direction (heave)	Z	w	z
Rotation about the x-axis (roll)	K	p	ϕ
Rotation about the y-axis (pitch)	M	q	θ
Rotation about the z-axis (yaw)	N	r	ψ

The WVAM method (Figure 3.3) starts with the AUV undergoing a straight-line, constant altitude mission through a region where the water column velocities are to be measured (i.e., in the turbulent water column). The vehicle's control system provides necessary commands to the propulsion motor and control surfaces (i.e., the propeller RPM commands and the control surface angle commands) to overcome the disturbances from the turbulent flow

and to continue the prescribed straight-line path while maintaining a constant altitude set point. These control commands, recorded in the vehicle log, are then executed with the simulation model that represents a calm water environment. Since there are no currents and flow disturbances in the simulated calm water condition, the vehicle velocities from the simulation model will be different to the actual velocities measured from the DVL aided INS of the AUV. The difference between the two motion responses provides a measurement of the water column velocities relative to the ground. Equation (3.1) gives the water velocity calculation in the general form. The requirement of the calm water manoeuvres is for initial development of the simulation model, which is applicable for a given vehicle configuration.

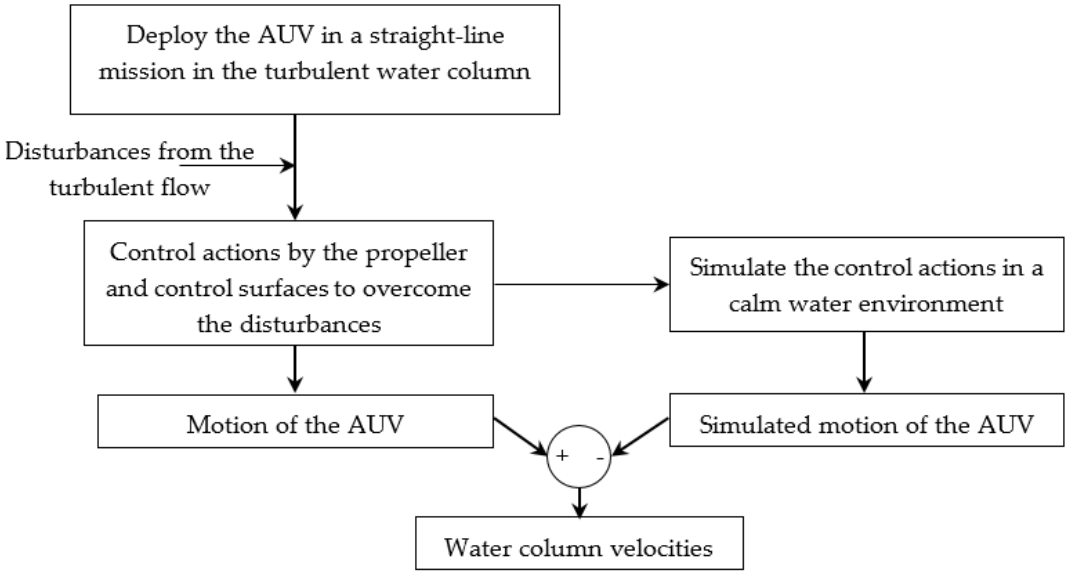

Figure 3.3 – The WVAM method flowchart to predict water column velocities from the observed vehicle motions. As given in Equation (3.1), the difference between the motion responses in the turbulent (i.e., experimental) and calm (i.e., simulated) water flow condition provides a measurement of the water column velocities relative to the ground.

$$\vec{V}_{water(t)} = \vec{V}_{AUV(turbulent)(t)} - \vec{V}_{AUV(calm)(t)} \tag{3.1}$$

where, $\vec{V}_{water}$ is the linear velocity vector of the surrounding water column (along the *x*, *y*, and *z* directions) relative to the earth in the body-fixed coordinate system (see Figure 3.4), $\vec{V}_{AUV(turbulent)}$ is the linear velocity vector of the AUV relative to the Earth measured in the turbulent environment using the DVL aided INS, and $\vec{V}_{AUV(calm)}$ is the linear velocity vector obtained from the calm water simulation model when the control commands recorded during the field tests were simulated. Subscript t indicates the time-step.

The AUV is required to be assumed as a particle if infinitely small water column velocity fluctuations are measured using Equation (3.1). However, an AUV is not sufficiently small in size to be assumed as a particle; therefore, due to the length of the vehicle, the water column velocity measurements derived from Equation (3.1) is restricted in terms of the length scale resolution. The minimum measurable velocity variation length scale is also limited by the sensor sampling frequency. This is further discussed in Section 3.4.

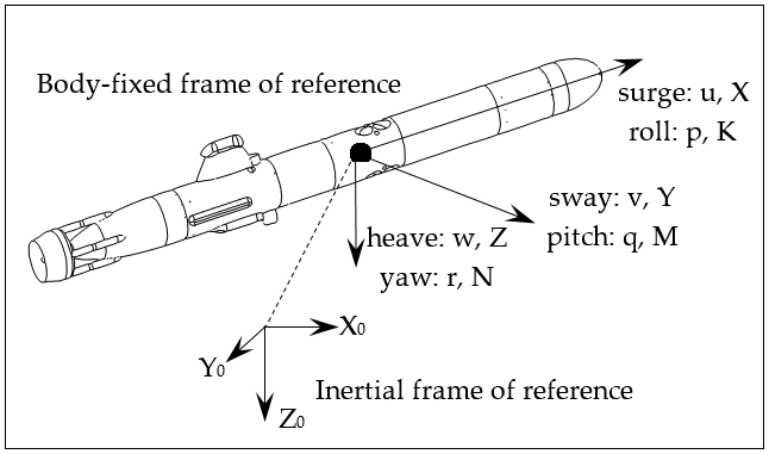

Figure 3.4 – Inertial and body-fixed frames of reference. The origin of the body-fixed coordinate system was at the centre of buoyancy of the vehicle (marked by the filled circle).

3.2.3.1. AUV Simulation Model

The motion simulation model of the Gavia AUV was developed to reproduce the vehicle's linear velocities in a calm water environment in response to the time series of the control commands. This included the propeller RPM command which was a direct input into the simulator. In order to simplify and reduce the associated uncertainties, the time series of pitch angle (Θ), pitch rate (q), pitch acceleration ($\dot{q}$), yaw rate (r) and yaw acceleration ($\dot{r}$) values recorded during the physical runs (i.e., measured by the gyroscopic sensors within the INS) were given as inputs to the simulator instead of providing the associated control surface angle commands. This simplification avoided the requirement of determining the control surface forces and moments, and using them to derive the rolling, pitching and yawing motions as the actual vehicle attributes were provided as inputs to the simulator. Therefore, the mathematical model was able to be limited to a 3-DOF (i.e., linear motions along the x, y, and z directions), thereby eliminating the requirement to model the angular motions of the vehicle.

The simulation model was developed using MATLAB Simulink software (developed by Mathworks, Massachusetts, USA) by modelling the rigid body dynamics and hydrodynamics

of the vehicle in accordance with Fossen (2011) for AUV dynamics and Prestero (2001) for the simulation model. The 6-DOF motion of an underwater vehicle can be described using the equations of motion given in Equation (3.2) in the vectorial form (Fossen, 2011).

$$M\dot{\vec{\nu}} + C(\vec{\nu})\vec{\nu} + D(\vec{\nu})\vec{\nu} + g(\vec{\eta}) = \tau_{control} \tag{3.2}$$

where, M is the system inertia matrix, $C(\vec{\nu})$ is the Coriolis-centripetal matrix, $D(\vec{\nu})$ is the damping matrix, $g(\vec{\eta})$ is the vector of the gravitational/buoyancy forces and moments, $\tau_{control}$ is the vector of propulsion, control surface forces, and moments, $\vec{\nu}$ is the velocity vector (i.e., [*u*, *v*, *w*, *p*, *q*, *r*] where p, q, and r are the angular velocities around the *x*, *y*, and *z* axes), and $\vec{\eta}$ is the vector of position/Euler angles (i.e., [*x*, *y*, *z*, φ, θ, ψ] where φ, θ and ψ are the roll, pitch, and yaw angles respectively). *M* and $C(\vec{\nu})$ are further expanded in Equations (3.3) and (3.4), where, M_{RB} and $C_{RB}(\vec{\nu})$ are the rigid body force components of *M* and $C(\vec{\nu})$ matrices, while M_A and $C_A(\vec{\nu})$ are their added mass components.

$$M = M_{RB} + M_A \tag{3.3}$$

$$C(\vec{\nu}) = C_{RB}(\vec{\nu}) + C_A(\vec{\nu}) \tag{3.4}$$

The 6-DOF force and moment matrices that appear in Equation (3.2) are given in Fossen (2011) in their full form. In this study, Equation (3.2) has been reduced to 3 DOF (i.e., to equations of motion in *x*, *y* and *z* directions) and simplified assuming the products of inertia (i.e., I_{xy}, I_{xz} and I_{yz}) are zero since they are negligibly small compared to the moments of inertia (i.e., I_{xx}, I_{yy}, and I_{zz}) of the vehicle (Prestero, 2001). Equations (3.5)–(3.7) represent the expanded forms of Equation (3.2) in the respective directions of *x*, *y*, and *z*. The left-hand sides of the equations demonstrate the rigid body dynamics and added mass terms while the right-hand sides show the hydrostatic, hydrodynamic damping and control forces (Prestero, 2001). The hydrodynamic coefficients are non-dimensionalised according to prime-system I notation (Fossen, 1994) using 2.7 m as the vehicle length (*L*), 1000 kg m^{-3} as the fresh water density, and 2 m s^{-1} as the prescribed forward speed (*U*) . The notation of the hydrodynamic coefficients presented in the equations below follow SNAME (1952). For example, $X_{u|u|}$ is the partial derivative of the surge force (*X*) with respect to the square of the surge speed ($u|u|$); i.e., $X_{u|u|} = \partial X / \partial(u|u|)$. $X'_{u|u|}$ represents the non-dimensionalised coefficient.

$$\frac{\rho}{2}L^3\left[\left(\frac{2}{\rho L^3}m-X'_{\dot{u}}\right)\dot{u}\right]+mz_g\dot{q}-my_g\dot{r}=-(W-B)\sin(\theta)+\frac{\rho L^2}{2U}\left[X'_{uuu}u^3\right]+\frac{\rho}{2}L^2\left[X'_{u|u|}u\,|u|\right]+$$
$$\frac{\rho}{2}L^2U\left[X'_u u\right]+\frac{\rho}{2}L^3\left[\left(X'_{wq}-\frac{2}{\rho L^3}m\right)wq+\left(X'_{vr}+\frac{2}{\rho L^3}m\right)vr\right]+X_n\times RPM^2 \tag{3.5}$$

$$\frac{\rho}{2}L^3\left(\frac{2}{\rho L^3}m-Y'_{\dot{v}}\right)\dot{v}-mz_g\dot{p}+\frac{\rho}{2}L^4\left(\frac{2}{\rho L^4}mx_g-Y'_{\dot{r}}\right)\dot{r}=+\frac{\rho}{2}L^2\left[Y'_{v|v|}v\,|v|\right]+$$
$$\frac{\rho}{2}L^2U\left[Y'_v v\right]+\frac{\rho}{2}L^3U\left[Y'_p p\right]+\frac{\rho}{2}L^3U\left[Y'_q q\right]+\frac{\rho}{2}L^3U\left[Y'_r r\right] \tag{3.6}$$

$$\frac{\rho}{2}L^3\left[\left(\frac{2}{\rho L^3}m-Z'_{\dot{w}}\right)\dot{w}\right]+my_g\dot{p}-\frac{\rho}{2}L^4\left[\left(\frac{2}{\rho L^4}mx_g+Z'_{\dot{q}}\right)\dot{q}\right]=(W-B)\cos(\theta)+$$
$$\frac{\rho}{2}L^2\left[Z'_{w|w|}w\,|w|\right]+\frac{\rho}{2}L^2U\left[Z'_w w\right]+\frac{\rho}{2}L^3U\left[Z'_p p\right]+\frac{\rho}{2}L^3U\left[Z'_q q\right]+\frac{\rho}{2}L^3U\left[Z'_r r\right] \tag{3.7}$$

where RPM is the vehicle's propeller revolutions per minute and X_n is the thrust coefficient, which is 95×10^{-6} for the Gavia AUV according to the estimation by Thorgilsson (2006).

Equations (3.5) – (3.7) were rearranged and parameterised to the forms given in Equations (3.8) – (3.10) in order to calculate the instantaneous linear accelerations of the AUV in *x*, *y*, and *z* directions, where α' β', and γ' are unknown parameters to be identified using system identification. The physical properties of the AUV, such as the mass, positive buoyancy force, and distances to the vehicle centre of gravity, were superimposed within the parameters, eliminating the requirement to measure them.

$$\dot{u}-X_n RPM^2=\alpha'_1\left[\frac{2}{\rho L^3}\sin(\theta)\right]+\alpha'_2\left[\frac{1}{UL}u^3\right]+\alpha'_3\left[\frac{1}{L}u\,|u|\right]+$$
$$\alpha'_4\left[\frac{U}{L}u\right]+\alpha'_5\left[wq\right]+\alpha'_6\left[vr\right]+\alpha'_7\left[\frac{2}{\rho L^3}\dot{q}\right]+\alpha'_8\left[\frac{2}{\rho L^3}\dot{r}\right] \tag{3.8}$$

$$\dot{v}=\beta'_1\left[\frac{1}{L}v\,|v|\right]+\beta'_2\left[\frac{U}{L}v\right]+\beta'_3\left[Up\right]+\beta'_4\left[Uq\right]+\beta'_5\left[Ur\right]+\beta'_6\left[\frac{2}{\rho L^3}\dot{p}\right]+\beta'_7\left[L\dot{r}\right] \tag{3.9}$$

$$\dot{w}=\gamma'_1\left[\frac{2}{\rho L^3}\cos(\theta)\right]+\gamma'_2\left[\frac{1}{L}w\,|w|\right]+\gamma'_3\left[\frac{U}{L}w\right]+$$
$$\gamma'_4\left[Up\right]+\gamma'_5\left[Uq\right]+\gamma'_6\left[Ur\right]+\gamma'_7\left[\frac{2}{\rho L^3}\dot{p}\right]+\gamma'_8\left[L\dot{q}\right] \tag{3.10}$$

As shown in the simulation model flowchart given in Figure 3.5, the instantaneous linear acceleration components of the current time-step is solved using the recorded input parameters

(i.e., propeller RPM, θ, q, r, $\dot{q}$, and $\dot{r}$) corresponding to the current time-step and linear vehicle velocities of the previous time-step. The calculated accelerations are then integrated with respect to time to obtain the linear velocity components in the body-fixed reference frame (i.e., u, v, and w), which is the key objective of the simulation model. These velocity components are also used as the input velocities for the future time-step.

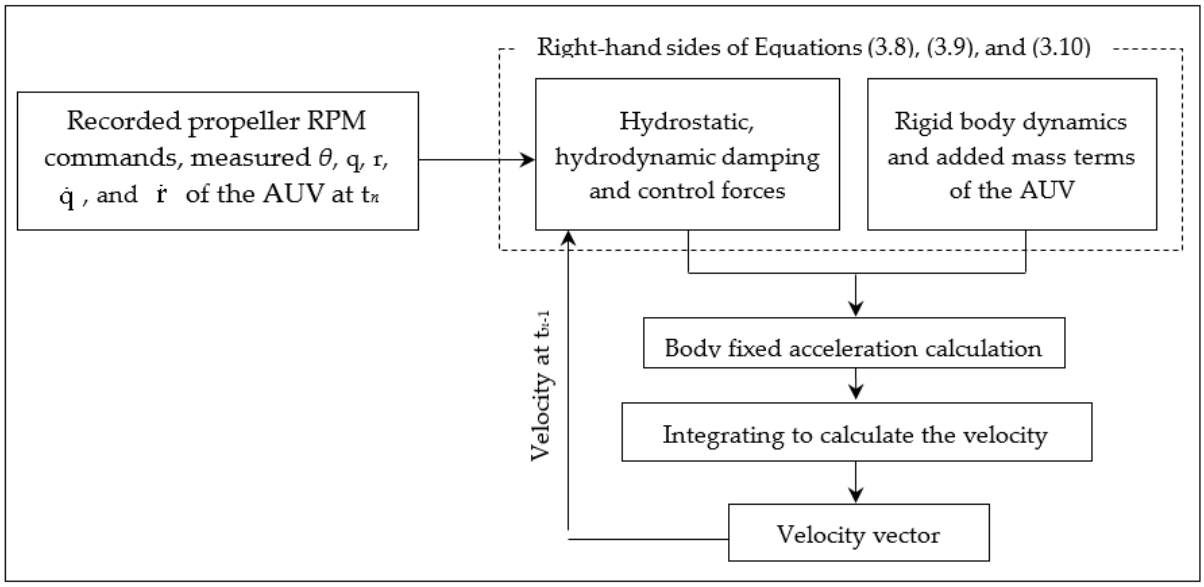

Figure 3.5 – Simulation model flowchart. The acceleration vector of the current time-step is solved using the velocity vector from the previous time-step and commanded propeller RPM while θ, q, r, $\dot{q}$, and $\dot{r}$ are subsequently replaced with the values recorded during field tests. The body-fixed velocity vector was obtained by integrating the acceleration vector with respect to time.

3.2.3.2. System Identification

The simulation model requires an accurate representation of the associated system parameters to precisely predict the motion of the AUV. Identification of the parameters was conducted in the MATLAB Simulink environment using the recursive least squares estimation block set of the MATLAB System Identification toolbox, which utilises the theoretical approach outlined in Ljung (1999). Equations (3.8) – (3.10) were modified to the format given in Equation (3.11):

$$y_{(t)} = H_{(t)}\Theta_{(t)} \tag{3.11}$$

where, $y_{(t)}$, $H_{(t)}$ and $\Theta_{(t)}$ vectors are as defined in Table 3.2 for models in x, y, and z directions.

Table 3.2 – $y_{(t)}$, $H_{(t)}$ and $\Theta_{(t)}$ vectors of Equation (11) for *x*, *y*, and *z* directions.

***x* Direction**	***y* Direction**	***z* Direction**
$y_{(t)} = \dot{u} - X_n RPM^2$	$y_{(t)} = \dot{v}$	$y_{(t)} = \dot{w}$
$H_{(t)} = \left[\frac{2}{\rho L^3}\sin(\theta) \quad \frac{1}{L}u\lvert u\rvert \quad wq \quad vr \quad Lq^2 \quad Lr^2 \quad \frac{2}{\rho L^3}\dot{q} \right]$	$H_{(t)} = \left[\frac{2}{\rho L^3}qr \quad \frac{1}{L}v\lvert v\rvert \quad \frac{1}{L}uv \quad ur \quad Lr\lvert r\rvert \quad L\dot{r} \right]$	$H_{(t)} = \left[\frac{2}{\rho L^3}\cos(\theta) \quad \frac{1}{L}w\lvert w\rvert \quad \frac{1}{L}uw \quad uq \quad Lq\lvert q\rvert \quad L\dot{q} \right]$
$\Theta_{(t)} = \left[\alpha_1' \quad \alpha_2' \quad \alpha_3' \quad \alpha_4' \quad \alpha_5' \quad \alpha_6' \quad \alpha_7' \right]$	$\Theta_{(t)} = \left[\beta_1' \quad \beta_2' \quad \beta_3' \quad \beta_4' \quad \beta_5' \quad \beta_6' \right]$	$\Theta_{(t)} = \left[\gamma_1' \quad \gamma_2' \quad \gamma_3' \quad \gamma_4' \quad \gamma_5' \quad \gamma_6' \right]$

The unknown parameter vectors (i.e., $\Theta_{(t)}$) were estimated by running the recursive least squares algorithm for the time series motion response data of zig-zag and straight-line manoeuvres conducted at Lake Trevallyn (further information regarding the utilised recursive squares technique could be obtained from Ljung (1999)). The values of the identified parameters given in Table 3.3.

The utilised system identification technique is a simple and robust method to determine the mathematical model parameters of a modular AUV, but it has limitations to estimate values for individual hydrodynamic derivatives as several coefficients and vehicle physical properties are overlaid within each parameter. System identification, in general, also has the risk of providing non-physical values for the parameters, limiting the applicability of the parameters to the propeller RPM range, pitch and yaw angle range of the identification manoeuvres. However, similar to most other AUV mapping missions, the AUV is prescribed to run in straight-line paths in the WVAM method, thus requiring the simulations to be conducted generally for straight-line and small pitch and yaw angle (generally below around 8°) manoeuvres, where the hydrodynamic coefficients are within the linear range (Wolkerstorfer, 1995). The identified parameters obtained from system identification were sufficient for the WVAM method and were verified by simulating a secondary set of manoeuvres conducted in the calm water environment. The results of the verification study are presented in Section 3.3 below.

Table 3.3 – Values of the parameters in Equations (3.8) – (3.10)

Parameter	Value	Parameter	Value	Parameter	Value
$\alpha_1' = \frac{-(W-B)}{\left(\frac{2}{\rho L^3}m - X_{\dot{u}}'\right)}$	-2.47×10^4	$\beta_1' = \frac{Y_{v\|v\|}'}{\left(\frac{2}{\rho L^3}m - Y_{\dot{v}}'\right)}$	1.20×10^{-1}	$\gamma_1' = \frac{(W-B)}{\left(\frac{2}{\rho L^3}m - Z_{\dot{w}}'\right)}$	1.53×10^1
$\alpha_2' = \frac{X_{uuu}'}{\left(\frac{2}{\rho L^3}m - X_{\dot{u}}'\right)}$	-4.64×10^1	$\beta_2' = \frac{Y_v'}{\left(\frac{2}{\rho L^3}m - Y_{\dot{v}}'\right)}$	-4.91×10^{-2}	$\gamma_2' = \frac{Z_{w\|w\|}'}{\left(\frac{2}{\rho L^3}m - Z_{\dot{w}}'\right)}$	-3.72×10^{-2}
$\alpha_3' = \frac{X_{u\|u\|}'}{\left(\frac{2}{\rho L^3}m - X_{\dot{u}}'\right)}$	6.02×10^1	$\beta_3' = \frac{Y_p'}{\left(\frac{2}{\rho L^3}m - Y_{\dot{v}}'\right)}$	4.32×10^{-4}	$\gamma_3' = \frac{Z_w'}{\left(\frac{2}{\rho L^3}m - Z_{\dot{w}}'\right)}$	-4.69×10^{-2}
$\alpha_4' = \frac{X_u'}{\left(\frac{2}{\rho L^3}m - X_{\dot{u}}'\right)}$	-4.42×10^1	$\beta_4' = \frac{Y_q'}{\left(\frac{2}{\rho L^3}m - Y_{\dot{v}}'\right)}$	-3.97×10^{-5}	$\gamma_4' = \frac{Z_p'}{\left(\frac{2}{\rho L^3}m - Z_{\dot{w}}'\right)}$	3.50×10^{-4}
$\alpha_5' = \frac{\left(X_{wq}' - \frac{2}{\rho L^3}m\right)}{\left(\frac{2}{\rho L^3}m - X_{\dot{u}}'\right)}$	-7.11	$\beta_5' = \frac{Y_r'}{\left(\frac{2}{\rho L^3}m - Y_{\dot{v}}'\right)}$	3.78×10^{-4}	$\gamma_5' = \frac{Z_q'}{\left(\frac{2}{\rho L^3}m - Z_{\dot{w}}'\right)}$	-5.26×10^{-4}
$\alpha_6' = \frac{\left(X_{vr}' + \frac{2}{\rho L^3}m\right)}{\left(\frac{2}{\rho L^3}m - X_{\dot{u}}'\right)}$	-1.35×10^1	$\beta_6' = \frac{mz_g}{\left(\frac{2}{\rho L^3}m - Y_{\dot{v}}'\right)}$	2.84×10^1	$\gamma_6' = \frac{Z_r'}{\left(\frac{2}{\rho L^3}m - Z_{\dot{w}}'\right)}$	5.34×10^{-5}
$\alpha_7' = \frac{-mz_g}{\left(\frac{2}{\rho L^3}m - X_{\dot{u}}'\right)}$	-8.94×10^2	$\beta_6' = \frac{-\left(\frac{2}{\rho L^4}mx_g - Y_r'\right)}{\left(\frac{2}{\rho L^3}m - Y_{\dot{v}}'\right)}$	4.93×10^{-3}	$\gamma_7' = \frac{-my_g}{\left(\frac{2}{\rho L^3}m - Z_{\dot{w}}'\right)}$	0.00×10^1
$\alpha_8' = \frac{my_g}{\left(\frac{2}{\rho L^3}m - X_{\dot{u}}'\right)}$	5.21×10^3			$\gamma_8' = \frac{\left(\frac{2}{\rho L^4}mx_g + Z_q'\right)}{\left(\frac{2}{\rho L^3}m - Z_{\dot{w}}'\right)}$	-2.17×10^{-3}

The utilised system identification technique is a simple and robust method to determine the mathematical model parameters of a modular AUV, but it has limitations to estimate values for individual hydrodynamic derivatives as several coefficients and vehicle physical properties are overlaid within each parameter. System identification, in general, also has the risk of providing non-physical values for the parameters, limiting the applicability of the parameters to the propeller RPM range, pitch and yaw angle range of the identification manoeuvres. However, similar to most other AUV mapping missions, the AUV is prescribed to run in straight-line paths in the WVAM method, thus requiring the simulations to be conducted generally for straight-line and small pitch and yaw angle (generally below around 8°) manoeuvres, where the hydrodynamic coefficients are within the linear range (Wolkerstorfer,

1995). The identified parameters obtained from system identification were sufficient for the WVAM method and were verified by simulating a secondary set of manoeuvres conducted in the calm water environment.

3.3. Assessment

3.3.1. Validation of the WVAM Method

The WVAM method was validated by comparing the calculated velocity components of the water column with velocity observations obtained with the on-board ADCP. Out of the three straight-line runs conducted at the Batman Bridge site, the one with the largest discrepancy with the ADCP results is presented in Figure 3.6. The vehicle path was aligned with the predominant tidal flow direction during this run.

Figure 3.6a compares the vertical velocity response of the AUV (i.e., the velocity component of the AUV in the *z* direction—w) observed in the turbulent environment (i.e., the Batman Bridge site) with the response obtained from the simulation model representing the calm water. During the experiments, the vertical velocity of the AUV was determined using the DVL aided INS. Since there are no flow variations in the calm water condition, there is no external forcing on the vehicle. Therefore, the velocity responses from calm and turbulent water surroundings vary from each other. As given in Equation (3.1), the difference between the two vertical velocity responses provides the vertical water velocity variation along the AUV track at the Batman Bridge site. The horizontal water velocity components in *x* and *y* directions were obtained by comparing the vehicle's measured and simulated surge and sway speed responses, respectively.

Figure 3.6b – 3.6d compares the WVAM estimates and ADCP measured water velocity components in the *x*, *y*, and *z* directions, respectively. The ADCP results were smoothed using a moving average filter using a backward scheme with a frame size of six time-steps. The filtered flow velocity components from the first bin of upward and downward looking transducers (i.e., 0.44 m away from the vehicle) were averaged together and taken as the ADCP measurements for the comparison.

The difference between velocities obtained from the WVAM method and the ADCP were calculated by quantifying the standard deviation between the two. The standard deviations of the velocity components in *x*, *y*, and *z* directions were 0.09 m s^{-1}, 0.07 m s^{-1}, and 0.06 m s^{-1}, respectively. The maximum error velocity of the ADCP vertical flow measurements estimated

with the redundant transducer was ±0.10 m s^{-1} and Fong and Jones (2006) indicated that the velocity measurements taken from an AUV-fixed ADCP typically has an uncertainty margin of ±0.1 m s^{-1}. Thus, the standard deviation of the WVAM method results are within the uncertainty margin of ADCP measurements for the *x* and *z* directions. The WVAM method provides the water column velocities at the vehicle while the ADCP velocity measurements are the averaged values of the first bins of the upward and downward looking transducers. The WVAM method was further validated by comparing the velocity measured by a stationary upward-looking ADCP moored to the seabed as discussed in Section 3.4.1.

Since the vehicle was moving against the predominant tidal flow direction, a negative water velocity along the *x* direction is seen in Figure 3.6b (positive water velocities were observed when the AUV was running with the flow direction as a result of the inverted body-fixed coordinate system). The best replica between the WVAM and ADCP velocities is noticed in the vertical velocity component. The largest mismatches in velocities along *y* and *z* directions are seen at the peaks. The estimated hydrodynamic coefficients of the simulation model using the system identification method could be less accurate for large angles of incidence of the vehicle, where the hydrodynamic forces and moments are in their nonlinear ranges. Therefore, as the yaw and pitch angle fluctuations become larger, the accuracy of the simulation model decreases; adversely affecting the WVAM velocity prediction (Randeni et al., 2016). The disparity at peaks of the velocity components is due to the hydrodynamic coefficients exceeding their linear ranges causing a reduction in the accuracy of the simulation model. Although the peak discrepancy is negligible for the tested runs, it is critical to ensure that the vehicle motion response remains within the applicable range of the hydrodynamic coefficients in order to use the WVAM method. The nonlinear hydrodynamic coefficients of an AUV could be obtained more accurately using techniques such as captive model experiments and computational fluid dynamics simulations (Randeni et al., 2015b, Phillips, 2010).

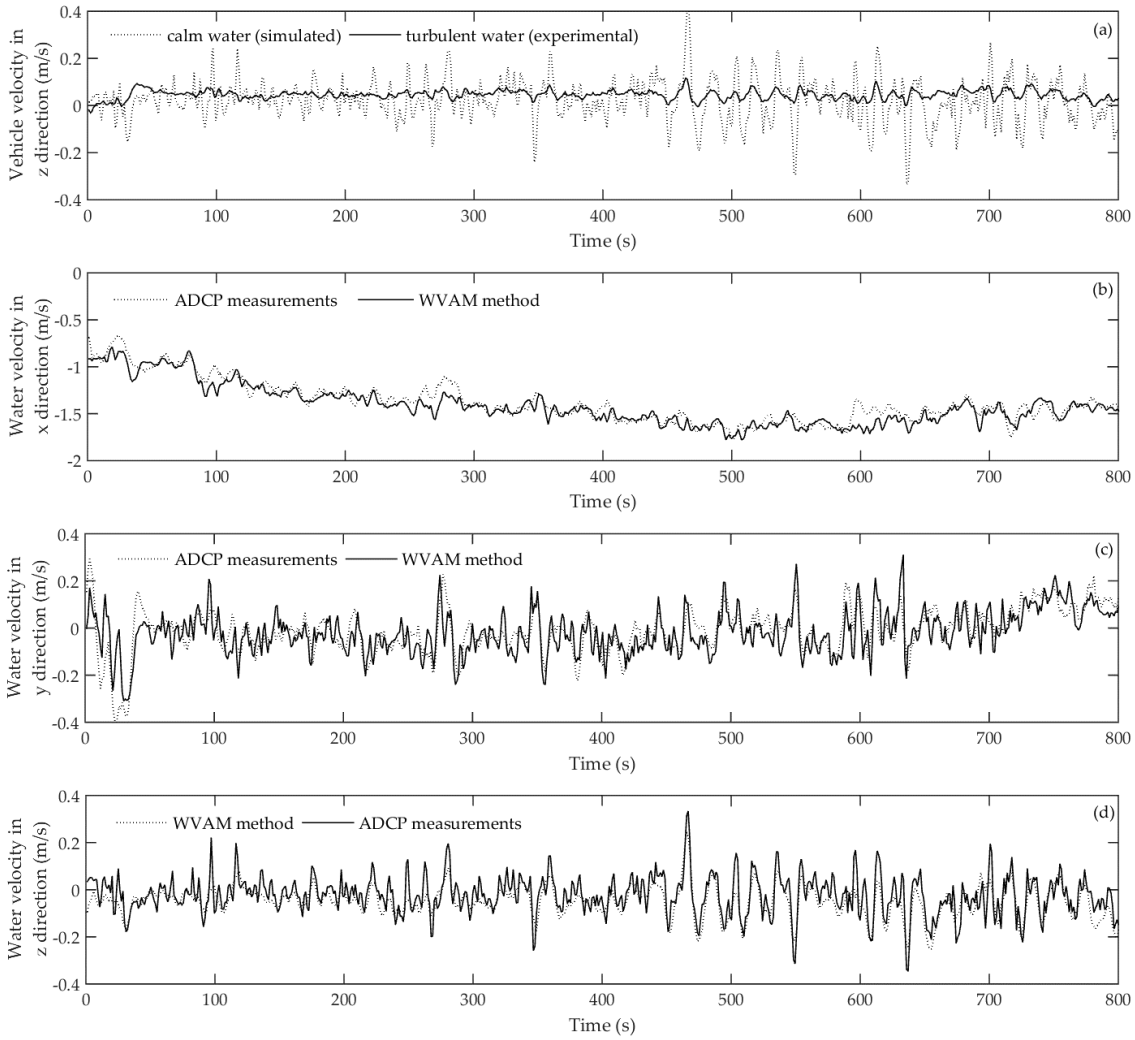

Figure 3.6 – (a) The vertical velocity of the vehicle observed in the turbulent (experimental) and calm (simulated) water environments. The difference between the two responses provides the velocity of the water column in the z direction. The comparison between the velocity components of the water column in *x*, *y* and *z* axes (panels (b), (c), and (d), respectively) was calculated using the WVAM method and those obtained from the ADCP measurements smoothed with a moving average filter.

3.3.2. Verification of the WVAM Method

The validation study discussed above demonstrates that the WVAM method is compatible with experimental measurements and could be used to calculate water column velocities in the vicinity of an AUV within the ADCP blanking distance. To gain further confidence, a verification study was conducted to identify the uncertainty margins of the results obtained from this method. The analysis was based on computing the error margins of individual steps, and adding them to obtain the total ambiguity.

The hydrodynamic coefficients of the Gavia AUV for the simulation model were identified by running the recursive least squares algorithm for the time series motion response data collected from the calm water environment at Lake Trevallyn. The uncertainty present in the identified coefficients may affect the water column velocity calculations and therefore it was necessary to quantify the ambiguity of the WVAM method. The performance of the determined coefficients was examined by applying them to the simulation model and simulating a different set of manoeuvres conducted at the Lake Trevallyn site. The AUV runs used for model estimation were not used for this verification process guaranteeing an unbiased verification. The accuracy of the identified coefficients was quantified by computing the standard deviation between the simulated and actual vehicle velocities in *x*, *y*, and *z* axes, which were 0.010 m s^{-1}, 0.005 m s^{-1}, and 0.002 m s^{-1}, respectively.

During the field tests at the Lake Trevallyn site (i.e., a calm water environment), the on-board ADCP showed minor variations of the water column velocities, with averaged values in the surge, sway and heave directions of less than 0.05 m s^{-1}. These minor water velocities indicate a calm water environment. Nevertheless, there is a minor contribution towards the ambiguity of the results from the WVAM method. Therefore, these velocity components were included in the final uncertainty calculation.

During the experiments, the velocities of the AUV over ground and the pitch and yaw rates were measured using the INS, which was aided with the velocity over ground measurements from the DVL bottom-tracking mode. The uncertainties associated with the DVL aided INS influence the calm water simulation results, as well as the measurements taken in the turbulent environment. These uncertainties were incorporated twice when calculating the total uncertainty margin of the WVAM method. The uncertainty of the DVL aided Kearfott T24 INS in measuring the speeds over ground is ±0.05 m s^{-1} (Hildebrandt and Hilljegerdes, 2010). The respective uncertainties of the INS in providing the pitch and yaw rates of the AUV are $\pm 7.96 \times 10^{-5}$ rad s^{-1} and $\pm 1.60 \times 10^{-4}$ rad s^{-1}.

The total uncertainty margin of the WVAM method was determined by adding the individual error components as discussed above and shown in Table 3.4. Using these values it can be determined that the WVAM method is able to provide velocity components of a turbulent water column in *x*, *y*, and *z* axes with respective uncertainty margins of ±0.160 m s^{-1}, ±0.155 m s^{-1}, and ±0.152 m s^{-1}. In comparison, the uncertainty margins of an ADCP mounted

on an AUV and a stationary ADCP in measuring water column velocities is around ±0.1 m s^{-1} and ±0.002 m s^{-1}, respectively, for velocity components in the *x*, *y*, and *z* directions.

Table 3.4 – Uncertainty margin of the WVAM method was determined by adding the individual error components of each step.

Uncertainty Components	Uncertainties Along		
	***x* Direction**	***y* Direction**	***z* Direction**
Due to hydrodynamic coefficients	±0.010 m s^{-1}	±0.005 m s^{-1}	±0.002 m s^{-1}
Due to the turbulence present in the calm water environment	±0.05 m s^{-1}	±0.05 m s^{-1}	±0.05 m s^{-1}
Due to sensor errors	±0.100 m s^{-1}	±0.100 m s^{-1}	±0.100 m s^{-1}
Total uncertainty of the WVAM method	±0.160 m s^{-1}	±0.155 m s^{-1}	±0.152 m s^{-1}

3.4. Discussion

3.4.1. Accuracy with the Distance from the AUV

The ADCP captures the water velocity components at each bin up to a distance of 10 m away from the AUV, whereas the WVAM method returns only a single estimate of flow velocity at, or near, the AUV. The reason for this is because the WVAM method measures the water column velocities by comparing the hydrodynamic forces acting on the vehicle, and these forces arise from the near AUV flow field. For example, the standard deviation between the ADCP and WVAM vertical water velocities at 0.5 m away from the AUV was 0.06 m s^{-1} and it increased up to 0.15 m s^{-1} at 9.5 m away from the vehicle. In turbulent environments, velocity fluctuations are typically larger and it is unlikely to have a single velocity value for a range of 10m. Figure 3.7 illustrates the variation of the difference between ADCP and WVAM vertical water velocity magnitudes with the vertical distance from the AUV. A good correlation with variations less than around 0.08 m s^{-1} is seen until a vertical distance of around 4 m. Beyond 4 m, the difference increases up to around 0.3 m s^{-1}; that is, the water column velocity pattern changes significantly compared to 0 – 4 m as a result of the seawater and fresh water mixing in the estuary. This shows that the WVAM method can be considered as accurate only in the vicinity of the vehicle.

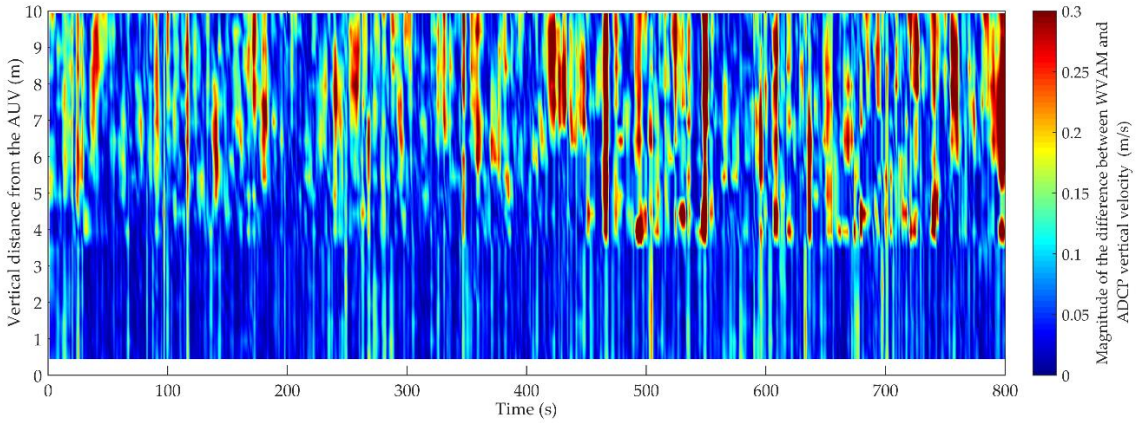

Figure 3.7 – The variation of the difference between ADCP and WVAM vertical water velocity magnitudes with the vertical distance from the AUV.

Both the WVAM and vehicle on-board ADCP measurements use the same Earth referenced AUV velocities. Therefore, in order to further validate the WVAM method Randeni et al. (2016) compared the WVAM estimations with those obtained from a stationary ADCP moored to the seabed. When the AUV was flying over the location of the stationary ADCP, it maintained an altitude of 11 m; hence, the ADCP water column velocities recorded from the bins at 11 m altitude were used for the comparison. The investigation was conducted using the same Gavia AUV at the same test location where the current study was carried out (i.e., Tamar estuary near the Batman Bridge) and the horizontal water column velocity recorded by the stationary ADCP was around 0.7 m s^{-1}. A good agreement between the two was observed with differences of 0.05 m s^{-1}, 0.08 m s^{-1}, and 0.01 m s^{-1} for the respective velocity components in the *x*, *y*, and *z* directions, further validating the WVAM method's ability to estimate flow velocities near, or at, the AUV and that the accuracy is independent of the vehicle velocities.

3.4.2. Length Scale of the WVAM Velocity Measurements

During the AUV field tests in the Tamar estuary, the motion response data of the vehicle were recorded at a rate of 0.87 Hz while the vehicle was travelling at an average forward speed of approximately 1.8 m s^{-1}. Hence, the data sampling distance was around 2.1 m (i.e., there was a horizontal distance of 2.1 m in between each data point). Therefore, the WVAM method neglects the velocity variations with length scales smaller than the data sampling distance. Also, the WVAM method assumes that the velocity components along the *y* and *z* axes are acting uniformly along the length of the AUV; i.e., the WVAM method estimates the mean velocity variation along the length of the AUV. Therefore, the smallest measurable length scale of the velocity variations in *y* and *z* axes is the data sampling distance or the length of the AUV,

whichever is greater. In this case, the length of the AUV is approximately 2.7 m. However, the length scale of the velocity variations in the *x* axis is limited only by the data sampling distance. Hayes and Morison (2002) estimated the vertical water velocity in the upper ocean by applying a Kalman filter to the AUV motion data. They reduced the measurement length scale down to half the AUV length by incorporating the phenomenon of pitching of the vehicle across a horizontal gradient of the vertical water velocity.

3.5. Recommendations

The WVAM method can be improved to capture the water velocity variations with length scales smaller than 2.7 m by overcoming the two limiting factors; i.e., the length of the AUV and the data sampling distance. The latter can be addressed by increasing the data sampling rate. Additionally, the scale restriction caused by the length of the AUV has to be resolved by identifying the variations of water velocities along the length of the AUV. This can be achieved by incorporating the difference between the vehicle angles of attack observed in the turbulent environment and that obtained from the calm water simulation model (i.e., pitch angle difference for vertical water velocity gradient and the yaw angle for the horizontal gradient). The WVAM method can be further improved by incorporating a more accurate representation of the linear and nonlinear hydrodynamic coefficients determined using techniques such as the captive model experiments and computational fluid dynamics simulations (Randeni et al., 2015b, Phillips, 2010). The accuracy of the WVAM method reduces in time periods where the AUV glides through the water column when the current is either accelerating or decelerating. Further improvements to the model to calculate the gliding effect of the AUV due to accelerating/decelerating water columns could improve the performance of the WVAM method.

Autonomous underwater gliders utilise a similar approach to determine the vertical water column velocities using the model predicted vertical velocity of the glider and the observed vertical velocity from the pressure sensor. The WVAM method can be adopted for such platforms to estimate the horizontal water column velocities by calculating difference between the model predicted horizontal position and the actual position from the GPS (i.e., when the glider comes to the surface).

3.6. Conclusions

This study presents the WVAM method to estimate the flow velocity components of a turbulent water column, relative to the Earth, in *x*, *y*, and *z* axes of the AUV body-fixed coordinate system using the motion response of the vehicle. The water column velocities were determined by calculating the difference between the motion responses of the AUV observed in calm and turbulent water column conditions. The motion of the vehicle in the calm water environment was obtained by simulating the control commands executed during the field experiments conducted in the turbulent condition with a mathematical model that represents the calm water. The simulation model was developed within MATLAB Simulink and the associated hydrodynamic coefficients of the AUV were obtained using a recursive least squares system identification method.

The estimated water column velocity components in *x*, *y*, and *z* direction agreed well with the measurements from the AUV's on-board ADCP with standard deviations of 0.09 m s^{-1}, 0.07 m s^{-1}, and 0.06 m s^{-1} for the respective components. These standard differences were well within the uncertainty margin of the ADCP results. WVAM velocity estimates were also compared with a bottom-mounted stationary ADCP data obtained while the AUV was flying over the stationary ADCP. Both datasets show good agreement with velocity differences of approximately 0.05 m s^{-1}, 0.08 m s^{-1}, and 0.01 m s^{-1} for the respective velocity components. An uncertainty analysis showed that the WVAM method estimates the respective velocity components within of ±0.16 m s^{-1}, ±0.16 m s^{-1}, and ±0.15 m s^{-1}. The advantage of the proposed method is to determine velocity components closer to the vehicle where standard ADCPs are incapable of capturing the flow velocities due to their blanking distance or if they are unavailable in the scientific payload. Estimating vertical and horizontal velocities around the boundary layer of the AUV is important to fill the blanking distance gap within a water column velocity profile, which is required for flow field characterisation.

Chapter 4: Feasibility of WVAM method for AUV localisation error counteraction

Chapter 4 is based on the journal article '*Autonomous Underwater Vehicle motion response: A non-acoustic tool for blue water navigation*' published in the '*Marine Technology Society Journal*'. The citation for the article is:

Randeni SAT, Forrest AL, Cossu R, Leong ZQ, King PD, Ranmuthugala D. Autonomous Underwater Vehicle Motion Response: A Non-acoustic Tool for Blue Water Navigation. Marine Technology Society Journal. 2016;50:17-26.

Chapter 4 has been removed for copyright or proprietary reasons.

Chapter 5: Counteracting AUV localisation error when operating beyond the range of bottom-tracking sonar

This chapter is based on the journal article '*Counteracting Autonomous Underwater Vehicle (AUV) localisation error as a precursor for blue water navigation*' that is submitted for publication in the '*IEEE Journal of Oceanic Engineering'*. This article is in review at the time of writing. The citation for the article is:

Randeni SAT, Forrest AL, Leong ZQ, Cossu R, Ranmuthugala D, King PD and Schmidt V. Counteracting Autonomous Underwater Vehicle (AUV) localisation error as a precursor for blue water navigation. IEEE Journal of Oceanic Engineering. *In review*.

Abstract

This study proposes a novel localisation technique for an Autonomous Underwater Vehicle (AUV) in the descent phase of a mission in water depths greater than the range of bottom-tracking Doppler Velocity Log (DVL) sonar. The proposed technique is based on a mathematical model-aided Inertial Navigation System (INS). The main components of the proposed technique is an Outlier Rejection (OR) filter, which removes the outliers present within the INS acceleration measurements and a flow profile estimator that determines the water column velocity profile along the AUV descent track relative to the ground. The flow profile estimator is a combination of the WVAM method and a forward and backward flow profile smoothing algorithm. The proposed localisation technique is tested using a *Gavia*-class AUV for six short diving missions conducted in a high energy river estuary with strong tidal currents. The performance of the proposed technique is evaluated in comparison to the localisations solutions from DVL bottom-track aided, DVL water-track aided, conventional model-aided and unaided INS. The proposed technique provides the highest correlation with DVL bottom-track aided localisation solution with a maximum positioning uncertainty of 5.5% of the distance travelled and a minimum of 1.1%, where the uncertainties of other non-bottom-tracking localisation methods are more than twice this. The proposed technique is most advantageous when the AUV was operating in environments with large water column velocities, where the uncertainty of conventional non-bottom-tracking localisation methods are in the orders of 10% to 35% of the distance travelled. The vehicle velocity solution from the proposed technique can also be used for navigation and control systems of AUVs when bottom-track is unavailable.

5.1. Introduction

Autonomous Underwater Vehicles (AUVs) are increasingly being recognised as a robust technology for a wide range of scientific, commercial and military applications in part, because they are decoupled from surface motions (Forrest et al., 2012, Forrest et al., 2008, Kimura et al., 2016). Accurate vehicle navigation; i.e., guiding the vehicle from one point to another, and localisation; i.e., awareness of its own position within the three dimensional domain, are crucial requirements in carrying out AUV missions successfully and effectively (Paull et al., 2014). For instance, when an AUV is conducting a bathymetric survey, precise navigation and localisation is critical to accurately geolocate the sampled data and to cover the target survey area (Randeni et al., 2016).

One of the key methods to localise and navigate AUVs is the use of an Inertial Navigation System (INS). Linear and angular accelerations of the vehicle measured by the INS using its Inertial Measurement Unit (IMU) are integrated to determine the velocity and position of the vehicle respectively (Panish and Taylor, 2011). During this process, the uncertainties within the IMU measurements are also integrated; creating an unbounded drift in the INS position estimate with time. To counteract this drift, true position and/or velocity measurements of the AUV are fed back into the INS localisation solution through the use of a predictor-corrector model such as a Kalman filter (Medagoda et al., 2010). True position measurements can be delivered using Global Positioning System (GPS) fixes while at surface and true velocity over ground measurements from bottom-tracking Doppler Velocity Logs (DVLs) are commonly used for INS aiding while underwater. The acoustic transmissions of DVLs are limited in terms of the frequency specific penetration through the water column. For example, a 300 kHz DVL has a maximum range of around 200 m from the instrument and the range of a 1200 kHz DVL is around 15-25 m (Randeni et al., 2017a). Therefore, DVL aiding is unavailable when the vehicle-to-seabed distance (i.e., altitude) is larger than the range of the DVL.

Blue water operations of AUVs often include long descents in the mid-water column without DVL bottom-track (Jalving et al., 2003). During such descents, the localisation error will increase rapidly if the INS is operating in its free inertial mode (i.e., unaided INS). Therefore, at altitudes larger than the DVL range, the INS is aided with the velocity of the AUV relative to the water column provided by the water-tracking mode of the DVL (Hegrenaes and Berglund, 2009). However, the DVL water-tracking mode assumes the movements of the water column relative to the bottom is negligible; hence, it is inaccurate in environments with

stronger underwater currents and is prone to position drifts (Medagoda et al., 2016). Once the AUV is at a depth relative to the seabed where it has acquired the DVL bottom-lock, the accuracy of the INS localisation solution will be maintained for the subsequent time steps. The positioning error that occurred during the descent phase prior to bottom-lock being achieved will remain as a steady state offset error to the geolocation of the data for the entire mission (Randeni et al., 2016). One of the solutions for this would be to deliver true position updates of the vehicle using acoustic transceivers to correct the INS drift. However, acoustic transceivers have disadvantages such as limited range, complexity and logistical difficulties; hence, they are less preferred, especially for deep water offshore applications; i.e., blue water operations (Jalving et al., 2003). Medagoda et al. (2016) proposed a mid-water column ADCP aided localisation technique using the correlation between bins of a descending ADCP as they pass through the same layers to restrain drift, with the assumption of near constant current profile layer velocities over short time periods.

Mathematical model based AUV motion response prediction systems have been recently introduced for INS aiding; i.e., a model-aided INS (Hegrenaes et al., 2008, Randeni et al., 2017b). One of the major advantages of model-aided localisation is that it does not require additional sensors beyond a typical AUV navigational payload and could be simply established with a modification to vehicle firmware. Such models characterise the hydrodynamic, hydrostatic and mass properties of the vehicle. For example, Yan et al. (2012) developed a model-aided INS using recursive identification for emergency navigation of AUVs when the DVL malfunctions. Hegrenaes and Hallingstad (2011) introduced a model-aided INS, including a Kalman Filter based sea current estimation technique for a *HUGIN 4500* class AUV to be used when DVL aiding is unavailable. The velocities of the sea currents are calculated within the navigation system Kalman filter by using the model velocities that are relative to the water column and INS measurements relative to the inertial space. While these are two excellent examples, the majority of models exclude environmental forces due to currents; i.e., parameters within the model represent the characteristics of the AUV in a calm operational environment. The estimated sea currents could be less accurate in high current environments due to erroneous INS velocity measurements; since a pre error filtering technique is not utilised. For all these reasons, the vehicle velocities predicted with a mathematical model-aided INS are inaccurate in strong non-uniform currents.

To address this, a mathematical model, together with a calibration technique, was previously introduced by Randeni et al. (2017b) to field calibrate the base-line model

parameters for diverse operational environments by identifying the true local environmental conditions and external forces acting on the vehicle. One of the advantages of this model was that it allows for changes in the vehicle configuration (Randeni et al., 2017b). Field calibration is conducted by running a Recursive Least Squares (RLS) based optimisation algorithm for the absolute motion response and control command data of an AUV run conducted in the anticipated field. The field calibrated model has proven capable of successfully aiding the INS position in low energy environments with flow velocities of around 0.2 m s^{-1}; however, its accuracy is limited when an AUV descends through a high energy environments with strong non-uniform currents.

This work presents an AUV localisation technique based on a mathematical model-aided INS to be used for AUVs diving in blue water without DVL bottom-track. Inputs to the algorithm are vehicle control commands and unaided acceleration measurements from the INS. The key components of the proposed technique is an Outlier Rejection (OR) filter, which removes the outliers present within the INS acceleration measurements and a flow profile estimator that determines the water column velocity profile along the AUV descent track relative to the ground. The flow profile estimator is a combination of the WVAM method (Randeni et al., 2015a, Randeni et al., 2017a) and a forward and backward flow profile smoothing algorithm. Using a *Gavia*-class AUV, the technique was tested for six short AUV descents conducted in a high energy river estuary with strong tidal currents. The localisation accuracy of the proposed technique is analysed, assuming the DVL bottom-track aided solution as the baseline measurement. The performance is evaluated in comparison to other conventional non-bottom-tracking localisation systems; i.e., DVL water-track aided, conventional mathematical model-aided and unaided. After demonstrating that the newly developed model produces better results than conventional non-bottom-tracking solutions, the implications for future blue water navigation work is discussed.

5.2. Field experimental setup

5.2.1. AUV setup

The proposed localisation technique was tested and validated using the unprocessed INS, DVL, Acoustic Doppler Current Profiler (ADCP) and pressure sensor data collected from a *Gavia*-class AUV (Forrest et al., 2012). Due to high modularity of the AUV, the vehicle configuration can be changed by changing the modules for any given deployment purpose,

which will alter the hydrodynamic, hydrostatic and mass properties of the vehicle. The vehicle in the tested configuration (see Figure 5.1) consisted of a Nose Cone Module, Battery Module, Geoswath Interferometric Sonar Module, 1200 kHz Teledyne RD Instruments ADCP / DVL Module, Kearfott T24 INS (KI-4902S model) Module, Control Module, and a Propulsion Module. The vehicle had a length of 2.7 m, a diameter of 0.2 m, and a dry weight in air of approximately 70 kg. The propulsion module was a three bladed ducted propeller system with four individually functioning control surfaces arranged in an 'X' configuration.

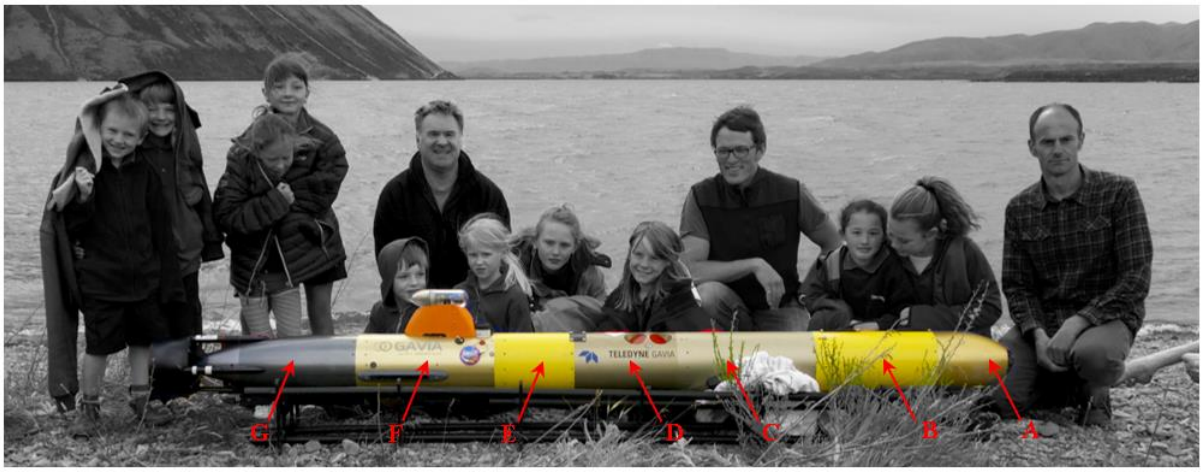

Figure 5.1 – Omarama Primary School students inspecting the utilised *Gavia* AUV. Configuration of the vehicle – (A) Nose Cone Module, (B) Battery Module, (C) Geoswath Module, (D) ADCP/DVL Module, (E) INS Module, (F) Control Module and (G) Propulsion Module.

The position and velocity estimation accuracies of the DVL aided Kearfott T24 INS, 1200 kHz Teledyne RD Instruments DVL and Keller Series 33Xe pressure sensor are given in Table 5.1. During field tests, the INS data were recorded in the vehicle log at a frequency of 25 Hz, DVL measurements at 0.5 Hz and other sensor measurements at the vehicle sampling frequency of 0.87 Hz.

Table 5.1 – Specifications of Gavia AUV sensor packages. "CEP" for Circular Error Probable and "RMS" for Root Mean Squared.

Sensor package	Measurements	Measurement accuracy
DVL bottom-track aided Kearfott T24 INS	Position estimate	0.1% of the distance travelled (CEP)
	Heading angle	±0.010° (RMS)
	Pitch angle	±0.005° (RMS)
1200 kHz Teledyne RDI DVL bottom – tracking mode	Velocity	±0.004 m s^{-1} (RMS) or 0.2% of the velocity
	Maximum range	30 m
	Minimum range	0.5 m
Keller Series 33Xe pressure sensor	Vehicle depth	0.1% of the depth

5.2.2. Test sites and experimental runs

Field tests were carried out in Tamar estuary, Tasmania, Australia – a high energy system with the water column velocities varying with the tidal cycle; see Figure 5.2. The test site was selected for the experimental runs to analyse the performance of the proposed localisation technique in comparison to other methods in different water column conditions.

Six short AUV diving missions (i.e., Mission 1 to Mission 6) were conducted in Tamar estuary near the Batman Bridge (Figure 5.2) on 14th and 15th of June, 2014. As a result of the main channel at this location being relatively narrow and shallow, the flow is constricted and typically exhibits strong tidal currents and water level fluctuations at different periods of the tidal cycle (Green et al., 2016). The six diving missions were conducted at different time periods of the tidal cycle in order to analyse the performance of the proposed localisation technique in different flow conditions. Missions 1-2 were conducted during slack water and Missions 3-4 and 5-6 were carried out at partially and fully developed tide conditions with strong tidal currents. Table 5.2 presents the average water column velocity of the site (i.e., measured with the vehicle on-board ADCP), the depth and duration of each diving mission. The flow conditions varied from 0.08 m s^{-1} to 0.86 m s^{-1}. Short diving missions were conducted so that the DVL bottom-track was available for the entire descent, facilitating the ability to analyse the performance of the proposed technique. All diving missions were conducted at a constant propeller Revolutions per Minute (RPM) of 700; i.e., a surge speed of around 2 m s^{-1} in calm water.

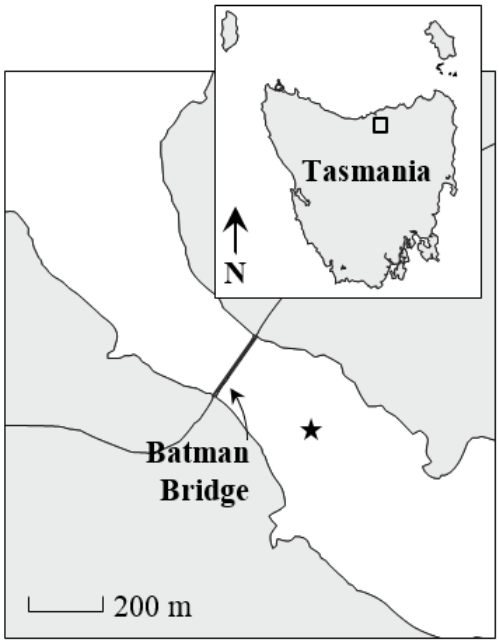

Figure 5.2 –Tamar estuary experimental field site near the Batman Bridge was located in Tasmania, Australia (inset). AUV diving missions were conducted at the location indicated with filled star.

Table 5.2 – Each mission's descent depth, time taken for the descent and the average of the water column velocity measured using the ADCP of the vehicle

Mission	Descend depth (m)	Descend time (s)	Average flow velocity (m s^{-1})
Mission 1	20	28	0.08
Mission 2	28	51	0.10
Mission 3	22	31	0.30
Mission 4	22	30	0.51
Mission 5	27	45	0.71
Mission 6	31	61	0.86

5.3. Methodology

5.3.1. Motion response predicting mathematical model

The mathematical model of the *Gavia* AUV was developed to estimate the vehicle's three-dimensional (3D) linear velocities relative to the water column in response to the time series of the control commands. The control commands included the propeller RPM commands,

and pitch angle (θ), pitch rate (q), pitch acceleration ($\dot{q}$), yaw rate (r) and yaw acceleration ($\dot{r}$) values recorded during the physical runs (i.e., measured by the gyroscopic sensors within the INS). The simulation model was developed within MATLAB Simulink environment by modelling the rigid body dynamics, hydrodynamics and hydrostatic properties of the AUV according to Randeni et al. (2017b) and Randeni et al. (2017a), which follows the theoretical aspects described by Fossen (2002).

The acceleration vectors of the current time step in the *x*, *y* and *z* directions were calculated with equations (5.1), (5.2) and (5.3) respectively using the controlling commands (i.e., the time stamps of propeller RPM_t, p_t, $\dot{p}_t$, q_t, $\dot{q}_t$, r_t and $\dot{r}_t$) of the vehicle and the linear velocity vector from the previous time step; i.e., $u_{(t-1)}$, $v_{(t-1)}$ and $w_{(t-1)}$. The calculated acceleration vector is then integrated with respect to the time in order to obtain the velocity vector of the current time step in the body-fixed reference frame. This process is repeated with a time step of 0.0001 s for the entire mission time. The selected time step is large enough to maintain a low computational time and small enough to converge the velocity solution between two control command sampling intervals.

$$\dot{u}_t = \alpha_1 \dot{r}_t + \alpha_2 \dot{q}_t + \alpha_3 \sin(\theta_t) + \alpha_4 u_{(t-1)}{}^3 + \alpha_5 u_{(t-1)} \left|u_{(t-1)}\right| + \alpha_6 u_{(t-1)} + \alpha_7 w_{(t-1)} q_t + \alpha_8 v_{(t-1)} r_t + X_n \times RPM_t{}^2 \tag{5.1}$$

$$\dot{v}_t = \beta_1 \dot{r}_t + \beta_2 \dot{p}_t + \beta_3 v_{(t-1)} \left|v_{(t-1)}\right| + \beta_4 v_{(t-1)} + \beta_5 p_t + \beta_6 q_t + \beta_7 r_t \tag{5.2}$$

$$\dot{w}_t = \gamma_1 \dot{q}_t + \gamma_2 w_{(t-1)} \left|w_{(t-1)}\right| + \gamma_3 w_{(t-1)} + \gamma_4 q_t + \gamma_5 r_t + \gamma_6 \tag{5.3}$$

where, *u*, *v*, *w* and *p*, *q*, *r* are the linear and angular velocities around the *x*, *y* and *z* axes of the AUV. Θ is the pitch angle, RPM is the vehicle's propeller revolutions per minute and X_n is the thrust coefficient, which is 95×10^{-6} for the *Gavia* AUV according to the estimation by Thorgilsson (2006). The thrust coefficient is only valid for the propeller speed range from 450 RPM to 975 RPM. $\alpha_1, \alpha_2 \ldots \alpha_8$, $\beta_1, \beta_2 \ldots \beta_7$ and $\gamma_1, \gamma_2 \ldots \gamma_6$ are parameters that characterise the hydrodynamic, hydrostatic and mass properties of the AUV, and the values for the utilised *Gavia* AUV are given in Table 5.3. Derivation of equations (5.1), (5.2) and (5.3), and identification of the parameters are given in Randeni et al. (2017b).

Table 5.3 – numerical values of the *Gavia* AUV's parameters

Parameter	value		Parameter	value		Parameter	value
α_1	0.5294		α_8	-13.5405		β_7	0.0008
α_2	0.0909		β_1	0.0133		γ_1	-0.0059
α_3	-2.5098		β_2	0.0029		γ_2	-0.0138
α_4	-8.5937		β_3	0.0444		γ_3	-0.0347
α_5	-22.3129		β_4	-0.0364		γ_4	-0.0011
α_6	-32.7171		β_5	0.0005		γ_5	0.0001
α_7	-7.1061		β_6	-0.0001		γ_6	0.0016

5.3.2. Conventional mathematical model-aided INS

The mathematical model (i.e., Block (1) of the proposed localisation technique flow chart illustrated in Figure 5.3) determines the velocities of the AUV relative to the water column in response to the provided control commands. Since the mathematical model predicts the vehicle velocities relative to the water column, the motion of the water column with respect to the ground could cause a disparity between the model predicted velocities in comparison to actual ground relative velocities. However, the INS measures the vehicle accelerations relative to the inertial space (i.e., with respect to the ground).

Conventional model-aided INS methods blend the model predicted velocities and INS acceleration measurements using a Kalman filter data fusion algorithm. A complimentary blending between the two can assist each other by avoiding the accumulation of INS instrumental errors as well as by reducing the mathematical model velocity drift due to water column velocities. Since the two measurements are relative to two different reference frames and the quantity desired is the vehicle velocity with respect to the ground, the ground relative INS measurements should have a higher weight in the fusion algorithm. INS acceleration measurements generally can contain outliers originated from sensor noise, temporary sensor failures, unanticipated environmental disturbances, etc. Due to these outlier measurements, the performance of the Kalman filter data fusion algorithm could be reduced (Ting et al., 2007, Wadehn et al., 2016, Hu et al., 2011), especially if there is a considerable difference between the two fusing measurements. That is, the conventional model-aided INS localisation solution could be inaccurate in environments with large underwater currents.

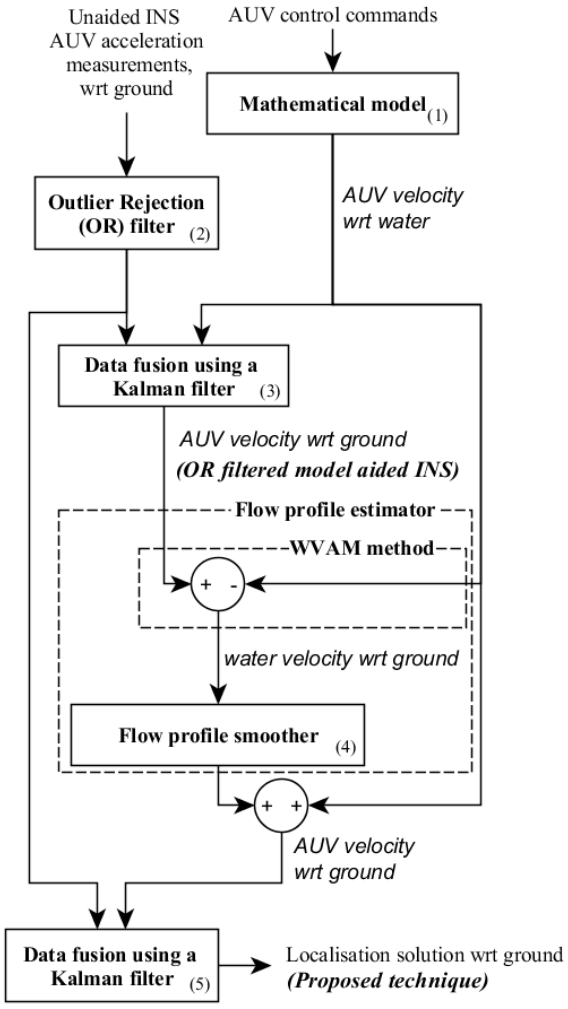

Figure 5.3 – Flowchart of the proposed technique of estimating the absolute position of the AUV using unaided INS acceleration measurements and AUV control commands. wrt stands for 'with respect to'.

5.3.3. Outlier Rejection (OR) filter

To overcome this, the proposed method utilises a simple OR filter (i.e., Block (2) of Figure 5.3) to clean the INS outlier measurements prior to the data fusion. The OR filter evaluates the reasonableness of the difference between two immediate INS acceleration measurements in *x* and *y* directions; that is, the variation of the acceleration within 0.04 seconds. If the difference exceeds a pre-set threshold value; the measurement of that time stamp is considered as erroneous and the time step is neglected. That is, no change in vehicle acceleration will be assumed during that time step.

The threshold value primarily depends on the performance of the vehicle control system; i.e., the ability to maintain the vehicle in the set constant velocities. For a straight line, constant

speed and constant depth mission, the tested *Gavia* AUV had an average acceleration fluctuation of 0.025 m s^{-2} between two consecutive time steps for both *u* and *v* (measured from the DVL bottom-track aided INS). The maximum fluctuations were 0.150 m s^{-2} and 0.225 m s^{-2} for the respective acceleration components. The maximum allowed difference for the vehicle velocities between two sampling time steps (i.e., the threshold) was defined as 0.25 m s^{-2}. That is, ten times the average acceleration fluctuation. The computed value ensured that the non-outlier measurements are not filtered out and the selected value was accurate for all tested missions. For the tested missions, the minimum amount of encountered outliers was 2% of the overall time steps and the maximum was 25%. The threshold value is applicable only if the dive is started after the set forward speed is fully developed while at surface. This is generally the common procedure as the flow speed around the control surfaces is required to be well developed in order to acquire the force and moment necessary to dive the AUV.

Outlier filtered INS measurements were aided with the vehicle velocity estimates from the mathematical model using the Kalman filter data fusion algorithm shown in Block (3) of Figure 5.3.

5.3.4. Kalman filter data fusion algorithm

The Kalman filter data fusion algorithm was developed using the MATLAB Kalman filter toolbox (Murphy, 2001, Murphy, 1999) to fuse the INS acceleration measurements with the aiding velocity; i.e., with model predicted velocities in Block (3), and estimates from the proposed technique in Block (5) of Figure 5.3. The fusion algorithm was also used to determine DVL bottom-track and water-track aided INS localisation solutions to evaluate the performance of the proposed technique. Only a brief description of the mechanisation equations used for the Kalman filter are provided here and the reader is referred to Farrell (2008) for detailed theoretical information on the Kalman filter's measurement and state prediction solvers.

According to Newton's law of motion, the state vector of the current time step is calculated using previous time step's state vector as given in Equation (5.4).

$$x_{(k)} = Fx_{(k-1)} + w_{(k-1)} \tag{5.4}$$

where, $x_{(k)} = \begin{bmatrix} \dot{u}_{(k)} \\ \dot{v}_{(k)} \\ u_{(k)} \\ v_{(k)} \end{bmatrix}$, $F = \begin{bmatrix} 1 & 0 & 0 & 0 \\ 0 & 1 & 0 & 0 \\ \Delta t & 0 & 1 & 0 \\ 0 & \Delta t & 0 & 1 \end{bmatrix}$

and $w_{(k)}$ is the plant noise matrix, a zero-mean Gaussian white noise matrix of covariance Q with a diagonal structure. The value of Q was empirically established as 1×10^{-8} followed by several data analyses.

The measurement vector is given by Equation (5.5).

$$y_{(k)} = Hx_{(k)} + v_{(k)} \tag{5.5}$$

where, $y_{(k)} = \begin{bmatrix} \dot{u}_{INS(k)} \\ \dot{v}_{INS(k)} \\ u_{aiding(k)} \\ v_{aiding(k)} \end{bmatrix}$, $H = \begin{bmatrix} 1 & 0 & 0 & 0 \\ 0 & 1 & 0 & 0 \\ 0 & 0 & 1 & 0 \\ 0 & 0 & 0 & 1 \end{bmatrix}$

and $v_{(k)}$ is an uncorrelated, zero-mean measurement noise matrix R, a diagonal matrix with the respective measurement variances:

$$R = \begin{bmatrix} \sigma^2_{\text{INS}} & 0 & 0 & 0 \\ 0 & \sigma^2_{\text{INS}} & 0 & 0 \\ 0 & 0 & \sigma^2_{u\ \text{aiding}} & 0 \\ 0 & 0 & 0 & \sigma^2_{v\ \text{aiding}} \end{bmatrix}$$

Equations (5.4) and (5.5) are used as respective state and measurement prediction equations for the Kalman filter. The acceleration and velocity measurements at the beginning of the descent obtained from the GPS aided INS were used as the initial condition of the state vector. $\dot{u}_{INS(k)}$ and $\dot{v}_{INS(k)}$ are INS acceleration measurements along surge and sway directions and σ^2_{INS} is the variance of INS acceleration measurements. $u_{aiding(k)}$ and $v_{aiding(k)}$ are the velocity measurements/estimates used to aid the INS; i.e., either DVL bottom-tracking velocities, DVL water-tracking velocities, model predicted velocities or velocities from the proposed technique. $\sigma^2_{u\ \text{aiding}}$ and $\sigma^2_{v\ \text{aiding}}$ are their respective measurement/estimation variances for u and v.

5.3.5. Flow profile estimator

Flow profile estimator compliments the proposed localisation technique by further refining the localisation solution using known physical properties of the operating water column. According to the WVAM method (Randeni et al., 2015a, Randeni et al., 2017a), the velocity of the surrounding water column can be obtained by computing the difference between velocity of the AUV relative to the bottom and the velocity predicted by a mathematical model relative to the water column as shown in Equation (5.6).

$$\vec{\nu}_{\text{water,ground(t)}} = \vec{\nu}_{\text{AUV,ground(t)}} - \vec{\nu}_{\text{AUV,water(t)}} \tag{5.6}$$

where, $\vec{\nu}_{\text{water,ground(t)}}$ is the linear velocity vector of the surrounding water column (along the *x*, *y* and *z* directions) relative to the earth in the body-fixed coordinate system, $\vec{\nu}_{\text{AUV,ground(t)}}$ is the linear velocity vector of the AUV relative to the earth, preferably measured using the DVL bottom-track aided INS, and $\vec{\nu}_{\text{AUV,water(t)}}$ is the linear velocity vector obtained from the simulation model representing a calm water environment when the control commands recorded during the field tests were simulated. Subscript 't' indicates the time step.

The WVAM method ideally requires the velocity of the AUV relative to the ground from a bottom-tracking DVL (Randeni et al., 2017a), which is unavailable during the mid-water column descent and also is the final goal of this work. As outlined in Algorithm 1, which represents Block (4) of Figure 5.3, the true velocity of the surrounding water column is estimated when the AUV is at the surface (i.e., when $\vec{\nu}_{\text{AUV,ground(t)}}$ can be measured from the GPS) using Equation (5.6) and is set as the initial value, i.e., $\vec{\nu}_{\text{water,ground(0)}}$. After beginning the descent, the vehicle velocity from OR filtered model-aided INS is used as $\vec{\nu}_{\text{AUV,ground(t)}}$; i.e., the vehicle velocities from Block (3). The forward correcting and smoothing loop starts from this point on. If the difference between $\vec{\nu}_{\text{water,ground(t)}}$ and $\vec{\nu}_{\text{water,ground(t–1)}}$ is larger than a pre-defined threshold value, $\vec{\nu}_{\text{water,ground(t)}}$ will be replaced with either $\left[\vec{\nu}_{\text{water,ground(t–1)}} + \text{threshold}\right]$ or $\left[\vec{\nu}_{\text{water,ground(t–1)}} - \text{threshold}\right]$, depending on the sign of the difference (see Algorithm 1). The main purpose of this filter is to remove any erroneous outliers within the flow velocity profile. It also allows to smoothly settle the initial $\vec{\nu}_{\text{water,ground(t)}}$ to the values during the descent phase of

the vehicle, and smooths the flow velocity along the depth profile. This loop continues until the DVL bottom-lock is reached.

Upon reaching the DVL bottom-lock, the true water column velocity is calculated using Equation (5.6) with $\vec{v}_{\text{AUV,ground(t)}}$ from the DVL bottom-track, and is set as the initial value for the back correction, i.e., $\vec{v}_{\text{water,ground(n)}}$ where n is the time step at which the DVL bottom lock is reached. As outlined in Algorithm 1, if the difference between $\vec{v}_{\text{water,ground(t–1)}}$ and $\vec{v}_{\text{water,ground(t)}}$ is larger than the pre-set threshold, $\vec{v}_{\text{water,ground(t–1)}}$ will be replaced with either $\left[\vec{v}_{\text{water,ground(t)}} + \text{threshold}\right]$ or $\left[\vec{v}_{\text{water,ground(t)}} - \text{threshold}\right]$ depending on the sign of the difference. This loop will continue till t = n/2.

The filtered water column velocity profile is considered as valid only if $\vec{v}_{\text{water,ground(n/2)}}$ from forward and back corrections are within the threshold limit. In situations where the water velocity back correction is unsuccessful, the AUV velocity from the OR filtered model-aided INS is used as the final localisation solution. It is required to reach the DVL bottom-lock in order to start the back correction algorithm. Therefore, only the forward correction is to be used to determine the localisation solution during the descent of the AUV. Upon obtaining a DVL bottom-lock, the back correction algorithm will be run to counteract the previously estimated localisation solution.

Algorithm 1 – flow profile smoother

1: determine $\vec{v}_{\text{water,ground(0)}}$ prior to the descend using $\vec{v}_{\text{AUV,ground}}$ from GPS
2: **set** $\vec{v}_{\text{water,ground(0)}}$ as the initial condition for the forward correction
3: **loop** – Begin the descend, start forward correction
4: **if** $\left[\vec{v}_{\text{water,ground(t–1)}} - \vec{v}_{\text{water,ground(t)}}\right]$ > threshold, **then**
5: $\left[\vec{v}_{\text{water,ground(t)}} = \vec{v}_{\text{water,ground(t–1)}}\right]$ + threshold
6: **else if** $\left[\vec{v}_{\text{water,ground(t–1)}} - \vec{v}_{\text{water,ground(t)}}\right]$ < -threshold, **then**
7: $\left[\vec{v}_{\text{water,ground(t)}} = \vec{v}_{\text{water,ground(t–1)}}\right]$ – threshold
8: **end if**
9: t = t + 1
10: **if** DVL bottom-lock is not reached, **then**
11: go to 4
12: **else**

13: **set** t = n
14: **end if**
15: **end loop** – descent complete

16: **loop** – start back correction
17: determine the true $\vec{v}_{water,ground(n)}$ upon DVL bottom-lock
18: **set** $\vec{v}_{water,ground(n)}$ as the initial condition for the back correction
19: **if** $\left[\vec{v}_{water,ground(t)} - \vec{v}_{water,ground(t-1)}\right]$ > threshold, **then**
20: $\left[\vec{v}_{water,ground(t-1)} = \vec{v}_{water,ground(t)}\right]$ + threshold
21: **else if** $\left[\vec{v}_{water,ground(t)} - \vec{v}_{water,ground(t-1)}\right]$ < -threshold, **then**
22: $\left[\vec{v}_{water,ground(t-1)} = \vec{v}_{water,ground(t)}\right]$ – threshold
23: **end if**
24: t = t – 1
25: **if** the simulation has not reached n/2 time step, **then**
26: **go to** 19
27: **end if**
28: **end loop** – back correction complete

The magnitude of the threshold depends on the dive angle and variation of the water column velocity along the depth profile. For the tested missions, the AUV dive angle was around 25º and the depth between two consecutively sampled data points was around 0.03 m. A threshold value of 0.001 m s^{-1} was selected after analysing the flow variation of the deployment site closer to the surface. For five out of six missions, the flow profile smoother was triggered less than 3.8% of the overall time stamps and, for Mission 4, it was 11.5%.

5.3.6. Computation of final localisation solution

The velocity of AUV relative to the ground is computed by adding the model predicted velocities relative to the water column to the velocity of the water column relative to the ground. This provides the velocity of the AUV relative to the ground and is used to aid the OR filtered INS acceleration measurements in Block (5) using a second Kalman filter data fusion algorithm, which computes the final vehicle velocity and localisation solutions from the proposed method.

5.4. Results and discussion

5.4.1. Comparison of vehicle velocity estimations

The velocity measurements from the DVL bottom-track aided INS was considered as the true vehicle velocity measurement as it is the most accurate localisation approach. Figure 5.4 compares the Root Mean Square (RMS) difference of the horizontal vehicle velocity (i.e., the magnitude of *u* and *v*) obtained from each method compared to the DVL bottom-track aided solution for six diving missions. The 'OR filtered model-aided' results represent the outcome from Block (3) of Figure 5.3 while the 'Proposed technique' results are the final localisation solution from Block (5). The average values of the water column velocities measured during each mission using the vehicle ADCP are also given.

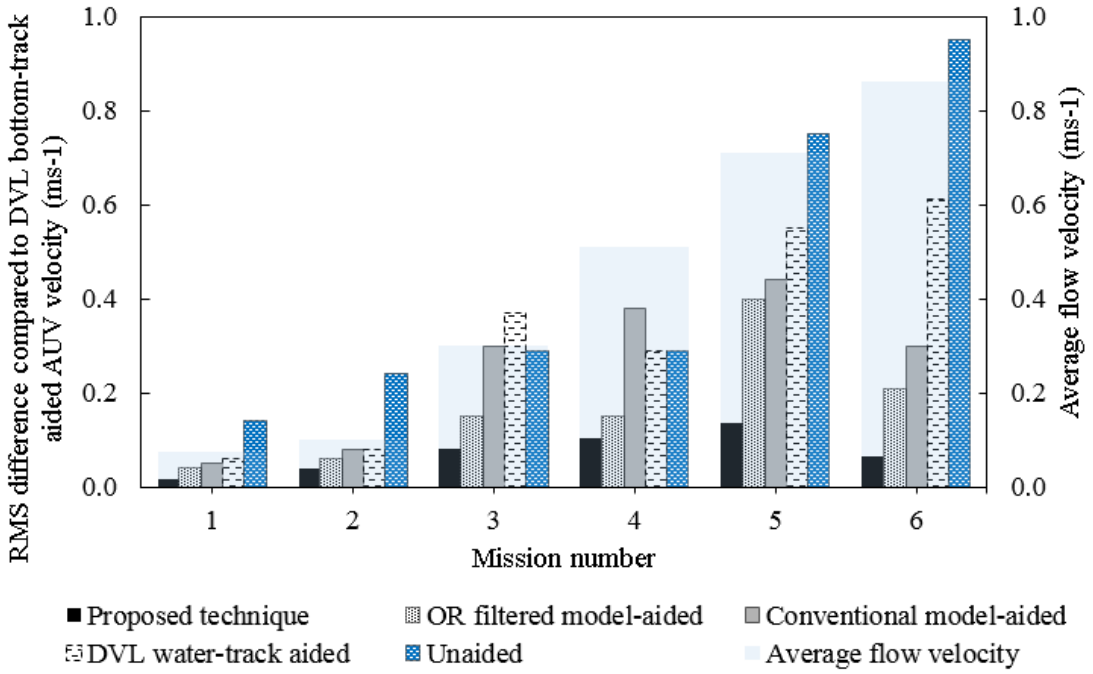

Figure 5.4 – RMS of the vehicle horizontal (i.e., the magnitude of u and v) velocity prediction difference of each method compared to the solution from DVL bottom-track aided INS. The 'OR filtered model-aided' results represent the outcome from Block (3) of Figure 5.3 while the 'Proposed technique' results are the final localisation solution from Block (5).

5.4.1.1. Unaided INS

Integration of uncertainties within raw INS measurements will develop drift in the vehicle velocity and position calculations unless they are corrected with true measurements or realistic estimates (e.g. acoustic fixes). The magnitude of drift of an unaided solution is a function of several factors including the time spent underwater after the last position correction,

and the number of outlier measurements present during the unaided period (Titterton and Weston, 2004). The latter varies with the type of manoeuvre; therefore, the performance of an unaided INS is mission dependant. As shown in Figure 5.4, the maximum RMS difference between the unaided and DVL aided velocities was 0.95 m s^{-1}, observed from Mission 6. Mission 6 had the highest average water column velocity of 0.86 m s^{-1}. The minimum RMS difference of 0.14 m s^{-1} was from the mission with the lowest flow velocity, Mission 1. The general trend was that, the higher the water column velocity, the higher is the velocity prediction uncertainty of the unaided INS (see Figure 5.4).

Figure 5.5a and 5.5b compare the horizontal vehicle velocities from all techniques for two sample missions; i.e., Mission 6 and Mission 5 respectively. The discrepancy between the DVL bottom-track aided and unaided velocity solutions are significantly large and they continue to diverge with time. This verifies that an unaided INS is unreliable for AUV localisation.

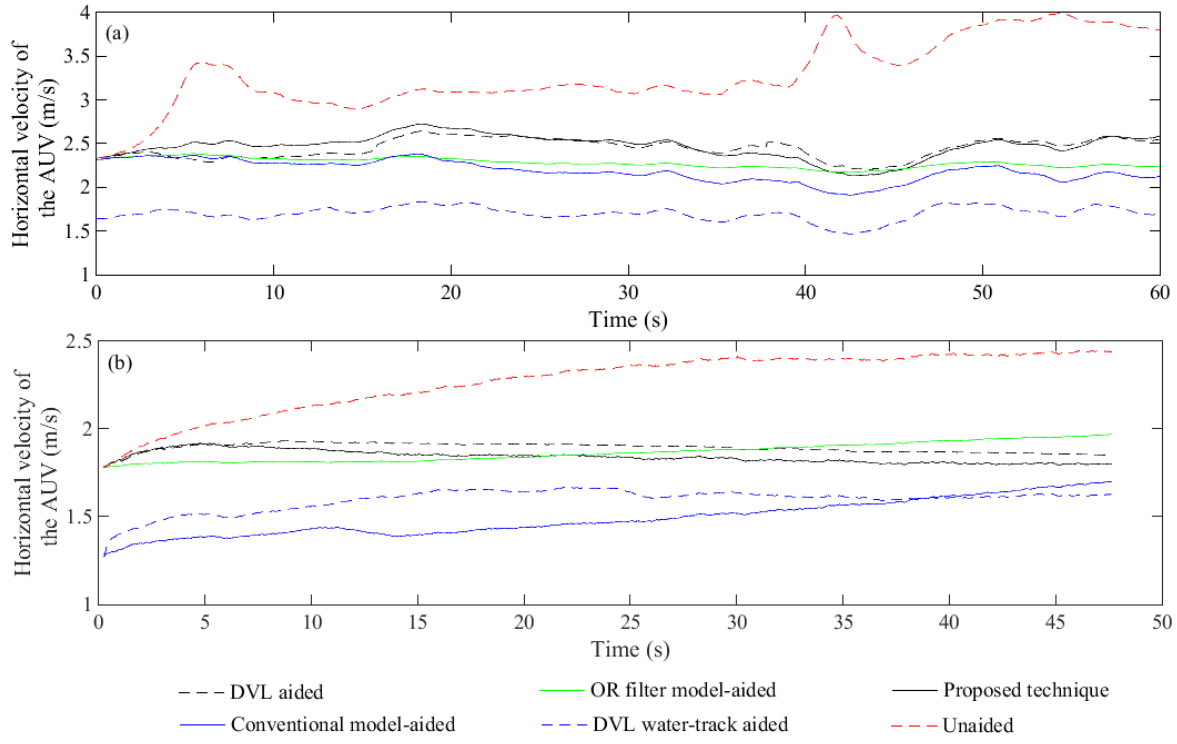

Figure 5.5 – comparison of the horizontal velocities from the proposed technique with other aiding mechanisms for (a) Mission 6 and (b) Mission 5. Velocity calculation from the OR filtered model-aided INS as well as the final estimate are given.

5.4.1.2. DVL water-track aided INS

Majority of the commercial AUVs utilise DVL water-track aided INS as the alternative localisation technique when DVL bottom-track is unavailable (Hegrenaes and Berglund, 2009, Jayasiri et al., 2016, Medagoda et al., 2016), which is determined by fusing the velocity measurements from the DVL water-track mode with raw INS accelerations. The key disadvantage of this method is that the movements of the water column relative to the ground are generally unaccounted for; therefore, it will cause drifts in the vehicle velocity and position estimate. The maximum uncertainty of the DVL water-track aided INS compared to the DVL bottom-track aided INS was recorded from Mission 6 as 0.61 m s^{-1}. The smallest difference of 0.06 m s^{-1} RMS was from Mission 1 that had the slowest moving water column (i.e., an average flow velocity of 0.08 m s^{-1}).

For tested missions, the accuracy of the DVL water-track aided INS velocity prediction is greater than that from the INS in its free inertial mode. When the INS is aided with water-tracked velocity, the data fusion algorithm delivers a compromised solution between the raw INS acceleration measurements relative to the inertial frame, and velocity measurements relative to the water column. This helps to avoid INS error accumulation. Figure 5.5 shows that the water-track aided solution is not as prone to divergence with time as the unaided solution. However, steady offsets in comparison to bottom-track solutions are present due to the movement of the water column.

5.4.1.3. Conventional model-aided INS

The conventional model-aided INS velocity solution was obtained by fusing the raw INS acceleration measurements with the vehicle velocity estimates from the mathematical model. The mathematical model represents the hydrodynamic, hydrostatic and mass properties of the *Gavia* AUV that operates in a calm water environment. Therefore, similar to the DVL water-track mode, the model predicts the vehicle velocities relative to the water column. For this reason, even though the INS measurements are relative to the ground, the aided solution could have a deviation compared to the bottom-track velocity if the velocity of the water column is significant. Furthermore, the outliers in raw INS acceleration measurements degrade the output of the aided solution, creating an error. For the tested missions, the largest discrepancy of 0.44 m s^{-1} was observed from Mission 5, the mission that had the second largest average water column velocity of 0.71 m s^{-1} (see Figure 5.4). The best correlation was for the mission with the lowest flow speed.

The accuracy of the velocities from the conventional model-aided INS was better than the DVL water-track aided INS for five out of six tested missions. The DVL water-track mode measures the velocity of the AUV relative to the particles suspended within the water column that moves with the fluid. Therefore, due to entrained air bubbles in the flow, water-track velocity measurements are prone to outliers and erroneous readings, especially in turbulent environments. Furthermore, they are likely to suffer from outages and instrument re-initialisations where the INS is run in its free inertial mode. In addition, the DVL had a lower measurement sampling frequency of around 2 Hz compared to the mathematical model that processes the vehicle control commands recorded at 25 Hz with a model update frequency of 10^4 Hz. Thereby, the DVL assumes a constant velocity in between measurements while the model provides a continuous variation of the vehicle velocities. All these factors have assisted the model solution to perform better than the DVL water-track mode aided INS.

5.4.1.4. OR filtered model-aided INS

The OR filter was successfully able to improve the model-aided INS velocity prediction by removing outliers within the INS measurements prior to the data fusion. The OR filter was triggered 2% of the number of time steps in Mission 2, which was the minimum outlier occurrence, and the maximum occurrence was 25%, in Mission 6. The minimum vehicle velocity prediction improvement of the OR filtered model-aided INS compared to conventional model-aided solution is 9% (i.e., from Mission 5) and the maximum improvement is 60% (i.e., from Mission 4). The RMS difference compared to DVL bottom-track aided solution is below 0.15 m s^{-1} for four out of six tested missions (see Figure 5.4). This shows that although the amount of outliers is less than 25%, the performance improvement once they are removed is significant.

Figure 5.5 illustrates that velocity predictions from the OR filtered model-aided INS are closely correlated with the DVL bottom-track aided velocities even though minor variations due to water column velocities are not well replicated. The general trend is that the uncertainty is directly proportion to the average velocity of the water column. The AUV velocity prediction accuracy of the OR filtered model-aided INS decreases in environments with large flow speeds.

5.4.1.5. Proposed technique

The water column velocity estimate from the flow profile smoothing algorithm was compared against the measurements from the AUV's on-board ADCP. The flow velocity

components from the first bin of the downward looking ADCP (i.e., 0.44 m away from the vehicle) were taken as the measurements for the comparison. Figure 5.6a and 5.6b present a comparison of the horizontal velocities of the water column (i.e., the magnitude of u_{water} and v_{water}) for two sample missions (i.e., Mission 5 and Mission 4 respectively). The proposed technique well replicated the ADCP measured flow profiles for all the tested missions with a maximum RMS difference of 0.23 m s^{-1} from Mission 5. The best agreement was from Mission 1; i.e., an RMS difference of 0.05 m s^{-1}.

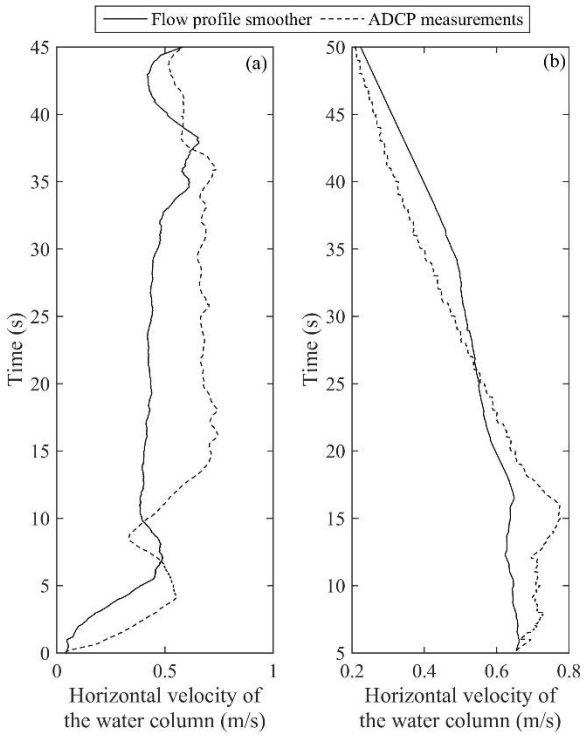

Figure 5.6 – comparison of horizontal water column velocities (i.e., the magnitude of u_{water} and v_{water}) from the proposed flow profile smoother against the ADCP measurements for (a) Mission 5 and (b) Mission 4.

The flow profile smoother was triggered 1.5% of the overall time steps in Mission 2 (i.e., the minimum occurrence) and 11.5% in Mission 6 (i.e., the maximum occurrence). The percentage occurrence was less than 3.8% for five out of six missions.

The final velocity prediction from the proposed localisation technique (i.e., the output from Block (5) of Figure 5.3) provided the best correlation with DVL bottom-track aided velocities for all tested missions (see Figure 5.4). The largest deviation of 0.14 m s^{-1} was from Mission 5 and the lowest of 0.02 m s^{-1} was from Mission 1. The performance of the proposed

technique has improved more than double of that of the conventional methods for the tested short descent missions. Hence, the vehicle velocity estimates from the proposed technique is likely to be able to use for the localisation, navigation and control systems of AUVs when bottom-track is unavailable.

Unlike in DVL water-track and conventional model-aided INS solutions, the proposed technique well replicates the small velocity fluctuations of the AUV. Such fluctuations are mainly initiated and caused by the velocity variations of the surrounding water column. Since the proposed technique accounts for flow velocities, it has been able to perform better than conventional methods. DVL water-track and conventional model-aided INS solutions tend to be unusably inaccurate in high turbulent environments with large water column velocities. However, as illustrated in Figure 5.4, the proposed technique is generally independent of the average velocity of the water column. Therefore, it can be utilised for operational environments with high as well as low flow speeds, although it is most useful when the vehicle is operating in environments with strong non-uniform currents. Furthermore, due to low uncertainty it could be used for long descents conducted in low energy environments.

5.4.2. Comparison of vehicle localisation solutions

Vehicle localisation solutions (i.e., vehicle travel track) from each method were calculated by integrating the relevant vehicle velocities with respect to time. Figure 5.7a and 6.7b illustrates the vehicle tracks from all techniques plotted in a local coordinate system for two sample missions (i.e., Mission 5 and Mission 6 respectively).

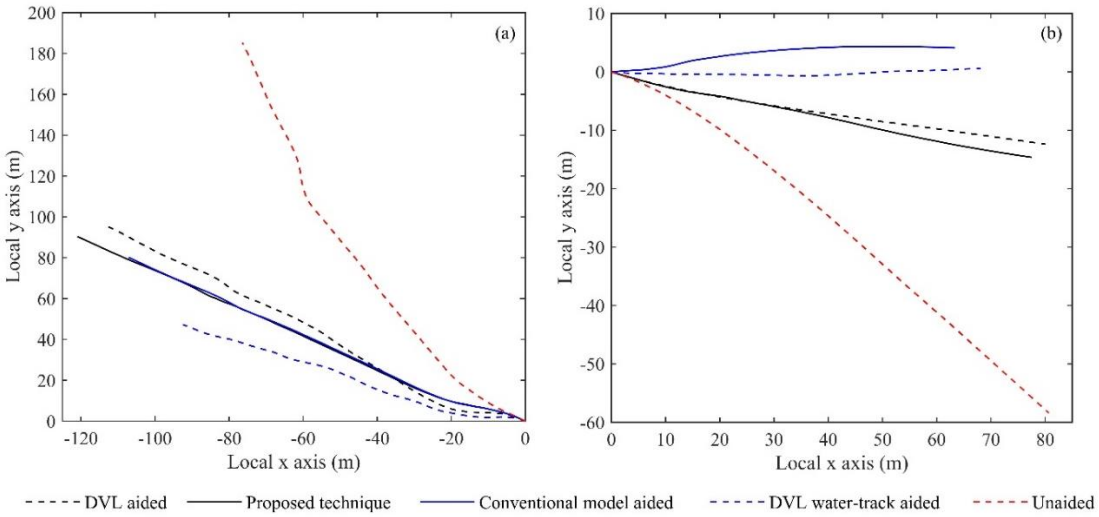

Figure 5.7 – the vehicle localisation solutions of (a) Mission 5 and (b) Mission 6, in a local coordinate system.

As seen from Figure 5.7a and 5.7b, the vehicle track provided by the unaided INS is extremely unreliable in comparison to the DVL bottom-track aided localisation solution. The estimated vehicle position at the end of the manoeuvre has an uncertainty of over 50% of the travelled distance. The performance has increased when the INS is aided with the DVL water-track mode or with the mathematical model; although, the vehicle track diverges with the distance travelled due to integration of drift due to current (see Figure 5.7). The proposed technique provided the highest accuracy with uncertainties less than 5.5% of the distance travelled for both Missions 5 and 6.

Figure 5.8 illustrates the positioning errors at the end of each mission as a percentage of the distance travelled, in comparison to the DVL bottom-track aided INS solution. The average values of the water column velocities measured during each mission using the vehicle ADCP are also given.

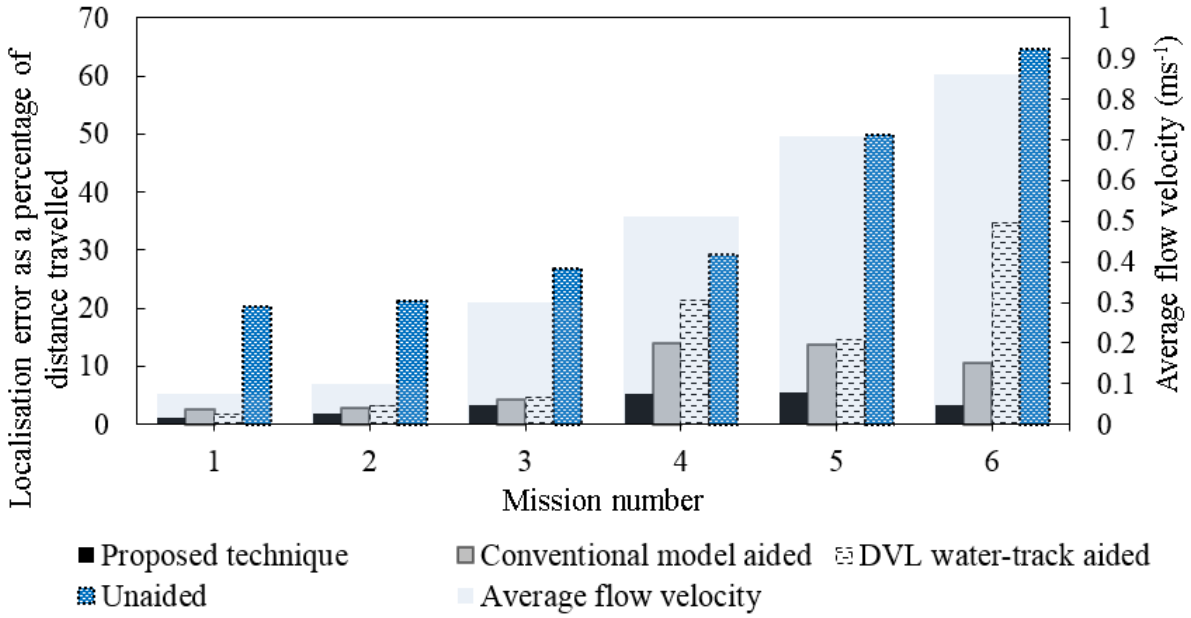

Figure 5.8 – the localisation errors at the end of each mission as a percentage of the distance travelled. The error is determined in comparison to the DVL bottom-track aided INS solution.

For all test cases, the localisation error of the unaided INS is unacceptably large to be used for AUV localisation, navigation and motion control. The general trend is that the uncertainty increases with the average velocity of the surrounding water column.

Localisation solutions from the DVL water-track aided INS is reasonably accurate for operational environments with lower surrounding water column velocities (see Figure 5.8). For instance, the positioning uncertainties at the end of Missions 1 to 3 (where the mean water

column velocities are below 0.1 m s^{-1}) were less than 5% of the distance travelled. However, the uncertainties were above 14% of the distance travelled when the average water column velocity was beyond around 0.4 m s^{-1}, making it an unreliable technique; although, it is the most typically used alternative approach for AUV localisation and navigation when DVL bottom-track is unavailable. The localisation uncertainty of the conventional model-aided INS was less than 5% of the distance travelled when the velocity of the surrounding water column was below 0.1 m s^{-1}. The uncertainty was beyond 10% of the distance travelled when the average water column velocity was more than around 0.4 m s^{-1}.

The proposed localisation technique has provided the most accurate solutions for all tested missions. The largest uncertainty of 5.5% of the distance travelled was observed from Mission 5, where the uncertainties of model-aided and DVL water-track aided INS are 13.7% and 14.6%. The lowest uncertainty of 1.1% of the distance travelled was from Mission 1, which had the smallest average surrounding water column velocity. The ambiguity of the flow profile prediction becomes more significant when the flow speed is larger. As a result, the accuracy of the proposed technique is proportional to the magnitude of the average water column velocity. However, in comparison to other techniques, the accuracy of the proposed technique is relatively consistent, regardless of the water column velocity.

Although the proposed technique performs better than conventional non-bottom-tracking localisation techniques, it is most advantageous when the AUV is operating in environments with large water column velocities. This is because conventional techniques tend to be erroneous in such conditions. Therefore, the proposed technique is beneficial for future AUV deployments of all sizes. One of the key advantages of this technique is that it could be implemented in the AUV with a software update, without additional instruments.

5.5. Limitations and future work

For this study, it was required to compare the vehicle velocity and position estimates from the proposed technique against the DVL bottom-track aided INS solutions. Therefore, the analysis was limited for short vehicle descending missions conducted in water columns that are less than 45 m deep, which was a key limitation. The forward and backward corrector section of the proposed flow profile smoother will perform better for shallower water depths compared to deeper waters. Nevertheless, the performance of the OR filter and the flow profile smoothing sections are independent of the depth of the water column. It is expected to further

test the proposed technique using AUV missions conducted in a deeper water column that has a previously geolocated object on the seabed. Once the AUV has completed its descent, a sonar imaging mission will be conducted above the object. The true position of the vehicle will be determined by calculating the position offset to the object recorded in the sonar images, which will then be used to evaluate the performance of the proposed method.

The accuracy of the flow profile estimator reduces in time periods where the AUV glides through the water column when the current is either accelerating or decelerating. This is a limitation of the WVAM method as stated in Chapter 3. Further improvements to the model to calculate the gliding effect of the AUV due to accelerating/decelerating water columns could improve the performance of the localisation solution in water columns with highly variable water column velocities.

This study was not implemented in the actual AUV to be run in real time. Furthermore, it was limited to determine the position of the vehicle and the improved position estimate was not used for the navigation and control systems of the AUV. Further studies are currently ongoing to develop the algorithm as a Mission Oriented Operating Suite – Interval Programming (MOOS-IvP) application (Benjamin et al., 2010), which will run in a backseat driver computer of the AUV and feed necessary vehicle localisation, navigation and control corrections to the front seat computer. The proposed localisation algorithm was able to process all the longest mission with a 61-second long dataset in less than 1 s utilising an Intel Core i7-4470 3.40 GHz central processing unit. That is, the measurement data can be processed in a rate of around 65 Hz. Real time measurement sampling rate of the AUV is around 25 Hz. Therefore, it is feasible to run the proposed technique is real time in a backseat driver computer.

5.6. Conclusions

This study presents a novel localisation technique for AUVs descending in altitudes larger than the range of the bottom-tracking DVL sonar. A mathematical model of the *Gavia* AUV was developed to determine the velocities of the AUV in response to the control commands, which assumes that the vehicle is operating in a calm water environment. The vehicle velocity estimates from the model were fused with OR filtered INS acceleration measurements to determine the model-aided velocity solution.

The OR filter was successfully able to remove the outliers present in the INS measurements and to improve the model-aided INS velocity prediction. The minimum

percentage improvement of the vehicle velocity prediction compared to conventional model-aided INS was 9% and the maximum improvement was 60%. The proposed flow profile smoother showed a good replication of the water column velocity measurements from the AUV on-board ADCP for all the tested missions with a maximum RMS difference of 0.23 m s^{-1}.

The proposed localisation technique provided the highest correlation with DVL bottom-track aided localisation solution compared to other non-bottom-tracking localisation techniques. The accuracy of the proposed technique was relatively consistent regardless of the water column velocity. Therefore, the technique could be utilised for operational environments with high as well as low flow speeds; although it is most advantageous when the AUV is operating in environments with large water column velocities.

Chapter 6: Summary, conclusions and future work

6.1. Research summary

In achieving the project objective, the literature review had the focus to improve the INS localisation performance when DVL aiding is unavailable. In comparison to other alternatives, model-aided localisation is most suitable for INS drift bounding since it does not require additional sensors beyond a typical AUV navigational payload or shadowing support vessels; unlike for LBL and USBL based localisation. That is, a model-aided INS could be simply established using either modifications to vehicle firmware or using a backseat driver (e.g. using MOOS-IvP). That said, cutting edge model aiding technology needs further improvements to handle the unpredictable environmental conditions.

This thesis establishes a technique to determine the linear and nonlinear parameters of a baseline mathematical model, utilising RLS and PEM based system identification algorithms. The model predicts the velocities of the AUV in response to the vehicle's control commands. The accuracy of the baseline model decreases if the operational environment or the configuration of the vehicle varies from the baseline environmental condition and vehicle configuration (Chapter 2). The model calibration method is introduced to calibrate the parameters within the baseline model to different environmental conditions and vehicle settings by conducting a calibration mission in the new environment. However, the model calibration could fail in flow fields with high spatial variations; for example, when the AUV is descending in a deep water column with strong non-uniform underwater currents that varies with the depth. The calibrated model approach is more suitable for low energy environments with a consistent flow field or to calibrate the model for a different vehicle configuration.

The WVAM method is introduced to measure the velocity of the water column using the AUV motion response (Chapter 3). It is capable of accurately estimating the flow velocity around the AUV within the vehicle boundary layer (e.g. in high energy environments). The performance of the method is evaluated and validated against the measurements from on-board as well as stationary ADCPs in different water column conditions (Chapters 4 and 5). A major drawback of the WVAM method is its requirement of vehicle velocity relative to the ground, which is typically unavailable without DVL bottom-lock.

The WVAM method is further improved in Chapter 5 to determine the water column velocity profile along the descend path of the AUV, diving from the surface to seabed in blue water, without DVL bottom-track. In combination with the model-aided INS, this technique provides an improved positioning accuracy in comparison to existing non-bottom-tracking localisation techniques. Its performance is validated with AUV diving missions conducted in low as well as high energy water column conditions.

A secondary, CFD and EFD based approach is also presented to determine the hydrodynamic parameters of the mathematical model in pre-defined complex flow conditions such as when operating in proximity to the pressure field of another underwater vehicle (Appendix C).

Following sections provide a point by point summary of the outcomes from the overall project.

6.1.1. Traditional non-bottom-tracking AUV localisation techniques

- The unaided INS localisation solutions are extremely unreliable in comparison to DVL bottom-track aided localisation solution. The positioning error ranges from 20% to 60% of the distance travelled. The magnitude of uncertainty is mission dependent. Although most commercial AUVs utilise the DVL water-track mode when bottom-tracking is unavailable, it has the disadvantage of poor performance in environments with underwater currents. The accuracy of DVL water-track aided INS localisation depends on the magnitude of the water column velocity. The higher the flow speed, the greater is the uncertainty (Chapter 5).

6.1.2. Model-aided AUV localisation in low energy environments

6.1.2.1. AUV localisation in calm-water environments

- The baseline model is capable of accurately predicting the linear velocities of the AUV using vehicle control commands for operations conducted in calm-water environments and baseline vehicle configuration. It assumes that the AUV is operating in a calm water environment as it neglects the parameters representing static and vehicle heading dependent environmental forces.
- For the tested zig-zag manoeuvres conducted in the calm-water environment, the baseline model estimates *u*, *v* and *w* with respective RMS errors of 0.15 m s^{-1}, 0.07 m

s^{-1} and 0.03 m s^{-1} in comparison to DVL bottom-track aided INS measurements (Chapter 2). However, should there be any movements of the water column relative to the ground, the drift of the vehicle due to current is not replicated by the baseline model (Chapter 2). Thus, the baseline model provides the vehicle velocities relative to the water column.

- Similar to DVL water-track aided mode, the performance of the baseline model-aided INS varies with the velocity of the water column. Higher water column velocities have been found to cause drifts in the position estimate (Chapter 5).
- The baseline model-aided INS provided more accurate solutions compared to DVL water-track aided INS for five out of six missions conducted in different water column conditions (Chapter 5). This is a result of DVL water-track mode's low measurement sampling frequency and liability to outliers, outages and erroneous readings. The mission that disagreed with this trend also had a small uncertainty difference of 0.9% of the distance travelled. Therefore, the baseline model-aided INS is a better approach for AUV localisation compared to the DVL water-track aided mode.

6.1.2.2. Calibrated model-aided localisation

- Once the baseline model is calibrated using the calibration technique (Chapter 2), it includes parameters representing static and vehicle heading dependent environmental forces. These parameters represent the flow field characteristics of the water column where the calibration run is being carried out. Therefore, the calibrated model precisely replicates the motion response of the AUV for missions conducted in the calibrated flow field. Therefore, it is substantially more accurate than the baseline model for operations conducted in water columns with different flow velocity conditions (i.e., an improvement up to 73%). It is also able to compute the position of the AUV within an uncertainty range of 1.5% of the distance travelled (Chapter 2).
- The accuracy of a calibrated model is restricted to flow fields with low spatial variations (i.e., even currents). If the velocity of the water column varies along the vehicle path, the parameters representing the environmental forces become invalid, adversely affecting the model accuracy. Therefore, the calibrated model should not be used in environments with strong non-uniform currents (Chapter 2).

6.1.2.3. Determining AUV models for complex flow conditions (Appendix C)

- The hydrodynamic parameters of a model vary when the AUV is operating within external pressure fields such as those created by another moving underwater vehicle. System identification is not suitable to determine a large number of parameters in such scenarios. Therefore, captive model experiments or CFD simulations should be utilised to determine the hydrodynamic parameters of a mathematical model in complex flow conditions. The simplified method introduced in Appendix C is able to estimate the hydrodynamic coefficients of an AUV when operating in a complex flow field by simply adding the steady-state interaction force coefficient to the baseline parameters (Appendix C).
- The anticipated operational condition should be predefined to determine the hydrodynamic coefficients of an AUV using captive model experiments and CFD simulations. That is, such techniques are most suitable for well-defined complex operations (Appendix C).

6.1.3. Model-aided AUV localisation in high energy environments

6.1.3.1. Water column velocity estimation

- Neither the baseline model nor the calibrated model is able to predict the motion response of the AUV accurately in environments with strong non-uniform currents. Therefore, it is required to link the model predicted vehicle velocities relative to the water column with the water column velocities relative to the ground (Chapter 2). The water velocity components estimated by the WVAM method agreed well with the measurements of the AUV's on-board ADCP with standard deviations of 0.09 m s^{-1}, 0.07 m s^{-1}, and 0.06 m s^{-1} for the respective components in *x*, *y*, and *z* directions (Chapter 3). WVAM method also showed a good agreement in comparison to water column velocity measurements from a stationary ADCP with differences of 0.05 m s^{-1}, 0.08 m s^{-1} and 0.01 m s^{-1} for the respective components (Chapter 4).
- When an AUV undertakes missions in environments with strong non-uniform currents, the yaw and pitch angles of the vehicle typically fluctuate around the target values due to the inability of the AUV's dynamic controller to adequately compensate for the external disturbing forces. Hydrodynamic forces and moments acting on the AUV moves into their nonlinear range as the angles of incidence of the vehicle become larger.

The parameters of the model identified using system identification are most accurate within their identified range; for example, the model parameters are limited to a forward speed range of around 1.4 m s^{-1} to 2.5 m s^{-1}. Therefore, if the vehicle motion exceeds the identified range, the accuracy of the model decreases adversely affecting predictions the WVAM method (Chapter 4).

- The WVAM method was tested for water column velocities up to around 1.7 m s^{-1}, and the method provided an acceptable accuracy with a maximum standard deviation of 0.09 m s^{-1}. Therefore, it could be incorporated to aid the INS navigation solution without further improvements. However, the applicable range of the method could be increased by extending the mathematical model for a wider range of speeds and angles of incidences (Chapter 4).
- A disadvantage of the WVAM method is that it requires the vehicle velocity measurements relative to the ground in order to measure the water column velocities. The flow profile smoothing algorithm introduced in Chapter 5 is able to accurately determine the water column velocity profiles along the descend paths of the AUV without DVL bottom track. The flow profile smoothing algorithm provided a good replication of the actual horizontal water column velocity measurements from the ADCP for all the tested missions with maximum and minimum RMS differences of 0.23 m s^{-1} 0.05 m s^{-1} respectively.

6.1.3.2. AUV localisation in high energy environments

- When outliers within the INS acceleration measurements are removed using the OR filter and aided with the baseline model, the performance improved considerably compared to conventional model-aided INS localisation system (Chapter 5). When combined with the water column velocity profile from the flow profile smoothing algorithm, it provided the most accurate localisation solution compared to other non-bottom-tracking localisation methods (i.e., DVL water-track aided, conventional model-aided, and unaided INS solutions). For the tested missions, the proposed technique was able to limit the positioning uncertainty to less than 5.5% of the distance travelled, even at extreme environmental conditions; whereas the other non-bottom-tracking techniques reveal an uncertainty up to 30%. This approach is relatively consistent regardless of the water column velocity. Therefore, the technique could be utilised for operational environments with both high and low flow speeds. However, it

is most advantageous when the AUV is operating in environments with large water column velocities since conventional techniques such as DVL water-track aided INS and conventional model-aided INS are less accurate in such environments.

6.2. Conclusions

AUVs operating in calm water environments without DVL bottom-track can utilise the baseline model-aided INS to improve the localisation performance, which is more accurate in comparison to conventional DVL water-track aided INS solution. Conducting a calibration mission prior to the actual survey mission can considerably improve the performance of the baseline model as it calibrates the model for any variations in the vehicle configuration as well as for environmental forces in the current operating condition. However, model calibration should not be done in environments with strong non-uniform underwater currents that largely vary with the depth and position.

The OR filtered baseline model-aided INS should be used with the flow profile smoothing algorithm to determine the localisation solution in high energy environments with strong non-uniform currents. This approach is more accurate compared to other conventional non-bottom-tracking localisation methods. It can also be used for calm water environments; although, the performance improvement compared to baseline model-aided INS is not significant.

6.3. Research implications

Novel techniques developed in this study also have many implications outside of the main objective of this project. For example, the WVAM method was well validated in this thesis as a tool to estimate water column velocities around the vehicle. This is an important outcome as the flow field around the vehicle is unresolvable with existing methods due to the ADCP blanking distance. Estimating water column velocities is essential to fill the blanking distance gap within a water column velocity profile, which is important for flow field characterisation. Furthermore, the flow velocities around the boundary layer of the AUV is critical for vehicle control system optimisation (Fan et al., 2016).

The AUV mathematical models are a prerequisite for vehicle control system optimisation (Kokegei et al., 2008). The models developed in this study accurately characterise the hydrodynamic, hydrostatic and mass properties of the vehicle. Real time model calibration

compliments this by adding the environmental influences from the current operating environment. Therefore, the models of this study have a great potential for being used to improve the performance of model based AUV control systems, especially when operating in high energy environments.

AUV simulators are used for a number of applications such as for operator training programs, for real time vehicle position tracking and to test new algorithms prior to the implementation in the actual vehicle. A mathematical model that characterises the vehicle properties is one of the key components of a simulator and the models developed in this project can be used for such applications. In addition, the system identification technique introduced to determine the models can be upgraded to obtain the model for autonomous surface vessels to be used for control system optimisation as well as to develop vehicle simulators (Keane et al., 2016).

The investigation on the hydrodynamic interaction between an AUV operating in close proximity to another moving underwater vehicle has a number of implications outside the scope of this project. The validated CFD simulation models developed in this study enabled investigation of the effects of relative size and position between the two vehicles. The interaction effects can be used to examine the feasibility to launch and recover AUVs from moving military submarines and to investigate the operational envelope of the AUV (Leong et al., 2015). CFD models can also be used to investigate the hydrodynamic interaction effects of AUVs operating near the bottom, surface ice layers and sidewalls. In addition, the variation of hydrodynamic coefficients can be used to optimise the model based control systems to enable the AUV to be safely launched and recovered from a moving submarine. The simplified method introduced in Appendix C to determine the variation of hydrodynamic coefficients by transforming the single body hydrodynamic coefficients with steady-state interaction forces facilitates to conduct high resolution investigations with a lower CFD computational cost.

6.4. Future work

Following future work is recommended for the continuance of this research program.

- AUV localisation techniques presented in this thesis are tested and validated by running simulations with sensor data from real vehicle missions conducted in the field. Implementing these techniques in the actual vehicle was out of the scope of this project. Therefore it is recommended to convert the developed algorithms as Mission Oriented

Operating Suite – Interval Programming (MOOS-IvP) application (Benjamin et al., 2010), which is to be run in a payload computer as a backseat driver for the AUV for real time localisation. The localisation solution computed by the MOOS-IvP application is to be used for the vehicle navigation and motion control systems to navigate the AUV more accurately when DVL bottom-track is unavailable.

- One of the key advantages of the techniques developed in this thesis is that they could be applied to any torpedo shaped AUV (e.g. *REMUS*, *Iver*, *Bluefin*, *Explorer*, etc.). For instance, the system identification techniques and the WVAM method have been tested for an *Iver III* AUV and a *Gavia* AUV with a different module configuration. It is recommended to implement the proposed localisation technique as a generalised algorithm that can be used for any torpedo shaped AUV. The MOOS-IvP software has made this possible as it runs platform independently in a payload computer, decoupled from the vehicle manufacturer's autonomy software. Furthermore, the applicability of the proposed technique for non-torpedo shaped AUVs is recommended to be investigated.
- The RLS and PEM based system identification techniques developed in this thesis to determine and to field calibrate the mathematical models have a vast applicability, not only for underwater vehicle, but also for surface vessels (Keane et al., 2016). For example, it can be used to determine the mathematical models of Autonomous Surface Vessels (ASVs) for a number of purposes, such as to develop vehicle simulators, for model based control system optimisation, etc. Therefore, it is recommended to transform the model equations for surface vessels to identify the mathematical models of surface platforms such as ASVs.
- The WVAM method is recommended to be used to develop and implement a water column velocity feedforward control algorithm to improve the vehicle motion control system when operating is high energy environments with strong non-uniform currents. Accurate motion control performance in strong currents is critical for better-quality survey data as well as for autonomous docking and launch and retrieval of AUVs from moving submarines.

Bibliography

ABKOWITZ, M. A. 1964. Lectures on ship hydrodynamics-Steering and manoeuvrability. Lyngby, Denmark: Hydro- and Aerodynamic's Laboratory.

ACOSTA, G. G., CURTI, H., IBÁÑEZ, O. C. & ROSSI, S. 2009. Some issues on the design of a low-cost autonomous underwater vehicle with an intelligent dynamic mission planner for pipeline and cable tracking. *I-Tech Online Books, Robotics Series, I-Tech Education and Publishing KG, Vienna, Austria, Editor: A. Inzartsev,(ISBN 978-953-7619-49-7)***,** 1-18.

AGUIAR, A. P. & PASCOAL, A. M. 2007. Dynamic positioning and way-point tracking of underactuated AUVs in the presence of ocean currents. *International Journal of Control,* 80**,** 1092-1108.

ALAMEDA JR, W. Seadevil-A totally integrated inertial navigation system (INS) solution. Proceedings of the 2002 Underwater Intervention Symposium, 2002.

ANANTHAKRISHNAN, P. 1998. AUV Hydrodynamics in Shallow Water During Adverse Weather Conditions. DTIC Document.

ANANTHAKRISHNAN, P. & ZHANG, K.-Q. AUV motion in a wave field. OCEANS'98 Conference Proceedings, 1998. IEEE, 1059-1063.

ANDERSON, B. & CROWELL, J. Workhorse AUV-a cost-sensible new autonomous underwater vehicle for surveys/soundings, search & rescue, and research. OCEANS, 2005. Proceedings of MTS/IEEE, 2005. IEEE, 1-6.

AUGENSTEIN, S. & ROCK, S. Estimating inertial position and current in the midwater. OCEANS 2008, 2008. IEEE, 1-6.

BARNEVELD, W. V. 2013. *Experimental Investigation into the Interactions between Two Underwater Bodies.* Bachelor of Engineering (Naval Architecture), University of Tasmania.

BENJAMIN, M. R., SCHMIDT, H., NEWMAN, P. M. & LEONARD, J. J. 2010. Nested autonomy for unmanned marine vehicles with MOOS-IvP. *Journal of Field Robotics,* 27**,** 834-875.

CARRICA, P. M., ISMAIL, F., HYMAN, M., BHUSHAN, S. & STERN, F. 2013. Turn and zigzag maneuvers of a surface combatant using a URANS approach with dynamic overset grids. *Journal of Marine Science and Technology,* 18**,** 166-181.

COSSU, R., FORREST, A., ROOP, H., DUNBAR, G., VANDERGOES, M., LEVY, R., STUMPNER, P. & SCHLADOW, S. 2015. Seasonal variability in turbidity currents in Lake Ohau, New Zealand, and their influence on sedimentation. *Marine and Freshwater Research.*

CURTIN, T. B., BELLINGHAM, J. G., CATIPOVIC, J. & WEBB, D. 1993. Autonomous oceanographic sampling networks. *Oceanography,* 6**,** 86-94.

DASH, A. K., NAGARAJAN, V. & SHA, O. P. 2016. Bifurcation analysis of a high-speed twin-propeller twin-rudder ship maneuvering model in roll-coupling motion. *Nonlinear Dynamics,* 83**,** 2035-2053.

DE SCHIPPER, M. A., DE ZEEUW, R., DE VRIES, S., STIVE, M. & TERWINDT, J. Horizontal ADCP measurements of waves and currents in the very nearshore. Current, Waves and Turbulence Measurements (CWTM), 2011 IEEE/OES 10th, 2011. IEEE, 159-166.

DEVORE, J. 2011a. *Probability and Statistics for Engineering and the Sciences,* Cengage Learning.

DEVORE, J. L. 2011b. *Probability and Statistics for Engineering and the Sciences*, Cengage Learning.
DOBLE, M. J., FORREST, A. L., WADHAMS, P. & LAVAL, B. E. 2009. Through-ice AUV deployment: Operational and technical experience from two seasons of Arctic fieldwork. *Cold Regions Science and Technology,* 56**,** 90-97.
DUFFY, J. & RENILSON, M. The Importance of the form of Time Domain Forces on Berthed Ship Interaction. The Second International Conference on Manoeuvring in Shallow & Confined Waters: Ship to Ship Interaction, 2011. 107-116.
FAN, S., XU, W., CHEN, Z. & ZHANG, F. Nonlinear observer design for current estimation based on underwater vehicle dynamic model. OCEANS 2016-Shanghai, 2016. IEEE, 1-5.
FARRELL, J. 2008. *Aided navigation: GPS with high rate sensors*, McGraw-Hill, Inc.
FONG, D. A. & JONES, N. L. 2006. Evaluation of AUV-based ADCP measurements. *Limnology and Oceanography: Methods,* 4**,** 58-67.
FORREST, A., TREMBANIS, A. & TODD, W. 2012. Ocean floor mapping as a precursor for space exploration. *Journal of Ocean Technology,* 7.
FORREST, A. L., LAVAL, B. E., PIETERS, R. & LIM, D. S. 2008. Convectively driven transport in temperate lakes. *Limnology and Oceanography,* 53**,** 2321.
FOSSEN, T. I. 1994. *Guidance and control of ocean vehicles*, John Wiley & Sons Inc.
FOSSEN, T. I. 2002. *Marine control systems: guidance, navigation and control of ships, rigs and underwater vehicles*, Marine Cybernetics.
FOSSEN, T. I. 2011. *Handbook of marine craft hydrodynamics and motion control*, John Wiley & Sons.
FRAJKA-WILLIAMS, E., ERIKSEN, C. C., RHINES, P. B. & HARCOURT, R. R. 2011. Determining vertical water velocities from Seaglider. *Journal of Atmospheric and Oceanic Technology,* 28**,** 1641-1656.
GANDHI, B., VERMA, H. & PATNAIK, S. Discharge measurement in small hydropower stations using acoustic doppler current profiler. Proc., 7th Int. Conference on Hydraulic Efficiency Measurements, IGHEM-2008, 2008. 3-6.
GÓRNICZ, T. & KULCZYK, J. 2011. Application of CFD Methods for the Assessment of Ship Manoeuvrability in Shallow Water. *Methods and Algorithms in Navigation: Marine Navigation and Safety of Sea Transportation***,** P45-50.
GRANLUND, K. 2009. *Steady and Unsteady Maneuvering Forces and Moments on Slender Bodies.* PhD in Aerospace Engineering, Virginia Polytechnic Institute and State University.
GRASMUECK, M., EBERLI, G. P., VIGGIANO, D. A., CORREA, T., RATHWELL, G. & LUO, J. 2006. Autonomous underwater vehicle (AUV) mapping reveals coral mound distribution, morphology, and oceanography in deep water of the Straits of Florida. *Geophysical Research Letters*, 33.
GREEN, S., COSSU, R., PENESIS, I. & NADER, J.-R. Tidal energy: a promising future resource for Tasmania. 3rd Asian Wave and Tidal Energy Conference (AWTEC 2016), 2016. 891-898.
GRIFFITHS, G. 2002. *Technology and applications of autonomous underwater vehicles*, CRC Press.
GROVES, N. C., HUANG, T. T. & CHANG, M. S. 1989. Geometric Characteristics of DARPA (Defense Advanced Research Projects Agency) SUBOFF Models (DTRC Model Numbers 5470 and 5471). DTIC Document.
HAMA, F. R. 1957. An efficient tripping device. *Journal of the Aeronautical Sciences,* 24**,** 236-237.

HARDY, T. & BARLOW, G. Unmanned Underwater Vehicle (UUV) deployment and retrieval considerations for submarines. 9th International Naval Engineering Conference and Exhibition, 2008.

HAYES, D. R. & MORISON, J. H. 2002. Determining turbulent vertical velocity, and fluxes of heat and salt with an autonomous underwater vehicle. *Journal of Atmospheric and Oceanic Technology,* 19**,** 759-779.

HEGRENAES, O. & BERGLUND, E. Doppler water-track aided inertial navigation for autonomous underwater vehicle. OCEANS 2009-EUROPE, 2009. IEEE, 1-10.

HEGRENAES, O., BERGLUND, E. & HALLINGSTAD, O. Model-aided inertial navigation for underwater vehicles. Robotics and Automation, 2008. ICRA 2008. IEEE International Conference on, 2008. IEEE, 1069-1076.

HEGRENAES, O. & HALLINGSTAD, O. 2011. Model-aided INS with sea current estimation for robust underwater navigation. *Oceanic Engineering, IEEE Journal of,* 36**,** 316-337.

HILDEBRANDT, M. & HILLJEGERDES, J. Design of a versatile AUV for high precision visual mapping and algorithm evaluation. Autonomous Underwater Vehicles (AUV), 2010 IEEE/OES, 2010. IEEE, 1-6.

HILLER, T., REED, T. & STEINGRIMSSON, A. 2011. Producing chart data from interferometric sonars on small AUVs. *The International Hydrographic Review*.

HONG, E. Y., MENG, T. K. & CHITRE, M. Online system identification of the dynamics of an autonomous underwater vehicle. Underwater Technology Symposium (UT), 2013 IEEE International, 2013. IEEE, 1-10.

HORSTMAN, E., BALKE, T., BOUMA, T., DOHMEN-JANSSEN, M. & HULSCHER, S. 2011. Optimizing methods to measure hydrodynamics in coastal wetlands: evaluating the use and positioning of ADV, ADCP AND HR-ADCP. *Coastal Engineering Proceedings,* 1**,** 51.

HU, S., MEINKE, K., OUYANG, H. & SUN, G. 2011. Outlier-Tolerant Kalman Filter of State Vectors in Linear Stochastic System. *International Journal of Advanced Computer Science and Applications,* 2**,** 37-41.

HUGHES, M. G., MASSELINK, G. & BRANDER, R. W. 1997. Flow velocity and sediment transport in the swash zone of a steep beach. *Marine Geology,* 138**,** 91-103.

ITTC 2011a. ITTC - Recommended Procedures and Guidelines: Full Scale Measurements Speed and Power Trials Instrumentation Installation and Calibration. International Towing Tank Conference.

ITTC 2011b. ITTC – Recommended Procedures and Guidelines: Guideline on Use of RANS Tools for Manoeuvring Prediction. International Towing Tank Conference.

JALVING, B., GADE, K., HAGEN, O. K. & VESTGARD, K. A toolbox of aiding techniques for the HUGIN AUV integrated inertial navigation system. OCEANS 2003. Proceedings, 2003. IEEE, 1146-1153.

JALVING, B., GADE, K., SVARTVEIT, K., WILLUMSEN, A. & SØRHAGEN, R. 2004. DVL velocity aiding in the HUGIN 1000 integrated inertial navigation system. *Modeling, Identification and Control,* 25**,** 223.

JAVIER, B. Low-cost AUV based on Arduino open source microcontroller board for oceanographic research applications in a collaborative long term deployment missions and suitable for combining with an USV as autonomous automatic recharging platform Autonomous Underwater Vehicles (AUV). 2012 IEEE/OES, 2012 Sauthampton, UK. ISSN.

JAYASIRI, A., GOSINE, R. G., MANN, G. K. & MCGUIRE, P. Simulation of aided AUV navigation and adaptive plume tracking. Electrical and Computer Engineering (CCECE), 2014 IEEE 27th Canadian Conference on, 2014. IEEE, 1-6.

JAYASIRI, A., GOSINE, R. G., MANN, G. K. & MCGUIRE, P. 2016. AUV-Based Plume Tracking. *Journal of Control Science and Engineering,* 2016**,** 12.

KEANE, J. R., T, D. J., HAASE, M., RANDENI, S. A. T., HUBBERT, H. R., KENT, R. L., FORREST, A. L., SAMMUT, K., LAMMAS, A., WHEARE, J. & BATTLE, D. 2016. Preparing a wave adaptive modular vessel for automation. *International Journal of Small Craft Technology***,** 113.

KEARFOTT CORPORATION. 2016. *Kearfott sea navigation unit data sheet* [Online]. Available: http://www.kearfott.com/wp-content/uploads/2016/09/Kearfott_SeaNav.pdf [Accessed 6th of January 2017].

KEMNA, S., HAMILTON, M. J., HUGHES, D. T. & LEPAGE, K. D. 2011. Adaptive autonomous underwater vehicles for littoral surveillance. *Intelligent Service Robotics,* 4**,** 245-258.

KIM, K. & URA, T. Fuel-optimal guidance and tracking control of AUV under current interaction. The Thirteenth International Offshore and Polar Engineering Conference, 2003. International Society of Offshore and Polar Engineers.

KIMURA, S., JENKINS, A., DUTRIEUX, P., FORRYAN, A., NAVEIRA GARABATO, A. C. & FIRING, Y. 2016. Ocean mixing beneath Pine Island Glacier ice shelf, West Antarctica. *Journal of Geophysical Research: Oceans*.

KOKEGEI, M., HE, F. & SAMMUT, K. Fully coupled 6 degrees-of-freedom control of autonomous underwater vehicles. OCEANS 2008, 2008. IEEE, 1-7.

LATAIRE, E., VANTORRE, M., DELEFORTRIE, G. & CANDRIES, M. 2012. Mathematical modelling of forces acting on ships during lightering operations. *Ocean Engineering,* 55**,** 101-115.

LEONG, Z., RANMUTHUGALA, D., PENESIS, I. & NGUYEN, H. 2012a. RANS-based CFD Prediction of the Hydrodynamic Coefficients of DARPA SUBOFF Geometry in Straight-Line and Rotating Arm Manoeuvres. *The Transactions of the Royal Institution of Naval Architects, Part A International Journal of Maritime Engineering [under review]*.

LEONG, Z., SAAD, K., RANMUTHUGALA, S. & DUFFY, J. Investigation into the Hydrodynamic Interaction Effects on an AUV Operating Close to a Submarine. Pacific 2013 International Maritime Conference, 2013. 1-11.

LEONG, Z. Q. 2013. CFD Simulations of Multiple Submerged Bodies in Relative Motion for Control Systems. Launceston: National Centre for Maritime Engineering and Hydrodynamics

LEONG, Z. Q., RANMUTHUGALA, D., PENESIS, I. & NGUYEN, H. 2015. Quasi-static analysis of the hydrodynamic interaction effects on an autonomous underwater vehicle operating in proximity to a moving submarine. *Ocean Engineering,* 106**,** 175-188.

LEONG, Z. Q., RANMUTHUGALA, D., PENESIS, I. & NGUYEN, H. D. 2012b. Computational fluid dynamics re-mesh method to generating hydrodynamic models for maneuvering simulation of two submerged bodies in relative motion. *Journal of Computer Science and Cybernetics,* 27**,** 353-362.

LEWIS, E. V. 1988. *Principles of Naval Architecture: Motions in waves and controllability*, Society of Naval Architects and Marine Engineers.

LIANG, X., LI, Y., PENG, Z. & ZHANG, J. 2016. Nonlinear dynamics modeling and performance prediction for underactuated AUV with fins. *Nonlinear Dynamics,* 84**,** 237-249.

LJUNG, L. 1998. *System identification*, Springer.

LJUNG, L. 1999. *System Identification: Theory for the User*, Prentice Hall PTR.

LU, Y. & LUECK, R. G. 1999. Using a broadband ADCP in a tidal channel. Part I: Mean flow and shear. *Journal of Atmospheric and Oceanic Technology,* 16**,** 1556-1567.

MARCO, D. B., MARTINS, A. & HEALY, A. J. 2005. Surge motion parameter identification for the NPS Phoenix AUV. DTIC Document.

MAWBY, A., WILSON, P., BOLE, M., P, F. S. & DUNCAN, J. 2006. Manoeuvring Simulation of Multiple Underwater Vehicles in Close Proximity. Hamburg: Ministry of Defence, Defence Procurement Agency.

MCLEOD, D., JACOBSON, J. R. & TANGIRALA, S. Autonomous inspection of subsea facilities-Gulf of Mexico trials. offshore technology conference, 2012. Offshore Technology Conference.

MEDAGODA, L., JAKUBA, M. V., PIZARRO, O. & WILLIAMS, S. B. Water column current profile aided localisation for autonomous underwater vehicles. OCEANS 2010 IEEE-Sydney, 2010. IEEE, 1-10.

MEDAGODA, L., WILLIAMS, S. B., PIZARRO, O., KINSEY, J. C. & JAKUBA, M. V. 2016. Mid-water current aided localization for autonomous underwater vehicles. *Autonomous Robots,* 40**,** 1207-1227.

MURPHY, K. 1999. Kalman filter toolbox for Matlab.

MURPHY, K. 2001. The bayes net toolbox for matlab. *Computing science and statistics,* 33**,** 1024-1034.

NEWMAN, J. N. 1977. *Marine hydrodynamics*, MIT press.

OSTERLOH, C., MEYER, B., AMORY, A., PIONTECK, T. & MAEHLE, E. MONSUN II-Towards Autonomous Underwater Swarms for Environmental Monitoring. International Conference on Intelligent Robots and Systems (IROS2012), Workshop on Robotics for Environmental Monitoring, Vilamoura, Algarve, Portugal, 2012. 7-12.

PANISH, R. & TAYLOR, M. Achieving high navigation accuracy using inertial navigation systems in autonomous underwater vehicles. OCEANS, 2011 IEEE-Spain, 2011. IEEE, 1-7.

PAULL, L., SAEEDI, S., SETO, M. & LI, H. 2014. AUV navigation and localization: A review. *IEEE Journal of Oceanic Engineering,* 39**,** 131-149.

PHILLIPS, A. B. 2010. *Simulations of a self propelled autonomous underwater vehicle.* Doctoral dissertation, University of Southampton.

POLIS, C., RANMUTHUGALA, D., DUFFY, J. & RENILSON, M. Enabling the prediction of manoeuvring characteristics of a submarine operating near the free surface. Pacific 2013 International Maritime Conference: The commercial maritime and naval defence showcase for the Asia Pacific, 2013. Engineers Australia, 281.

PRESTERO, T. T. J. 2001. *Verification of a six-degree of freedom simulation model for the REMUS autonomous underwater vehicle.* Massachusetts institute of technology.

RANDENI, S. A. T., FORREST, A. L., COSSU, R., LEONG, Z. Q., KING, P. D. & RANMUTHUGALA, D. 2016. Autonomous Underwater Vehicle Motion Response: A Nonacoustic Tool for Blue Water Navigation. *Marine Technology Society Journal,* 50**,** 17-26.

RANDENI, S. A. T., FORREST, A. L., COSSU, R., LEONG, Z. Q. & RANMUTHUGALA, D. Estimating flow velocities of the water column using the motion response of an Autonomous Underwater Vehicle (AUV). OCEANS '15 MTS/IEEE, 2015a Washington D.C.: IEEE.

RANDENI, S. A. T., FORREST, A. L., COSSU, R., LEONG, Z. Q. & RANMUTHUGALA, D. 2017a. Determining the Horizontal and Vertical Water Velocity Components of a Turbulent Water Column Using the Motion Response of an Autonomous Underwater Vehicle. *Journal of Marine Science and Engineering,* 5**,** 25.

RANDENI, S. A. T., FORREST, A. L., COSSU, R., LEONG, Z. Q., RANMUTHUGALA, D. & SCHMIDT, V. 2017b. Parameter identification of a nonlinear model: replicating the

motion response of an autonomous underwater vehicle for dynamic environments. *Non-linear Dynamics*.

RANDENI, S. A. T., LEONG, Z., RANMUTHUGALA, D., FORREST, A. & DUFFY, J. 2015b. Numerical investigation of the hydrodynamic interaction between two underwater bodies in relative motion. *Applied Ocean Research,* 51**,** 14-24.

RODGERS, J., WHARINGTON, J., TYNAN, A. & COXHEAD, M. 2008. A concept for the deployment of unmanned maritime systems from submarines: MURULA integration impact modelling and results.

RUDNICK, D. L., JOHNSTON, T. & SHERMAN, J. T. 2013. High-frequency internal waves near the Luzon Strait observed by underwater gliders. *Journal of Geophysical Research: Oceans,* 118**,** 774-784.

SAKAMOTO, N., CARRICA, P. M. & STERN, F. 2012. URANS simulations of static and dynamic maneuvering for surface combatant: part 1. Verification and validation for forces, moment, and hydrodynamic derivatives. *Journal of marine science and technology,* 17**,** 422-445.

SIMONSEN, C., OTZEN, J., KLIMT, C., LARSEN, N. & STERN, F. Maneuvering predictions in the early design phase using CFD generated PMM data. 29th symposium on Naval Hydrodynamics, Gothenburg, Sweden, 2012.

SIMPSON, M. R. 2001. *Discharge measurements using a broad-band acoustic Doppler current profiler*, US Department of the Interior, US Geological Survey.

SNAME 1952. Nomenclature for treating the motion of a submerged body through a fluid JR. *New York: Technical and Research Bulletin***,** 1-5.

SONG, F., AN, P. E. & FOLLECO, A. 2003. Modeling and simulation of autonomous underwater vehicles: design and implementation. *IEEE Journal of Oceanic Engineering,* 28**,** 283-296.

SPRINTALL, J., GORDON, A. L., FLAMENT, P. & VILLANOY, C. L. 2012. Observations of exchange between the South China Sea and the Sulu Sea. *Journal of Geophysical Research: Oceans,* 117.

STEEL, V. 2010. *Investigation into the Effect of Wave Making on a Submarine Approaching the Free Surface.* Bachelor of Engineering (Naval Architecture), University of Tasmania.

STERN, F., WILSON, R. V., COLEMAN, H. W. & PATERSON, E. G. 2001. Comprehensive approach to verification and validation of CFD simulations—part 1: methodology and procedures. *Journal of fluids engineering,* 123**,** 793-802.

STUTTERS, L., LIU, H., TILTMAN, C. & BROWN, D. J. 2008. Navigation technologies for autonomous underwater vehicles. *IEEE Transactions on Systems, Man, and Cybernetics, Part C (Applications and Reviews),* 38**,** 581-589.

SUN, X. J., SHI, J. & YANG, Y. Neural Networks Based Attitude Decoupling Control for AUV with X-Shaped Fins. Advanced Materials Research, 2013. Trans Tech Publ, 222-228.

THORGILSSON, H. 2006. *Control of a small undermanned underwater vehicle using zero optimizing controllers.* Master's thesis, Department of Electrical and Computer Engineering, University of Iceland, Reykjavík, Iceland.

TING, J.-A., THEODOROU, E. & SCHAAL, S. A Kalman filter for robust outlier detection. Intelligent Robots and Systems, 2007. IROS 2007. IEEE/RSJ International Conference on, 2007. IEEE, 1514-1519.

TITTERTON, D. & WESTON, J. L. 2004. *Strapdown inertial navigation technology,* IET.

TREMBANIS, A. C., CARY, C., SCHMIDT, V., CLARKE, D., CREES, T. & JACKSON, E. Modular autonomous biosampler (MAB)—A prototype system for distinct biological size-class sampling and preservation. Oceans, 2012, 2012. IEEE, 1-6.

TU, J., INTHAVONG, K. & AHMADI, G. 2012. *Computational fluid and particle dynamics in the human respiratory system*, Springer.

VANTORRE, M., VERZHBITSKAYA, E. & LAFORCE, E. 2002. Model test based formulations of ship-ship interaction forces. *Ship Technology Research,* 49**,** 124-141.

VICKERY, K. Acoustic positioning systems. A practical overview of current systems. Autonomous Underwater Vehicles, 1998. AUV'98. Proceedings of the 1998 Workshop on, 1998. IEEE, 5-17.

WADEHN, F., BRUDERER, L., DAUWELS, J., SAHDEVA, V., YU, H. & LOELIGER, H.-A. Outlier-insensitive Kalman smoothing and marginal message passing. Signal Processing Conference (EUSIPCO), 2016 24th European, 2016. IEEE, 1242-1246.

WALKER, C. R., STRINGFIELD, J. Q., WOLBRECHT, E. T., ANDERSON, M. J., CANNING, J. R., BEAN, T. A., ODELL, D. L., FRENZEL, J. F. & EDWARDS, D. B. 2013. Measurement of the magnetic signature of a moving surface vessel with multiple magnetometer-equipped AUVs. *Ocean Engineering,* 64**,** 80-87.

WHITE, F. W. 2011. *Fluid Mechanics, 7th edition.*, New York, McGraw-Hill.

WILSON, R. V., STERN, F., COLEMAN, H. W. & PATERSON, E. G. 2001. Comprehensive approach to verification and validation of CFD simulations—Part 2: Application for RANS simulation of a cargo/container ship. *Journal of fluids engineering,* 123**,** 803-810.

WOLKERSTORFER, W. J. 1995. *A Linear Maneuvering Model for Simulation of Slice Hulls.* DTIC Document.

YAN, Z., WU, D., ZHOU, J. & HAO, L. 2014. Recursive Subspace Identification of AUV Dynamic Model under General Noise Assumption. *Mathematical Problems in Engineering,* 2014.

YAN, Z., WU, D., ZHOU, J. & ZHANG, W. Recursive identification of autonomous underwater vehicle for emergency navigation. Oceans, 2012, 2012. IEEE, 1-6.

YEO, R. Surveying the underside of an Arctic ice ridge using a man-portable GAVIA AUV deployed through the ice. OCEANS 2007, 2007. IEEE, 1-8.

Appendix A: WVAM method in high energy environments

Appendix A is based on the conference article '*Estimating flow velocities of the water column using the motion response of an Autonomous Underwater Vehicle (AUV)*' published in the Proceedings of the '*MTS/IEEE Oceans 2015*'. The citation for the article is:

Randeni SAT, Forrest AL, Cossu R, Leong ZQ, Ranmuthugala D. Estimating flow velocities of the water column using the motion response of an Autonomous Underwater Vehicle (AUV). OCEANS '15 MTS/IEEE. Washington D.C.: IEEE; 2015.

Abstract

The WVAM method is a non-acoustic method to calculate the velocity components of a turbulent water column using the motion response of an Autonomous Underwater Vehicle (AUV) without the aid of an Acoustic Doppler Current Profiler (ADCP). This study analyses water velocity measurements estimated using the WVAM method as a function of the turbulence level of the environment by testing the method in an estuary that exhibits strong tidal currents (around 2.5 m s^{-1}). The uncertainty of this method at different water column conditions was computed by comparing the velocity measurements from the WVAM method with those obtained from the AUV mounted ADCP. The WVAM method determines the water velocities by comparing the motion response of the vehicle when operating within turbulent and calm water environments respectively. The motion of the vehicle in the calm water environment was obtained by conducting simulations of the vehicles in calm water under the same control commands executed during the field experiments in turbulent conditions. A reduction in the accuracy of the method in rougher water environments was observed due to the hydrodynamic coefficients of the simulation model reaching their nonlinear range limits. A possible strategy to overcome this limitation and improve the WVAM method's ability to accurately estimate the flow field in the vicinity of AUVs operating in highly turbulent environments is also provided.

Introduction

Many marine surveys, from physical oceanography to hydraulic engineering, involves measuring water column velocities; for example, determining the sediment load in a stream (Hughes et al., 1997) and assessing the turbulent flux in the surface mixed layer (Hayes and Morison, 2002). Traditionally, equipment such as broadband Acoustic Doppler Current Profilers (ADCPs), Acoustic Doppler Velocimeters (ADVs) and High Resolution (HR) profilers are used to measure the water column velocities (Horstman et al., 2011, de Schipper et al., 2011). These acoustic instruments determine the water column velocity profiles using the Doppler frequency shift of a sound wave transmitted by the device and reflected from particles in the water column itself (Simpson, 2001). These devices are used as stationary moorings to determine the flow speeds at fixed locations as well as on moving platforms in order to map spatial distributions of velocity fields.

ADCPs mounted on Autonomous Underwater Vehicles (AUVs) are gradually being adopted to capture water column velocities due to their capability to undertake missions in areas logistically difficult or inaccessible to surface vessels and other types of underwater vehicles such as under-ice operations (Doble et al., 2009). In addition, their relative manoeuvring stability and the decoupling from surface noise and reflectance allows them to provide enhanced flow measurements as compared to other moving platforms (Fong and Jones, 2006).

Acoustic instruments such as ADCPs are generally expensive and therefore, not feasible for low-cost AUVs that are being developed for commercial and scientific applications (Acosta et al., 2009, Anderson and Crowell, 2005, Javier, 2012). Furthermore, ADCPs have a blanking distance (i.e., a dead zone) in proximity to the device (typically around 0.5 m to 5 m, depending on the sampling frequency and selected bin size of the instrument), in which the flow velocity data remains unresolved (Simpson, 2001). In order to minimise these effects, the authors previously introduced a new method to calculate the water velocity components of a turbulent water column using the AUV motion response without the aid of an ADCP, referred to as the WVAM Method (Randeni et al., 2017a). In this method, the water velocities are determined by comparing the performance (i.e., the motion response) of the vehicle when operating within turbulent and calm water environments.

The study presented in the paper investigates the variation of the WVAM method's accuracy with the turbulence level of the water column through field deployments in the Tamar

estuary located in Tasmania, Australia that exhibits strong tidal currents. The uncertainty of the method was calculated by comparing with the velocity measurements obtained from the AUV's ADCP at different stages within the tidal range. A potential technique to improve the capability of the WVAM method is also discussed.

Methodology

Instruments

A *Gavia*-class modular AUV (Yeo, 2007) was used to test the WVAM method, with the AUV configured to an overall length of 2.7 m, diameter of 0.2 m, and a dry weight in air of approximately 70 kg. The modularised vehicle in the tested configuration consisted of a Nose Cone, Battery, Geoswath Interferometry Sonar, 1200 kHz RDI ADCP, Inertial Navigation System (INS), Control and Propulsion Modules. The ADCP module of the AUV included two 4-beam ADCPs arranged in a vertical plane to scan up and downwards from the vehicle (see Figure A.1). The ADCPs were set to profile the 9.94 meters of water column in 0.5 m range bins so that the three directional water velocity components in the vehicle's body-fixed coordinate system are measured in each bin. However, adjacent to the transducers (both above and below) there was a blanking distance of 0.44 m as shown in Figure A.1.

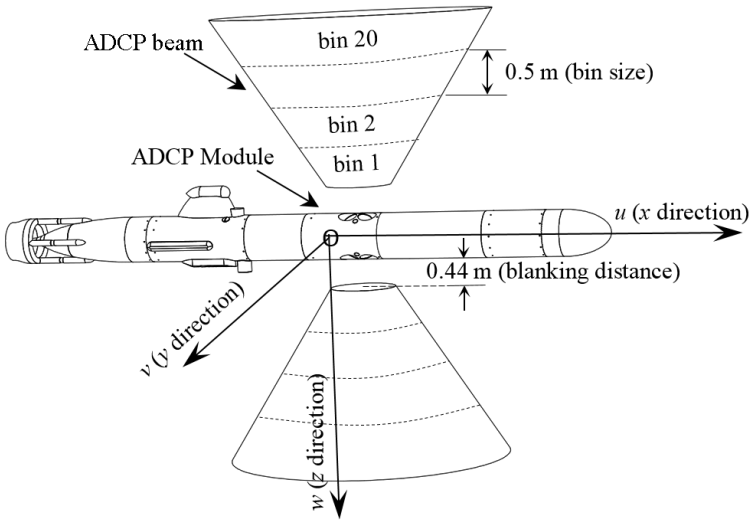

Figure A.1 – Body-fixed coordinate system of the *Gavia* AUV showing the ADCP beam geometry. The origin of the coordinate system is at the centre of buoyancy of the vehicle (marked by the 'O').

Site description

The objective of this study was to determine the variation of the WVAM method's accuracy at water columns with different flow velocities. To achieve this, the WVAM method was tested in the Tamar estuary near the Batman Bridge, which is located in Tasmania, Australia (see Figure A.2a and A.2b). Due to the proximity to the open sea, Tamar estuary exhibits strong tidal currents with maximum flow velocities of up to 2.5 m s^{-1}.

Nine AUV runs were conducted along the track line shown in Figure A.2b. Out of the nine, the first five were conducted on 14 April, 2015 and the last four on 15 April, 2015. Runs 1 to 3 and 6 to 9 were conducted during slack water as shown in the tidal curve given in Figure A.2c. The velocity of the tidal currents during the first runs on each day (i.e., runs 1 and 6) was approximately 0.25 m s^{-1}. Due to the development of the strong flood tide, the flow speeds increased rapidly during the following next runs. Runs 4 and 5 were carried out at partially and fully developed flood tide conditions with strong tidal currents (around 2 m s^{-1}).

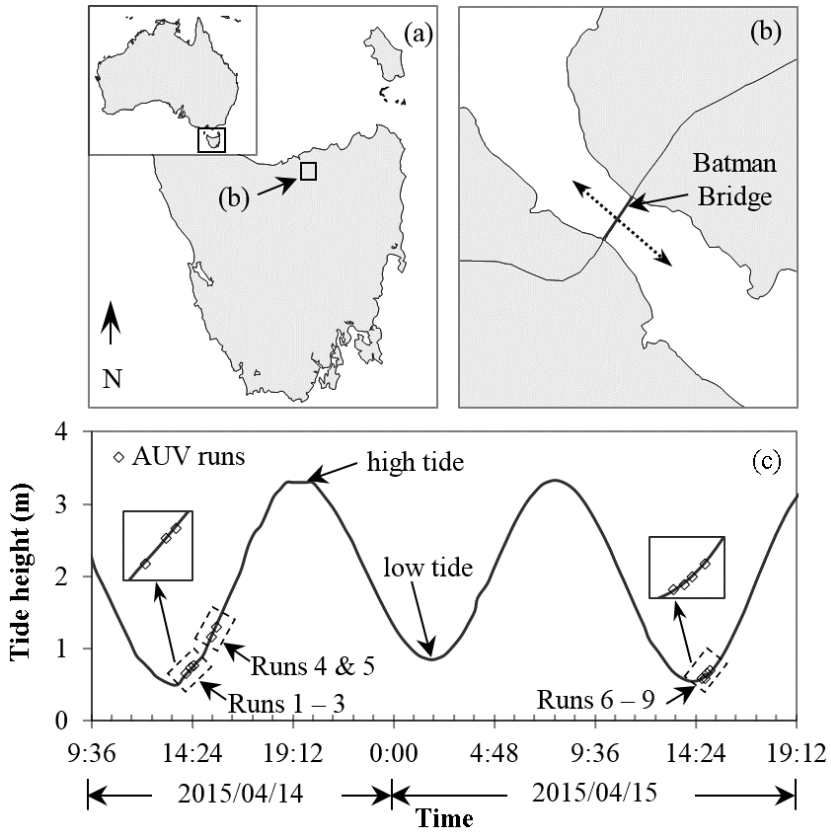

Figure A.2 – (a) The experimental field site in Tasmania, Australia (inset); (b) Tamar estuary with the AUV track illustrated by the dotted line. (c) The tidal heights observed on 14th and 15th April, 2015. The time periods the AUV runs were conducted are shown by the diamond markers.

WVAM method

For the WVAM method (Randeni et al., 2017a), the AUV needs to undergo a straight-line, constant depth mission through the region where the water column velocities are to be measured. Typically, when an AUV is operating in an environment with fluctuating water velocities, the forces and moments induced by these velocities can interrupt the control stability and change the vehicle speed, depth, pitch and yaw angles (i.e., motion response of the AUV) from the pre-set values. In order to compensate for such changes in performance, the vehicle's dynamic control system adjusts the revolution speed of the propeller and the angles of the four control surfaces. According to these adjustments, the motion response of the AUV will change and the AUV will return to the initially prescribed mission track unless the propeller and the control surfaces are unable to compensate for the external forces (Kim and Ura, 2003).

The WVAM method uses the compensation commands given by the vehicle's controller to the propulsion motor and control surfaces (recorded in the vehicle log) and executes these commands within a simulation model representing a calm water environment. Since there are no disturbing forces due to flow variations in calm water conditions, the simulated vehicle motion will be different to the actual motion. The difference between the two motion responses provides an estimation of the water column velocities relative to the earth.

Equation (A.1) gives a generalised form of the water velocity calculation:

$$\bar{v}_{water(t)} = \bar{v}_{AUV(turbulent)(t)} - \bar{v}_{AUV(calm)(t)} \quad \text{(A.1)}$$

where, $\bar{v}_{water}$ is the velocity component of the surrounding water column relative to earth in the body-fixed coordinate system, $\bar{v}_{AUV(turbulent)}$ is the velocity component of the AUV observed in the turbulent environment and $\bar{v}_{AUV(calm)}$ is the velocity component of the vehicle obtained from the calm water simulation utilising the control commands recorded from the field tests. Subscript *t* indicates the time-step. To estimate the water velocity component in the *x*, *y* and *z* axes, $\bar{v}_{AUV}$ is replaced with the surge, sway and heave velocity components (i.e., *u*, *v* and *w*) of the vehicle in the body-fixed frame of reference respectively.

Simulation model and hydrodynamic coefficients

The manoeuvring simulation model of the *Gavia* AUV was developed to reproduce the vehicle's trajectory in a calm water environment in response to the time series input of the

control commands. It requires an accurate approximation of the associated hydrodynamic coefficients (i.e., a representation of the forces and moments acting on the vehicle at different orientations and velocities) to adequately predict the motion of the AUV. Generally, the forces and moments acting on submerged bodies in Six-Degree-of-Freedom (6-DOF) are highly nonlinear (Lewis, 1988). For example, the vertical hydrodynamic force acting on the AUV varies linearly with its pitch angle up to a value of around ±8º, beyond which it becomes nonlinear (see Figure A.3). Similarly, threshold values exist for other hydrodynamic forces and moments as well. Therefore, the hydrodynamic coefficients estimated for the linear ranges are only valid up to a certain threshold angle (Lewis, 1988).

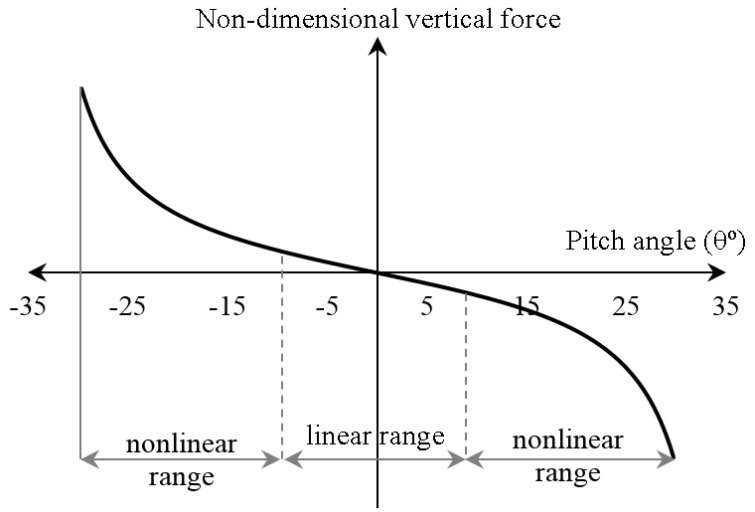

Figure A.3 – Typical variation of the force acting on the AUV in *z* direction with the pitch angle (Granlund, 2009). The threshold angle that the linear variation changes to nonlinear is around ±8º.

During the initial development of the WVAM method, a basic curve fitting method was utilised to determine the hydrodynamic coefficients due to its relative simplicity. The coefficients obtained from this method were limited to small angles of incidence (i.e., generally below 8º) restricting them to their linear range. When an AUV operates in turbulent environments, its pitch and yaw angles typically fluctuate around the baseline values. The magnitude of these fluctuations increases with increasing levels of turbulence due to the inability of the AUV's dynamic controller to adequately and/or quickly compensate for the severe disturbance forces (Kim and Ura, 2003). Therefore, in extremely turbulent water columns, these fluctuation angles will be greater than ±8º. Thus, a simulation model that is limited to linear hydrodynamics data will not be able to adequately replicate the motion of the vehicle in extreme environments.

Results and Discussion

The water velocity components determined using the WVAM method were compared with the ADCP velocity measurements in order to validate the former method. Figure A.4a, A.4b and A.4c compare ADCP water velocity components in the *x*, *y* and *z* directions obtained from the first AUV run with WVAM estimates. The ADCP results were smoothed using a moving average filter with a backward scheme and a frame size of six time-steps. It is evident from these plots that the WVAM method provides a good replication of the flow velocities measured using the on-board ADCP.

The uncertainty of the water velocity measurements from the WVAM method compared to the ADCP results was quantified using equation (A.2) that approximates the Standard Error (SE) with a percentage confidence of 99.7% (Devore, 2011a),

$$SE = \frac{3}{\sqrt{n}} \sqrt{\frac{\sum_{t=1}^{n} \left(\bar{v}_{water(ADCP)} - \bar{v}_{water(WVAM)} \right)^2}{n}} \tag{A.2}$$

where, $\bar{v}_{water(ADCP)}$ is the water velocity measured using the ADCP, $\bar{v}_{water(WVAM)}$ is the water velocity calculated using the WVAM method, and *n* is the number of time-steps.

The standard errors for the velocity components in the *x*, *y* and *z* directions for the first run were ±0.068 m s^{-1}, ±0.017 m s^{-1} and ±0.045 m s^{-1} respectively. These numbers represent the difference between WVAM and ADCP velocity predictions in each of the three directions, with the greatest error seen in the *x*-direction.

Runs 1 to 3 and 6 to 9 were conducted in lower turbulent environments compared to the Runs 4 and 5. Due to the developing flood tide, the level of turbulence increased gradually with each run; i.e., the flow conditions were usually more turbulent than in previous runs. Figure A.5a to A.5e presents the vertical velocity component of the water column obtained from the AUV runs conducted on 14th April, 2015 (i.e., Runs 1 to 5). The standard errors between the WVAM and ADCP results (also called as the uncertainty of the WVAM method) for these runs are given in Table A.1. The uncertainty of the vertical water velocity prediction generally increases with the increasing turbulence level of the water column. The development of increased divergence between the two results with the level of turbulence is clearly seen in Figure A.5.

The averaged fluctuation of the vehicle's yaw angle, pitch angle and surge speed from the target values are given in Table A.1. If the AUV's control system is capable of guiding the vehicle accurately along the prescribed path in turbulent environments, these values would be close to zero.

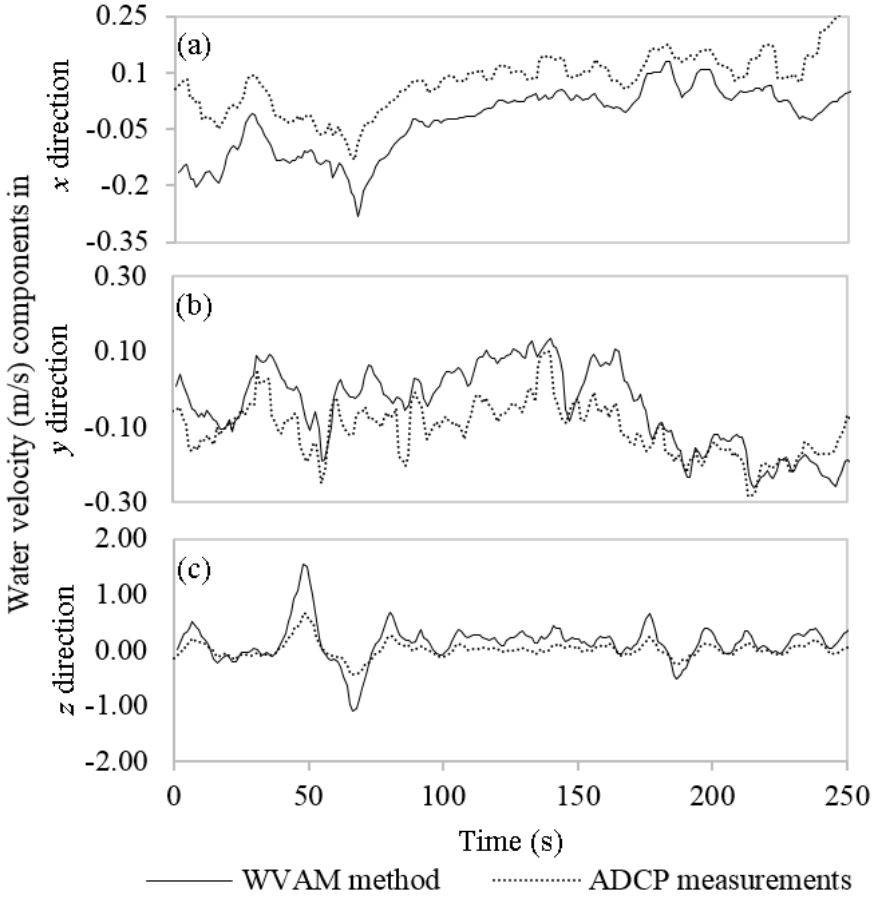

Figure A.4 – Comparison between the velocity components of the water column in the *x*, *y* and *z* directions (panels a, b and c respectively) calculated using the WVAM method (solid black line) and those obtained from the on-board ADCP (dashed grey line). Data were obtained from Run 1 when the AUV was moving with the predominant tidal currents.

The uncertainties of the vertical and transverse water velocity predictions are larger when the averaged fluctuations of the pitch and yaw angles (respectively) increase (see Table A.1). For example, in Run 2 the averaged deviation of the yaw angle is around ±17º and the standard error of the transverse velocity prediction is much larger than for Run 1 (i.e., 0.153 m s^{-1}). Run 1 has a smaller deviation of the yaw angle of around ±1.5º results in a much smaller uncertainty in the vicinity of 0.017 m s^{-1}. A similar outcome is seen in the vertical water velocity component. In Run 9, the averaged deviation of the pitch angle is ±7.5º giving a standard error in the vertical water velocity prediction of around 0.1 m s^{-1}. However, in Run 6 the deviation of the pitch

angle is comparatively lower at ±3.1º resulting in a smaller standard error of the velocity of around 0.05 m s^{-1}.

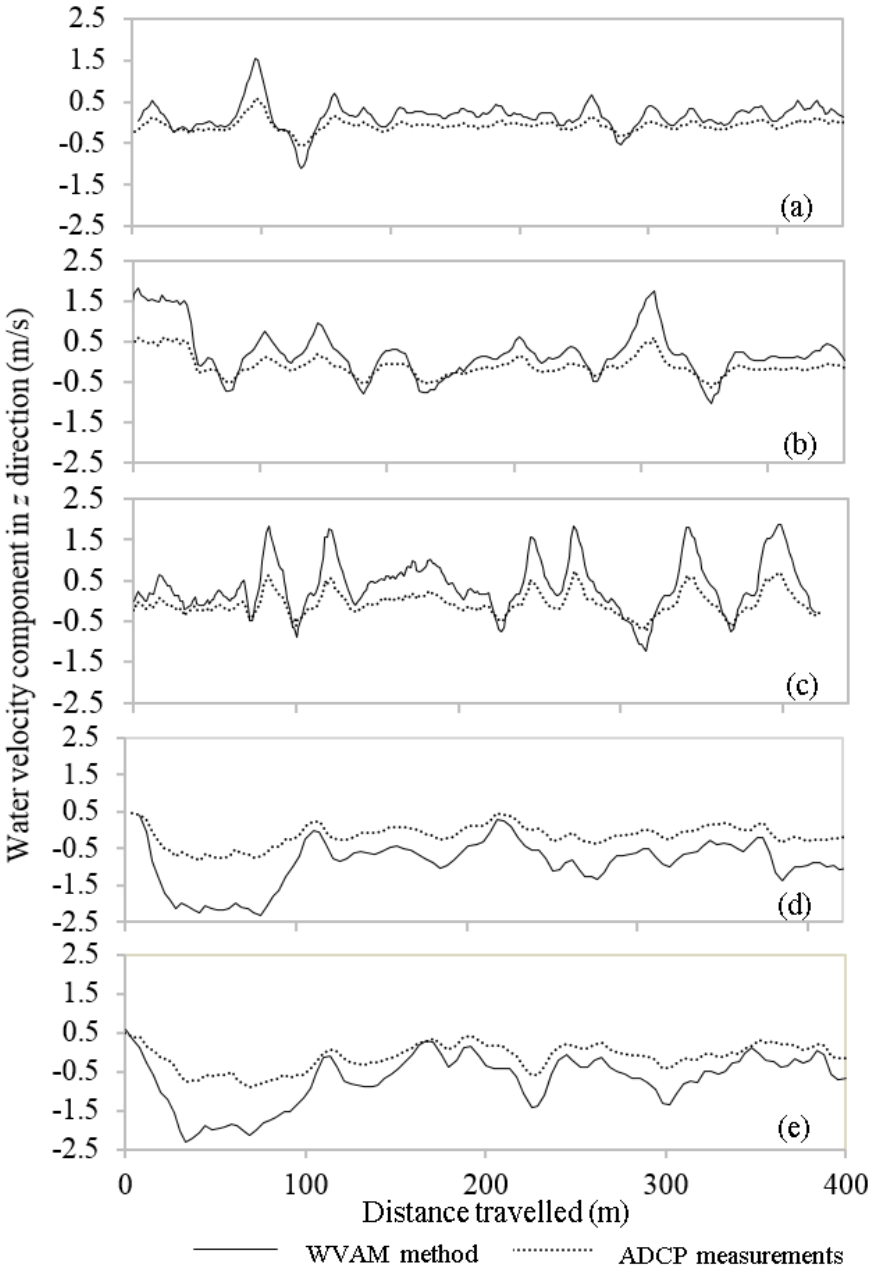

Figure A.5 – The vertical water velocity components from the WVAM method and ADCP measurements for AUV runs 1 to 5. Panels (a) to (e) sequentially present the data for these runs.

Generally, a standard error up to 0.1 m s^{-1} is acceptable as the uncertainty of the measurements from an AUV mounted ADCP is around ±0.1 m s^{-1} (Fong and Jones, 2006). The threshold averaged deviation of the pitch and yaw angles that provide the water column velocities with a standard error below 0.1 m s^{-1} is around 7º to 8º. Above this threshold angle the hydrodynamic coefficients usually become nonlinear. The hydrodynamic coefficients

estimated for the simulation model using the curve fitting method are only valid for small angles of incidence of the vehicle, i.e., where the coefficients are in the linear range. Therefore, when yaw and pitch angles are larger, the accuracy of the simulation model decreases and hence the uncertainty of the vertical and transverse water velocity components obtained from the WVAM method increases.

Table A.1 – Standard errors of the water velocity components determined from the WVAM method compared to the on-board ADCP measurements and the associated averaged deviations for the prescribed parameters.

Run Number	Standard error			Averaged deviation from the prescribed value		
	u	***v***	***w***	**Yaw angle (º)**	**Pitch angle (º)**	**Surge speed (m s^{-1})**
1	0.068	0.017	0.045	±1.5	±3.6	±0.2
2	0.029	0.153	0.075	±17.4	±7.1	±0.6
3	0.041	0.095	0.108	±3.5	±7.5	±0.7
4	0.063	0.061	0.241	±2.8	±9.2	±1.6
5	0.035	0.079	0.191	±5.6	±9.7	±1.6
6	0.042	0.063	0.052	±3.1	±3.1	±0.1
7	0.048	0.058	0.067	±2.6	±6.4	±0.3
8	0.025	0.104	0.092	±14.5	±7.4	±0.4
9	0.054	0.082	0.097	±5.8	±7.5	±0.6

The accuracy of the water velocity component in the *x* direction remains generally the same for all the runs regardless of the turbulence level of the environment. During the development of the simulation model, the hydrodynamic coefficients dominating the motion in the *x* direction were estimated for a propeller RPM range of 525 to 825 (i.e., a speed range of 1.43 m s^{-1} to 2.46 m s^{-1} in a calm environment). During this study, the AUV runs were conducted at 700 RPM, which typically provides a mean forward speed of around 2.04 m s^{-1} in calm water with a standard deviation of 0.01 m s^{-1}. The observed speed during the runs varied as much as ±1.6 m s^{-1} from the calm water speed of 2.04 m s^{-1}, especially in Runs 5 and

6 due to the AUV being 'dragged' by the strong tidal currents. Even though the actual speed deviated, the prescribed propeller speed of 700 RPM provides a calm water speed of around 2.04 m s^{-1} which is within the identified limits of the hydrodynamic coefficients dominating the forward motion. Therefore, the simulation model provided accurate prediction of the calm water based forward speed response of the AUV. Hence, the standard error between the WVAM and ADCP results in the *x* direction generally remained unrelated to the turbulence level of the water column.

Recommendations and future work

In order to expand the threshold of the WVAM method to higher turbulent environments, the simulation model should be improved to enable it to replicate the motion response of the vehicle in linear as well as nonlinear ranges. The hydrodynamic coefficients of an AUV could be obtained more accurately using techniques such as captive model experiments (Randeni et al., 2015b), Computational Fluid Dynamics (CFD) simulations (Randeni et al., 2015b) and system identification (Ljung, 1998). These methods could be employed to determine the coefficients within the linear and nonlinear ranges to improve the associated simulations and thus the predictions of the WVAM method.

Conclusions

The WVAM method is a non-acoustic technique to determine the water velocity components of a turbulent water column using the motion response of an AUV. This study investigated the accuracy of the WVAM method subject to the levels of turbulence in the water column. Nine AUV runs were conducted along the same AUV track line within the Tamar estuary in Tasmania, Australia, at different times in the tidal cycle.

Typically, when an AUV undertakes missions in rough water environments, the yaw and pitch angles of the vehicle fluctuate around the target values due to the inability of the AUV's dynamic controller to adequately compensate for the external disturbing forces. The greater the turbulence level of the water, generally larger are the fluctuations. The estimated water velocity components in the *y* and *z* directions using the WVAM method agreed well with the measurements from the AUV's on-board ADCP for low turbulent conditions where the averaged deviations of the vehicle's yaw and pitch angles are below 7º to 8º.

The hydrodynamic coefficients for the simulation model utilised in the WVAM method were determined using a curve fitting technique. These estimated coefficients were only valid for small angles of incidence of the vehicle, where the coefficients are in their linear range. Therefore, as the yaw and pitch angle fluctuations become larger, the accuracy of the simulation model decreases adversely affecting prediction of the vertical and transverse water velocity components using the WVAM method. During the AUV missions, the vehicle speed was maintained within the identified limits for the hydrodynamic coefficients dominating the forward motion. Therefore, the simulation model was able to provide an accurate prediction of the forward speed of the vehicle enabling the WVAM method to accurately determine the water velocities in x direction.

The WVAM method can be improved by upgrading the simulation model to replicate the motion response of the vehicle in both the linear and nonlinear ranges. The authors are expecting to achieve this by determining the hydrodynamic coefficients of the simulation model for a larger range using a comprehensive system identification study.

Appendix B: Least squares based system identification algorithm to obtain a mathematical model of an AUV

Appendix B is based on the conference article '*Least Squares Optimisation Algorithm Based System Identification of an Autonomous Underwater Vehicle*' published in the proceedings of the '*Third Vietnam Conference on Control and Automation*'. The citation for the article is:

Tran, M.Q., Randeni SAT, Nguyen, H.D., Binns, J., Chai, S. and Forrest, A.L., 2016. Least Squares Optimisation Algorithm Based System Identification of an Autonomous Underwater Vehicle. PROCEEDING of Publishing House for Science and Technology, 1(1).

Appendix B has been removed for copyright or proprietary reasons.

Appendix C: Numerical Investigation of the Hydrodynamic Interaction between Two Underwater Bodies in Relative Motion – A secondary CFD based approach of determining the hydrodynamic coefficients of an AUV

Appendix C is based on the journal article '*Numerical Investigation of the Hydrodynamic Interaction between Two Underwater Bodies in Relative Motion*' that is published in the journal '*Applied Ocean Research*'. The citation for the article is:

Randeni SAT, Leong Z, Ranmuthugala D, Forrest A, Duffy J. Numerical investigation of the hydrodynamic interaction between two underwater bodies in relative motion. Applied Ocean Research. 2015;51:14-24.

Abstract

The hydrodynamic interaction between an Autonomous Underwater Vehicle (AUV) manoeuvring in close proximity to a larger underwater vehicle can cause rapid changes in the motion of the AUV. This interaction can lead to mission failure and possible vehicle collision. Self-piloted, and comparatively small, an AUV is more susceptible to these interaction effects than the larger body. In an aim to predict the manoeuvring performance of an AUV under the effects of the interaction, the Australian Maritime College (AMC) has conducted a series of computer simulations and captive model experiments. A numerical model was developed to simulate pure sway motion of an AUV at different lateral and longitudinal positions relative to a larger underwater vehicle using Computational Fluid Dynamics (CFD). The variables investigated include the surge force, sway force and the yaw moment coefficients acting on the AUV due to interaction effects, which were in turn validated against experimental results. A simplified method is presented to obtain the hydrodynamic coefficients of an AUV when operating close to a larger underwater body by transforming the single body hydrodynamic coefficients of the AUV using the steady-state interaction forces. This method is considerably less time consuming than traditional methods. Furthermore, the inverse of this method (i.e., to obtain the steady state interaction force) is also presented to obtain the steady-state interaction force at multiple lateral separations efficiently. Both the CFD model and the simplified methods have been validated against the experimental data and are capable of providing adequate interaction predictions. Such methods are critical for accurate prediction of vehicle performance under varying conditions present in real life.

Introduction

Autonomous Underwater Vehicles (AUVs) are used in civilian, academic, and military applications due to their ability to undertake complicated tasks underwater without real time user control. A few examples of such applications include underwater surveillance (Kemna et al., 2011) and sampling physical transport processes in lakes (Forrest et al., 2008). AUVs are increasingly required to operate close to larger underwater vehicles such as submarines and larger Remotely Operated Vehicles (Rodgers et al., 2008), as well as to operate in swarms of AUVs of similar size (Osterloh et al., 2012). When operating in close proximity to a larger moving vehicle like a submarine, an AUV can experience motions resulting from the interaction of the wake and pressure fields generated by the larger body (Hardy and Barlow, 2008). Being relatively small and self-piloted, the AUV is more susceptible to these interaction effects, which can result in mission failure and, in extreme cases collision between the two vehicles. For this reason, it is critical to understand the manoeuvring performance of an AUV under these interaction effects in order to develop adequate control strategies (Leong et al., 2013).

While there have been considerable studies on hydrodynamic interactions between surface ships (Duffy and Renilson, 2011, Lataire et al., 2012, Vantorre et al., 2002) there is currently very little information on the interaction between submerged vessels in the public domain. Mawby et al. (2006) developed a high level architecture model to simulate the interaction between a moving submarine and a rescue submersible manoeuvring to the escape hatch of the submarine. This earlier model utilised pre-processed hydrodynamic interaction data obtained by solving the Laplace's equation using a boundary element method for the inviscid, irrotational flow past the vehicles' surfaces. The limitation of the utilised potential flow approach is that it does not account for fluid viscosity or wake field effects of the vehicles and will potentially oversimplify the interaction effects.

Previous numerical and experimental studies by Leong et al. (2013) have investigated the interaction effects on an AUV operating close to a larger vehicle for diameter ratios between the vehicles ranging from 2.237:1 up to 13.425:1 (i.e., displacement ratio from 10.419:1 to 139.878:1 respectively). The influence of different lateral and longitudinal distances between the two bodies over a range of speeds were investigated through Computational Fluid Dynamic (CFD) simulations and validated with captive model experiments. Leong (2013) also carried

out dynamic CFD simulations, modelling the pure sway motion of a smaller AUV model in close proximity to a larger AUV at one relative longitudinal position.

The work presented in this paper complements this previous work by considering a larger range of longitudinal positions and sway motion frequencies, with the information presented for a diameter ratio of 2.237:1 (i.e., displacement ratio of 10.419:1). The authors have also extended the capabilities of the CFD numerical model to simulate pure yaw motion of the AUV in close proximity to a larger body; however, will not be presented in this work. The numerical model was developed in ANSYS-CFX, utilising re-meshing techniques and was validated against experimental work conducted in the Towing Tank of the Australian Maritime College (AMC) at the University of Tasmania. Once validated, this numerical model can be extended to investigate the interaction between vehicles of larger diameter ratios, thus better representing the interaction between typical submarines and AUVs. A simplified method is presented to obtain the hydrodynamic coefficients of an AUV when operating close to a larger underwater body by transforming the single body hydrodynamic coefficients, using the steady state interaction forces. Using this method, the variation of hydrodynamic coefficients due to a second body could be estimated by conducting a less time consuming steady-state simulation, rather than time intensive dynamic pure sway motion simulations. Furthermore, the inverse of this method (i.e., to obtain the steady state interaction force) is also presented and validated. Inverse method is an efficient way of obtaining the steady-state interaction force at multiple lateral separations.

Methodology

Geometric models

The hydrodynamic characteristics of an AUV operating close to a larger underwater body were investigated through CFD and Experimental Fluid Dynamics (EFD) using two axisymmetric barehull underwater vehicle geometries. The research utilised a 1:2.801 scaled model of the SUBOFF submarine hullform developed by the Defence Advanced Research Projects Agency (DARPA) (Groves et al., 1989) as the smaller AUV, and a larger torpedo-shape body designated as NP01, with the principal dimensions of the models are shown in Figure C.1(a) and Table C.1. The diameter ratio of the NP01 model to the SUBOFF model is 2.237:1. The model scales were selected to ensure that they were sufficiently small to fit within

AMC's towing tank without causing blockage effects, but large enough to provide magnitudes of interaction forces that are larger than the experimental error levels.

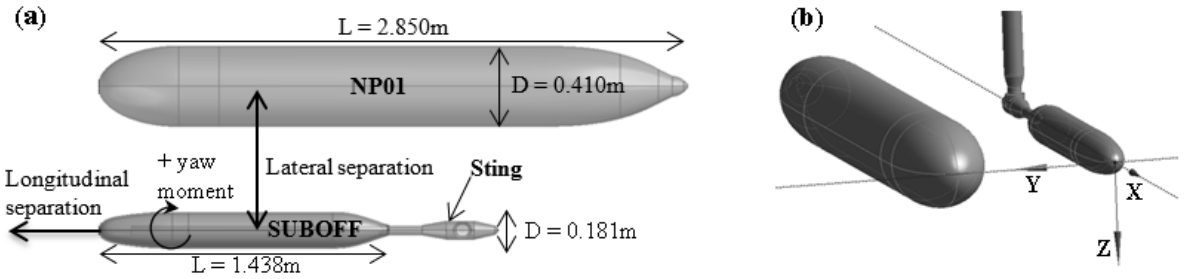

Figure C.1 – (a) The SUBOFF model alongside the larger NP01 model indicating the model dimensions and test rig arrangement along with (b) the assumed coordinate system

Table C.1 – Principal particulars of the two models

	SUBOFF Model	NP01 Model
Length (L)	1.438 m	2.850 m
Diameter (D)	0.181 m	0.410 m
Displacement (Δ)	0.031 m^3	0.323 m^3

Test parameters

The test runs consisted of straight-line and pure sway motions of the SUBOFF at different relative longitudinal and lateral positions to the larger NP01, with the investigated variables consisting of the surge force, sway force and the yaw moment experienced by the SUBOFF model. The lateral distance between centrelines of the two bodies was assumed to be the lateral separation distance, while the longitudinal separation distance was measured from the nose tip of the larger NP01 vehicle to that of the smaller SUBOFF vehicle; a 'positive' distance signifying that the SUBOFF model is located in front of the larger vehicle as shown in Figure C.1a. The longitudinal and lateral distances were non-dimensionalised as given in Equations C.1 and C.2. The coordinate system was selected according to ITTC (2011a) as shown in Figure C.1b.

$$\text{Longitudinal Separation Ratio } (R_{long}) = \frac{\text{Distance SUBOFF nose tip to NP01 nose tip}}{\text{Length of NP01}} \quad \text{(C.1)}$$

$$\text{Lateral Separation Ratio } (R_{lat}) = \frac{\text{Lateral Separation Distance}}{\text{Diameter of NP01}} \quad \text{(C.2)}$$

In order to isolate the interaction forces due to the larger second body, single body testings of the SUBOFF were conducted to provide baseline data. A summary of the single-body and two-body test parameters is outlined in Table C.2. The estimated Reynolds number (Re_{L_S}) is based on the length of the SUBOFF model, which is 1.438m.

Table C.2 – Test programme

Investigated parameters	**Straight-line Motion**	**Pure Sway Motion**
Forward Speed (m s^{-1})	1.2	
Reynolds number (Length)	19.39 $x10^5$	
Forces measured	Surge Force, Sway Force, and Yaw moment	
Single body tests		
Sway amplitudes (m)	-	0.145
Sway frequency (Hz)	-	0.2, 0.15, and 0.05
Two body tests		
Sway amplitudes (m)	-	0.145
Sway frequency (Hz)	-	0.2, 0.15, and 0.05
Longitudinal separation ratios	0.737, 0.491, 0.246, 0, -0.246, -0.491, -0.737	0.737, 0.491, 0.246, 0, -0.246, -0.491, -0.737
Lateral separation ratio	1.829	1.829

Definition of test motions

Straight-line motion

In the straight-line motion experiments, the bodies were moved in an equal forward velocity with a zero angle of attack. The aim of these tests was to obtain the sway and drag forces on the smaller SUBOFF body due to the forward motion when it is alongside the larger body. The obtained forces are referred to as the forces due to 'steady state straight-line motion'.

Pure sway motion

In the pure sway motion experiments, the SUBOFF model was moved forward at a constant velocity while undergoing sinusoidal oscillations in the *y* direction around its centre line (see Figure C.2) in order to obtain the surge force, sway force and the yaw moment due to sway velocity and sway acceleration. The angle of attack was maintained at zero. In pure sway motion, the sway displacement (y) is 90° out-of-phase with the sway velocity (v). The sway acceleration ($\dot{v}$) is in-phase with the sway displacement, while being 90° out-of-phase with the sway velocity. The forces and moments acting on the SUBOFF model due to sway motion is composed of both inertial and damping components, with the former is dependent on the acceleration while the latter is dependent on the velocity. The acceleration dependent component of the sway force becomes zero when the force is 90° out-of-phase with the displacement (i.e., when the velocity is at its peak and the acceleration is zero). This is termed as the 'sway force due to sway velocity (Fy_{out})', with its hydrodynamic coefficient obtained by differentiating Fy_{out} with respect to sway velocity (Lewis, 1988) as shown in Equation (C.3). Similarly, the acceleration component dominates when the sway force is in-phase with the displacement (Fy_{in}; i.e., when the acceleration is at its peak and the velocity is zero), with the coefficient (referred to as the added mass coefficient) obtained by differentiating Fy_{in} with respect to sway acceleration (Lewis, 1988) as shown in Equation (C.4).

$$Y_v = \frac{\partial Y}{\partial v} = \frac{Fy_{out}}{-a_0\omega} \tag{C.3}$$

$$Y_{\dot{v}} = \frac{\partial Y}{\partial \dot{v}} = \frac{Fy_{in}}{-a_0\omega^2} + m \tag{C.4}$$

where, Y_v is the sway force coefficient due to sway velocity; $Y_{\dot{v}}$ is the sway force coefficient due to sway acceleration (i.e., added mass coefficient); a_0 is the sway amplitude; ω is the sway frequency; and, m is the mass of the model.

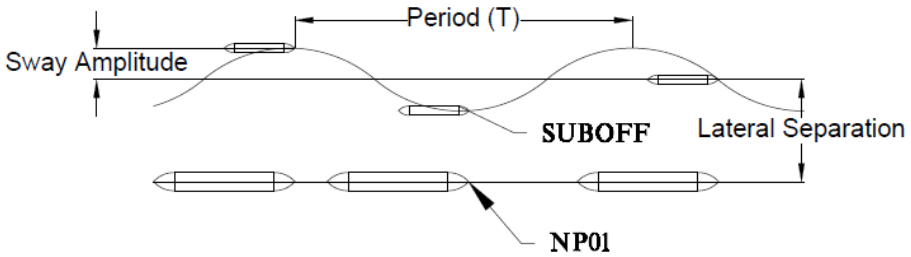

Figure C.2 – SUBOFF model undergoing the pure sway motion close to the larger NP01

Experimental setup

The captive model experiments were conducted in AMC's Towing Tank with the dynamic motion of the SUBOFF obtained using a Horizontal Planer Motion Mechanism (HPMM). The SUBOFF model was mounted to the HPMM using a 'sting', which connects to the model through the aft end as shown in Figure C.3a. The forces acting on the SUBOFF model were recorded using two 6-Degree of Freedom (6-DOF) load cells positioned in-line with the force balance located inside the model. The force balance is an extension of the sting that connects to the model via the load cells as shown in Figure C.3a. The SUBOFF model is not watertight, with vent holes allowing it to fill with water during testing. A gap in between the aft end of the model casing and the sting avoids contact between them eliminating friction and pre-tensioning effects. A Hama boundary layer transition strip device (Hama, 1957) was attached at 5% of the overall hull length aft of the model's leading edge to trip the laminar boundary layer into a turbulent one. The forces on the larger model were not recorded as modelling the larger vehicle was not an objective of this work. Figure C.3b shows the two models, with the NP01 attached to the towing tank carriage at an R_{lat} of 1.829. The NP01 had a 1m gap from its longitudinal centreline to the nearest side wall and was shifted longitudinally to achieve the desired R_{long} between the bodies. The R_{lat} was obtained by moving the SUBOFF laterally using the HPMM.

The variation of forces acting on the SUBOFF model due to the free surface was investigated by Steel (2010), concluding that the surface interference is negligible for non-dimensional depths of H/D greater than 3.3 (where H is the submerged depth from the surface waterline to the centreline of the vehicle as shown in Figure C.3a, and D is the model diameter). For this reason, the vehicles were positioned 0.75m below the waterline at mid-depth of the tank in order to minimise free surface effects as well as tank floor effects (i.e., the SUBOFF and the NP01 at non-dimensional depths of 4.147 and 1.852 respectively). The distance from the tank floor to the SUBOFF's and the NP01's bottom surface edges were 0.66m and 0.55m respectively. Further information with regard to the experimental setup is given in Barneveld (2013).

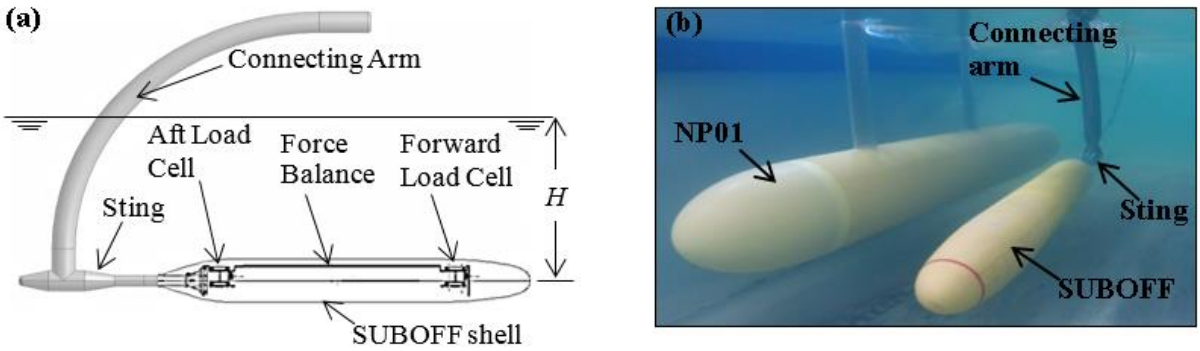

Figure C.3 – Experimental set up of (a) the SUBOFF model and (b) both the SUBOFF and NP01 model together

Numerical simulations

To assist with the validation of CFD results against EFD, the width and depth of the AMC towing tank were replicated in the numerical fluid domain. The numerical domain length was reduced to 20m from the towing tank length of 100m to reduce the computational effort while still capturing the wake field generated by the vehicles at the stern (see Figure C.4). Thus, it is assumed that reducing the modelled length of the towing tank has a negligible effect on the results.

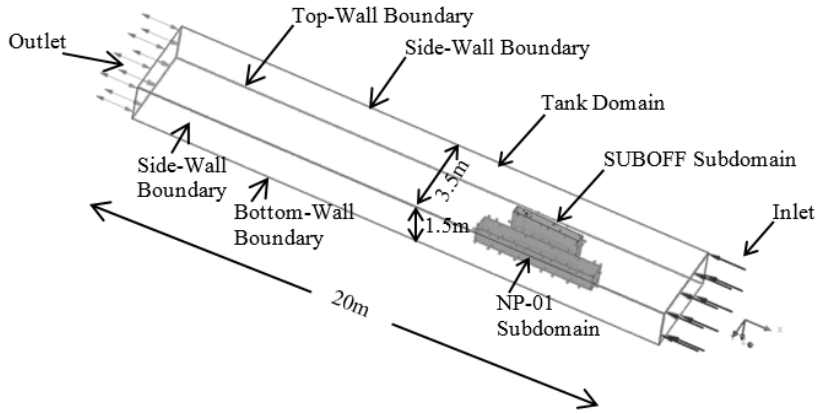

Figure C.4 – Numerical fluid domain subdivided to represent the tank domain, SUBOFF subdomain and NP01 subdomain

In simulating the fluid flow around the submerged bodies, the Reynolds Averaged Navier Stokes (RANS) equations were utilised. Leong et al. (2012a) evaluated the performance of two RANS-based turbulence models (i.e., Baseline Reynolds Stress Model (BSLRSM) and Shear Stress Transport with Curvature Correction (SSTCC)) in predicting the flow around the SUBOFF model and obtaining hydrodynamic coefficients under translation and rotational flow

conditions. Leong et al. (2012a) showed that the BSLRSM solution was the closest in comparison to the experimental results and was thus utilised in this investigation. This low Reynolds wall treatment model is recommended only when accurate prediction of separation wall-bounded flows are desired and $y^+ < 1$ (where y^+ is the non-dimensional value of the distance from the surface of the body to the first node of the mesh) is utilised, conditions that were adhered to in all simulations.

The ANSYS Meshing Platform (AMP) re-meshing method was used to simulate the relative motion between the two bodies. The essential aspect of this method is that the mesh in the fluid domain deforms locally around the moving object as it moves, and re-meshes when the mesh quality is deemed compromised in terms of accuracy and stability (Leong et al., 2012b). This overcomes the limited motions imposed by using a pure mesh deformation approach and allows rotation of the bodies to be compared to other re-meshing methods. Although mesh deformation is fully supported in ANSYS CFX, currently the re-meshing requires the use of a user-defined script. The latter, triggered by the mesh quality criterion, interrupts the simulation and transfers the positional state of the SUBOFF into ANSYS Workbench in order to update the geometry and the mesh. The script then transfers the new mesh into the solver where the simulation information from the previous mesh is interpolated into the new mesh and the simulation is resumed. The mesh quality criterion was defined as the orthogonality angle in the mesh cells of no less than 10° (Leong, 2013). The fluid domain of the study was formed from three sub-domains (see Figure C.4): the SUBOFF sub-domain, the NP01 sub-domain and the tank domain. In order to reduce the re-mesh time, the vehicle sub-domains were pre-meshed and were kept rigid during the solver process, while the tank domain underwent mesh deformation and re-meshing.

Meshing

To aid the validation, the experimental setup was identically replicated by the CFD mesh model. The mounting arrangement of the SUBOFF model to the HPMM (i.e., the sting) can cause pressure field variations and generate an additional wake field. Thus, the sting arrangement was modelled in the CFD simulations. During the experiments, the internal hollow section of the SUBOFF shell was filled with water and, as the tests involved accelerative motions, the inertial effects produced by the water inside the SUBOFF model were proven to be significant. Therefore, the internal water was meshed and interfaced with the surrounding water as shown in Figure C.5 (inset). The inertial effects due to the mass of the SUBOFF's

shell was modelled by defining the density of the shell material (i.e., fibreglass plastic) to the mesh within the shell. Predictions of the inertial forces may vary from exact physical values as the internal water volume and the mass of the SUBOFF shell cannot be accurately modelled due to the complexity of the force balance arrangement inside the shell and due to the uneven shell density.

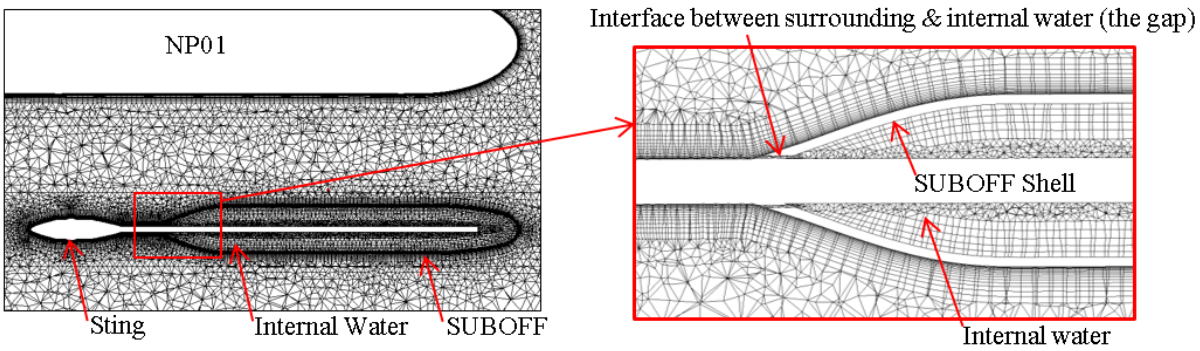

Figure C.5 – Mesh model around the sting and two submerged model bodies and the internal water of the SUBOFF (Inset) to closely replicate the EFD. The mesh of the SUBOFF shell is removed in the inset to provide a detail illustration of the interface gap.

It is well documented that the total thickness of the inflation prism layers should be at least the thickness of the boundary layer (White, 2011), where the inflation prism layer is a layer with very small mesh elements in the direction normal to the wall that resolves the wall region to aid the turbulent model to capture the boundary layer (Tu et al., 2012). If the thickness of the inflation prism layers is under-prescribed, this will 'squash' the predicted boundary layer in the simulation and correspondingly affect the forces acting on the vehicle. Overprescribing the thickness does not affect the force predictions; however, it will increase the number of mesh elements. Thus, the total thickness of the inflation layers around the SUBOFF was matched to Prandtl's theoretical estimate of the turbulent boundary layer thickness over a flat plate (White, 2011) using $0.16L_S/\,Re_{L_S}{}^{1/7}$, where L_S is the surface length of the vehicle and Re_{L_S} has previously been defined.

Mesh independence study

The mesh independence studies were conducted to select the optimum mesh size that provides sufficiently accurate results while maintaining a low computational effort. The studies were first conducted for the pure sway manoeuvres to investigate the effects of the vehicles' surface and the surrounding mesh sizes on the interaction prediction. This research work utilised an unstructured mesh type and it is not possible to make completely systematic mesh

refinements in unstructured meshes since the size of individual cells cannot be controlled directly (Simonsen et al., 2012). Therefore, it is difficult to estimate the mesh uncertainty. However, four meshes (i.e., S1, S2, S3 and S4, where the S1 is the finest mesh and S4 is the coarsest) were generated by carrying out mesh refinements with an approximate refinement ratio of $\sqrt{2}$ and, the surge force, sway force and yaw moment solutions were obtained from each mesh. The finest mesh contained 4.86 million elements, while the coarsest mesh contained 1.49 million elements. Figure C.6 illustrates the maximum percentage difference of the force predictions from each mesh size compared to the results from the finest mesh. The computational time taken for each mesh size simulation is also provided. The mesh convergence and the mesh uncertainty were investigated according to the procedure recommended by Stern et al. (2001) and Wilson et al. (2001). The mesh convergence ratios (i.e., R_G) for the surge force, sway force and yaw moment calculated from the finest three (i.e., S1, S2 and S3) and the coarsest three (i.e., S2, S3 and S4), out of the four meshes were within the range of 0.56 and 0.67. The convergence is deemed to be achieved since the convergence ratios were within $0<R_G<1$ (Stern et al., 2001). Therefore, the Richardson extrapolation (Simonsen et al., 2012, Stern et al., 2001) was used to estimate the mesh uncertainty. The estimated mesh uncertainties for the surge force, sway force and yaw moment were less than 1.6% of the S1 mesh solutions (i.e., the solutions from the finest mesh) and were less than 2.4% of the solutions from the S2 mesh. The S2 mesh (i.e., the 2.8 million element mesh) was selected as the optimum mesh since both the surge and sway force predictions were within 1% of the finest mesh force predictions (see Figure C.6) and within 2.4% of the corrected solutions. The selected mesh maintained around 53% less computational time compared to the finest mesh; i.e., run time reduced from 9.5 days to 4.5 days.

The mesh independence studies for the steady-state straight-line simulations were conducted by carrying out mesh refinements on the vehicle surfaces and the pressure interaction region between the vehicles. The finest mesh contained 6 million elements, while the coarsest mesh contained 1.2 million elements. The mesh convergences for the surge force, sway force and yaw moment were calculated similar to the pure sway simulations and were found to be within the converging range (i.e., $0<R_G<1$). The estimated mesh uncertainties were less than 2% of the solutions from the selected three million element mesh.

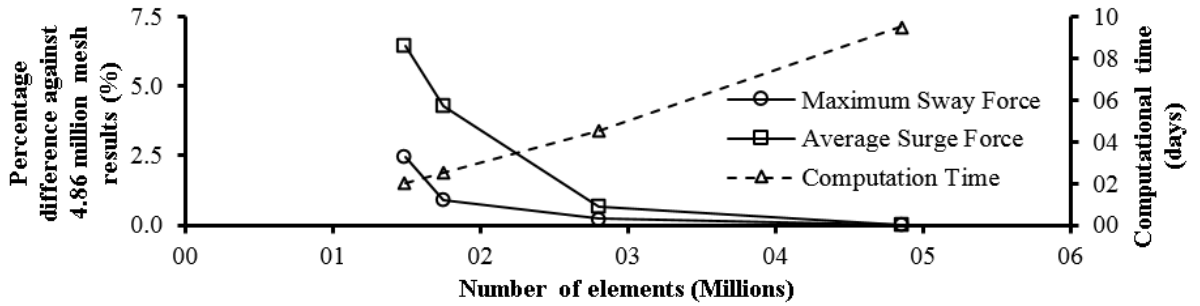

Figure C.6 – Percentage uncertainty of the sway force and surge force with respect to the finest mesh

To ensure numerical accuracy and stability, all simulations were performed using a high order advection and second order backwards Euler transient scheme. Convergence was deemed achieved when solution residuals reduced to below 10^{-4} and reduced by more than three orders of magnitude using a maximum of 10 inner iteration loops per time-step.

Time-step independence study

The dynamic simulations tend to fail if the utilised time-step was too large, since moving wall particles may cross more than one element per time-step and will pass their node solutions into an unknown element (Leong et al., 2012b). The largest possible time-step that could successfully carry-out the simulation for the selected mesh size was estimated to be 0.01s. The influence of the simulation time-step was investigated by comparing the sway force responses for three time-steps (i.e., 0.01s, 0.008s, and 0.006s) with the predictions found to be relatively consistent with respect to the different time-steps (see Figure C.7).

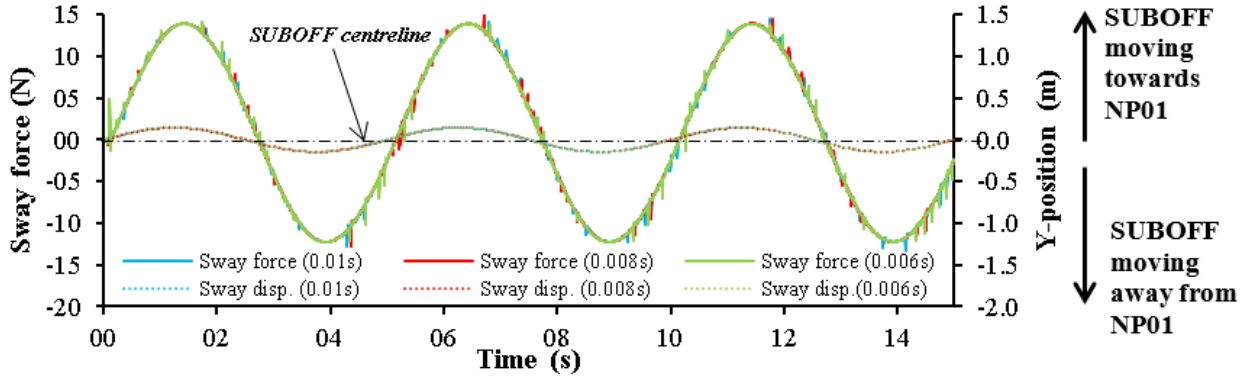

Figure C.7 – Sway force responses for simulation time-steps of: 0.01s, 0.008s & 0.006 (note that the sway forces from the three time-steps coincide each other).

The maximum percentage difference between the sway force predictions for the time-steps 0.01s and 0.006s was 0.4%. Therefore, a 0.01s time-step was utilised for the simulations

to reduce the simulation time. The spikes observed in force responses seen in Figure C.7 are due to the simulation initiations at re-mesh events, and are filtered out using a low pass filter.

Validation of numerical results

For validation purposes, the force responses obtained from CFD simulations were compared against those obtained from EFD. Figure C.8 shows the CFD and EFD sway force responses obtained from a two body pure sway motion test. It is seen that CFD and EFD responses vary in both magnitude and phase. The maximum magnitude deviation was below 5.58% for all validated cases.

Phase difference between CFD and EFD sway force responses

A phase shift between the CFD and EFD force responses obtained from such Planner Motion Mechanism (PMM) tests and other similar tests is usually observed (Carrica et al., 2013, Górnicz and Kulczyk, 2011, ITTC, 2011b, Sakamoto et al., 2012). Whilst some predict that it is due to inaccurate initial conditions (Sakamoto et al., 2012), others consider these to be possible experimental errors. However, this is an area of ongoing research. The minimum phase difference of 0.4% was seen at the lowest sway frequency (i.e., 0.05 Hz) and the maximum difference of 4.8% was observed at the highest sway frequency (i.e., 0.2 Hz). The phase difference between the CFD and EFD sway forces was directly proportional to the sway frequency. The effects of modelling uncertainties of the internal hollow section and the shell density of the SUBOFF are more significant at higher sway frequencies due to the higher acceleration. Thus, the phase uncertainty of CFD results could be partly due to the modelling uncertainties of the internal hollow region and internal free flood water section of the SUBOFF model. The other possible reasons for the difference could be an over prediction of the added mass within CFD and/or due to experimental errors. As the phase difference of the results are less than 5% for all the sampled frequencies and is within the experimental uncertainty, it was considered to have minimal effect to the main findings of the paper.

Validation of hydrodynamic coefficients between CFD and EFD results

In this section, the hydrodynamic coefficients derived through CFD results are compared against those obtained through EFD. The sway force coefficient due to sway acceleration ($Y_{\dot{v}}$) is derived using Equation (C.4) from the sway forces recorded in-phase with displacement (i.e., Fy_{in} as shown in Figure C.8). A positive (+) displacement indicates that the lateral separation

between the SUBOFF model and NP01 is less than that at the starting position and a negative (-) displacement indicates that the lateral separation between the models is larger than that at the starting position (for single body tests, this represents the SUBOFF model at the starboard and the port sides from the starting position respectively). The non-dimensionalised CFD & EFD force coefficients, recorded in-phase with displacement, are presented in Table C.3. The forces were non-dimensionalised using Equation (C.5),

$$\text{Non-dimensional sway force } (Fy') = \frac{2F}{\rho L^2 u^2} \qquad \text{(C.5)}$$

where, F is the force, ρ is the specific density of fresh water, L is the length of the model, and u is the surge velocity component.

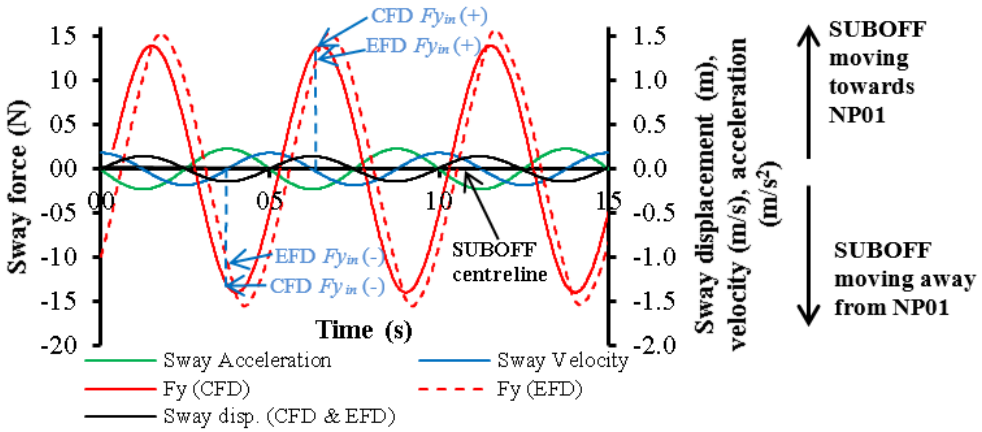

Figure C.8 – CFD and EFD sway force responses for pure sway motion at 0.2 Hz

Table C.3 – Variation of $F'y_{in}$ with sway frequency

Frequency	CFD $Fy'_{in}(+)$	EFD $Fy'_{in}(+)$	Difference	CFD $Fy'_{in}(-)$	EFD $Fy'_{in}(-)$	Difference
0.2 Hz	0.0081	0.0077	5.4%	-0.0081	-0.0079	2.7%
0.15 Hz	0.0046	0.0048	3.2%	-0.0047	-0.0048	2.0%
0.05 Hz	0.0005	0.0006	18.0%	-0.0005	-0.0007	19.4%

It is seen that the CFD Fy'_{in} are in good agreement with EFD (with the greatest percentage difference of 5.4%) for sway frequencies of 0.2 Hz and 0.15 Hz. Even though the difference for 0.05 Hz is around 20%, the actual difference in forces predicted using CFD and those measured from EFD is smaller due to the lower frequency and is within the experimental bias

error of +/- 0.2 N. For this reason, it is proposed that the numerical models can be used to obtain $Y_{\dot{v}}$.

Results and discussion

The sway force response due to the pure sway motion of the SUBOFF model tested alone (termed as $Fy_{(SUBOFF)}$ in the following discussion) is a symmetric sinusoidal response along the time axis. Thus, the hydrodynamic coefficients (i.e., Y_v and $Y_{\dot{v}}$) derived from positive or negative displacement cycles of motion (i.e., when the SUBOFF model is on the starboard or port sides from its starting position respectively) are equal in magnitude (see Figure C.9). However, when the SUBOFF model is operating in proximity of the larger NP01 body, the sway force response is influenced by the interaction with the pressure field of the latter. Figure C.9 shows that the two body response is shifted towards the positive y-direction as compared to the single body response. The shift is not uniform (i.e., the interaction force is higher when the SUBOFF is closer to NP01). This is due to the increasing influence of the pressure field generated by the NP01 as the SUBOFF draws nearer, compared to that when the SUBOFF is further away. Due to the asymmetry of the two body sway force response; the hydrodynamic coefficients obtained from positive and negative displacement cycles are not equal in magnitude. Thus, the hydrodynamic coefficients of the SUBOFF, when moving towards and away from the NP01 are different.

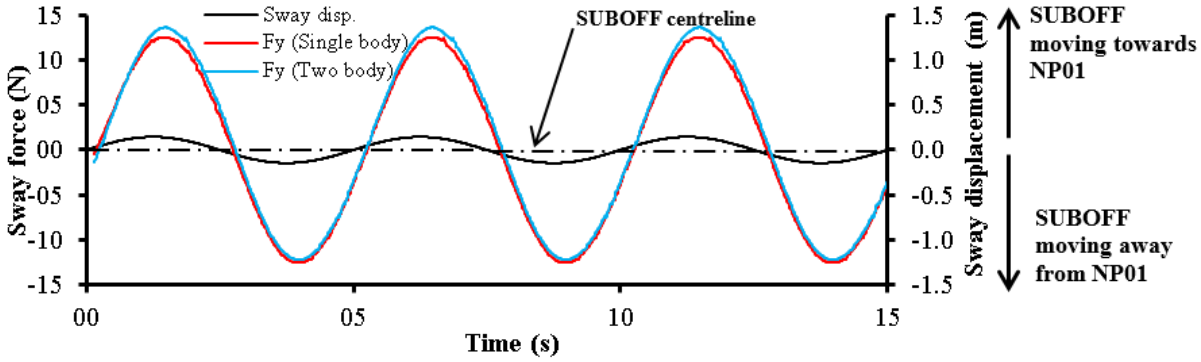

Figure C.9 – Sway force responses for single and two body simulations (at R_{long} of 0 and R_{lat} of 1.829)

Interaction forces and moments

With the aim of quantifying the interaction forces (i.e., $Fy_{(interaction)}$) acting on the SUBOFF model due to the pressure of the larger body, the interaction forces are defined as,

$$Fy_{(two\ body)} = Fy_{(SUBOFF)} + Fy_{(interaction)} \quad \text{(C.6)}$$

The interaction sway force was non-dimensionalised to obtain the interaction sway force coefficient using Equation (C.5) by substituting $Fy_{(two\ body)}$ as the force.

Interaction sway force against lateral separation

The variation of the isolated interaction force coefficient when the SUBOFF model is moving towards and away from the larger body is plotted against the sway displacement in Figure C.10. For all the analysed cases, the interaction force when the SUBOFF is moving away from the larger body was observed to be higher than when it is moving towards it. Figure C.11 shows that a low pressure field is generated throughout the span of the larger body, which becomes significant in the regions with longitudinally curved surfaces (i.e., just after the bow and just before the stern). When the SUBOFF model sways while moving forward, a low pressure region is generated at the opposite side to the SUBOFF's sway direction. In Figure C.11a when the SUBOFF model moves towards the larger body, the low pressure fields due to the larger body and the SUBOFF's sway motion are at opposite sides of the SUBOFF. Thus, the interaction sway force due to resultant pressure field is lower, as the SUBOFF's pressure field due to the sway motion is opposing the interaction force of the NP01. However, when the model moves away from the larger body as seen in Figure C.11b, the low pressure fields due to the larger body and the SUBOFF's sway motion are both in between the two bodies. Thus, the SUBOFF's own pressure field complements the interaction sway force, resulting in a higher attraction force.

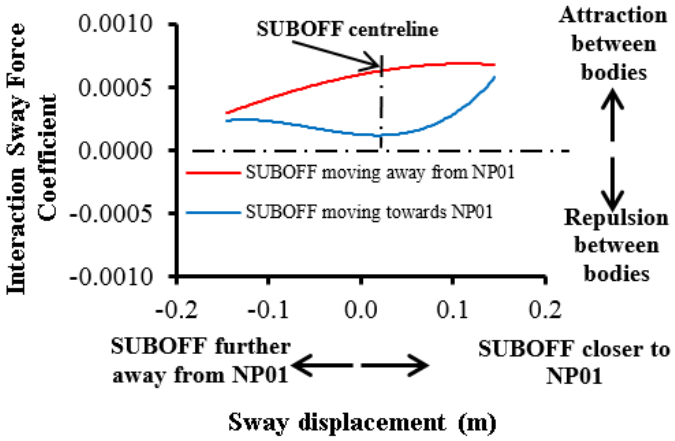

Figure C.10 – Interaction sway force coefficient against sway displacement (at R_{long} of 0)

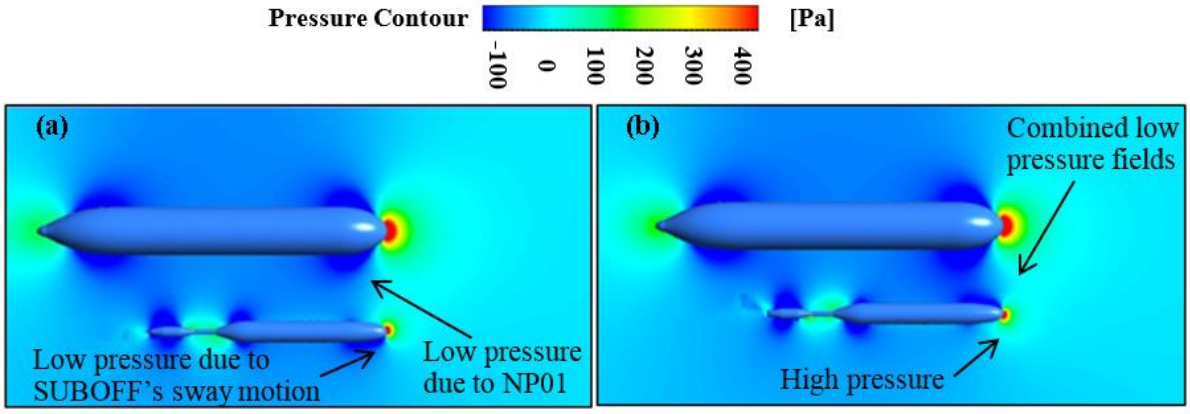

Figure C.11 – Visualisation of the predicted two-body pressure interaction field with (a) the SUBOFF moving towards NP01 and (b) the SUBOFF moving away from NP01 (at R_{long} of 0 and R_{lat} of 1.829)

Interaction sway force and yaw moment against longitudinal separation

The variation of the interaction sway force and yaw moment coefficients against the longitudinal separation of the two bodies are shown in Figure C.12 and Figure C.13 respectively. The forces and moments were recorded at positive peaks of the sway displacement (i.e., when the SUBOFF is closest to the NP01 model during each cycle). The sway forces were quantified for three sway frequencies of 0.2 Hz, 0.15 Hz and 0.05 Hz. The yaw moment was calculated at a reference point where the single body yaw moment reached zero (i.e., 0.701 m aft of the SUBOFF nose tip). Therefore, the yaw moment shown in Figure C.13 is purely due to the interaction with the larger body. The positive yaw moment represents the SUBOFF bow attempting to yaw towards the NP01 as shown in Figure C.1a. The yaw moment was non-dimensionalised using Equation (C.7).

$$\text{Non-dimensional yaw moment } (N') = \frac{2N}{\rho L^3 u^2} \qquad \text{(C.7)}$$

where, N is the yaw moment, ρ is the specific density of fresh water, L is the length of the model, and u is the surge velocity component.

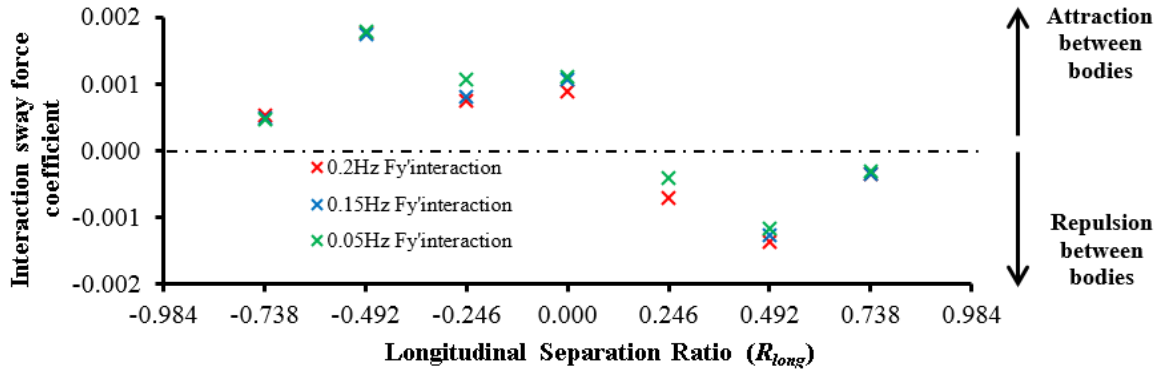

Figure C.12 – Interaction sway force coefficient due to sway acceleration vs R_{long} (at R_{lat} of 1.475, sway amplitude of 0.145m and sway frequency of 0.2 Hz)

Figure C.14 illustrates the pressure visualisation with longitudinal separation. When R_{long} is -0.737, the SUBOFF nose tip reaches the low pressure region around the aft section of the NP01 model. Furthermore, the confined area between the SUBOFF bow and the NP01 causes an increase in the flow velocity between the two bodies, resulting in the intensification of the low pressure field (in accordance with Bernoulli's theorem). The low pressure field between the two bodies attracts the SUBOFF towards the NP01 (i.e., a positive interaction force as shown in Figure C.12). However, the stern of the SUBOFF is still within the relatively higher pressure region aft of the NP01. Thus, the combination of the high and low pressure fields acting on the stern and forward regions of the SUBOFF respectively results a positive yaw moment as shown in Figure C. 13 (i.e., a moment acting on the SUBOFF yawing its bow towards the larger body).

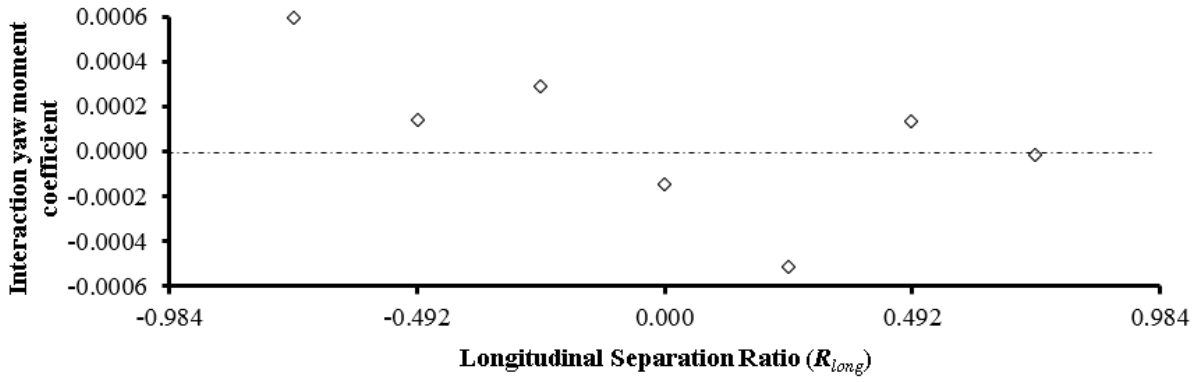

Figure C.13 – Interaction yaw moment coefficient vs. R_{long} (at R_{lat} of 1.475, sway amplitude of 0.145m and sway frequency of 0.2 Hz)

When R_{long} is -0.491, the entire SUBOFF model is within the low pressure interaction field created by the aft section of the NP01. Furthermore, the restricted space between the two

bodies creates a second low pressure field along the length of the SUBOFF. These two low pressure fields attract the SUBOFF towards the NP01, causing the highest attraction force. However, the yaw moment is relatively small as both the bow and the stern of the SUBOFF are attracted towards the NP01 model.

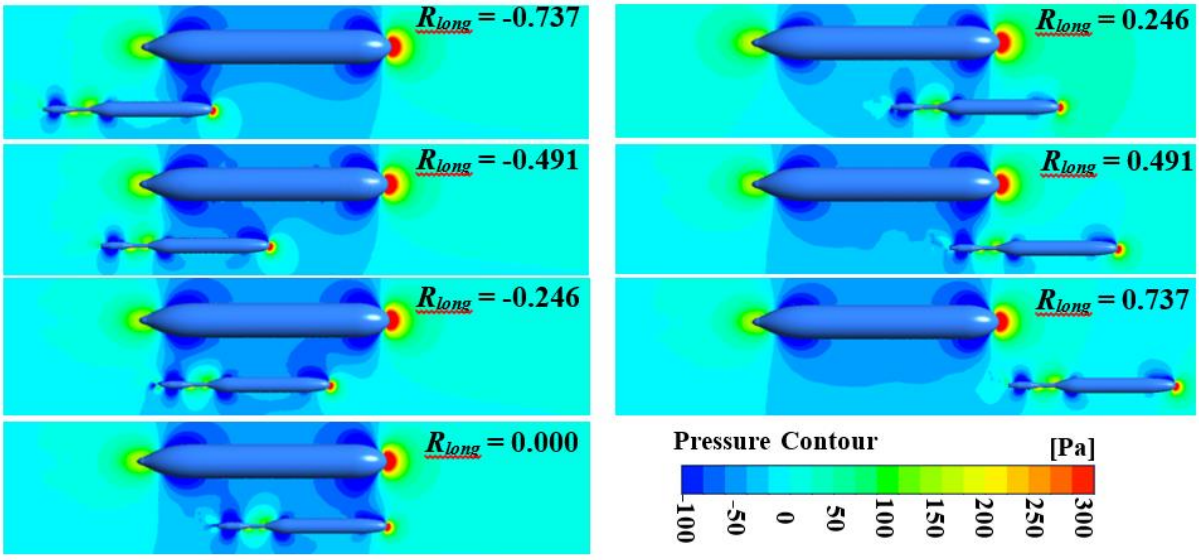

Figure C.14 – Pressure visualisation for different R_{long} (at R_{lat} of 1.829)

When R_{long} is -0.246, the SUBOFF is located within the mid-body region of the larger NP01 model. The intensity of the low pressure field due to the NP01 reduces in this region due the parallel mid-body section. However, the low pressure created due to the accelerated flow field between the two bodies attracts the SUBOFF towards the NP01, producing the lowest interaction force. The SUBOFF bow is attracted towards the NP01 due to the low pressure field created at the bow of the NP01, resulting in a positive yaw moment.

The attraction force again increases when the R_{long} is 0, due to the increase in the low pressure field located just aft of the bow of the larger body. The SUBOFF bow is pushed away from the NP01 by the high pressure field around the stagnation point of the latter, while the SUBOFF stern is attracted towards the NP01, resulting in a negative yaw moment.

As the SUBOFF moves further along the length of NP01 to a R_{long} of 0.246, the bow of the SUBOFF model moves into the high pressure region around the stagnation point of the NP01, which pushes the bow of the SUBOFF further away from the larger body, The stern of the SUBOFF is pulled towards the NP01 by the low pressure field located just after the bow of the latter. This results in an overall negative sway force and a yaw moment.

When R_{long} is +0.491, the entire SUBOFF is within the forward high pressure region, causing the highest repulsive interaction force. The stern of the SUBOFF is pushed away from the NP01 due to the high pressure region at the stagnation point of the NP01 causing a slightly positive yaw moment. When R_{long} is 0.737 the smaller body moves further away from the high pressure region, progressively reducing the repulsive interaction sway force as well as the positive yaw moment.

Although the trends of interaction force variations for the three frequencies shown in Figure C.12 are similar, their magnitudes do vary as much as 24%, especially when the two bodies are alongside. This shows that the interaction force is frequency dependent.

Interaction surge force

A similar analysis was carried out for the interaction surge force ($Fx_{(interaction)}$), which varies with the sway displacement and the direction of sway (i.e., whether towards or away from the larger body). However, unlike the interaction sway force, the interaction surge force is higher when R_{long} is below 0.246 and the SUBOFF model is moving away from the larger body than when moving towards it, but opposite when R_{long} is above 0.246 (see Figure C.15).

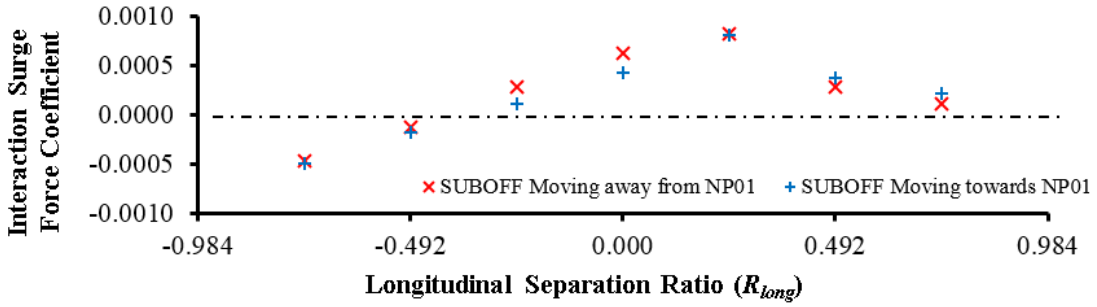

Figure C.15 – Interaction surge force coefficient vs. R_{long} (at R_{lat} of 1.475, sway amplitude of 0.145m and sway frequency of 0.2 Hz)

According to the pressure visualisations shown in Figure C.14, at R_{long} of -0.737 and -0.491, a low pressure region is located ahead the SUBOFF, effectively reducing the drag force. Thus, when R_{long} is lower than -0.491, the drag force acting on the SUBOFF model due to the interaction with the larger body is lower than the drag force for the single body (see Figure C.15). When the R_{long} is higher than -0.246, the high pressure region located forward of the SUBOFF model increases the drag force, resulting in it being greater than the single body drag force. Leong et al. (2013) investigated the steady state surge force acting on the SUBOFF model when operating in close proximity to the NP01, and concluded that it is unaffected by the larger body when the R_{long} is above 1.02 and below -1.19.

The above results indicate that the hydrodynamic coefficients of an AUV vary with the influence of interactions caused by third party objects; in this case a larger moving body. However, similar outcomes could be expected for other types of boundaries such as jetty walls, seabed, and surface ice layers (Ananthakrishnan, 1998, Ananthakrishnan and Zhang, 1998).

Proposed simplified method to predict interaction sway force

A simplified method was developed to obtain the two body hydrodynamic coefficients using single body hydrodynamic coefficients and steady-state interaction force due to straight-line motion. The inverse of this approach was also validated, i.e., obtaining the steady-state interaction force from two body hydrodynamic coefficients. The following section introduces the method, its validation and limitations

Simplified method: obtaining the two body hydrodynamic sway forces

A new term called the 'quasi-static' sway force is defined by adding the steady-state interaction force due to straight-line motion to the single body pure sway force as shown in Equation C.8.

$$Fy_{(quasi\text{-}static)} = Fy_{(two\ body,\ steady\ state)} + Fy_{(single\ body,\ dynamic)} \quad (C.8)$$

where, $Fy_{(two\ body,\ steady\ state)}$ is the steady state sway force on the smaller body due to straight-line forward motion of the two bodies together; and $Fy_{(single\ body,\ dynamic)}$ is the sway force on the smaller body obtained from single body pure sway motion. The lateral separation ratio of the tests should be maintained at the ratio at which the quasi-static sway force is required.

The quasi-static sway forces are compared against the sway forces obtained from two body pure sway motion tests (i.e., $Fy_{(two\ body,\ dynamic)}$) in Figure C.16. The sway forces were recorded in phase with displacement (i.e., the sway force due to sway acceleration). The positive (+) and negative (-) signs indicate that the forces were measured when the SUBOFF model is closer or further away from the centreline of motion to the larger NP01 body respectively. The maximum percentage difference between $Fy_{(quasi\text{-}static)}$ and $Fy_{(dynamic)}$ is below 14% for all the test cases. Therefore, it could be deduced that the quasi-static sway force ($Fy_{(quasi\text{-}static)}$) is a good indicator of the two body dynamic sway force acting on the smaller body ($Fy_{(two\ body,\ dynamic)}$).

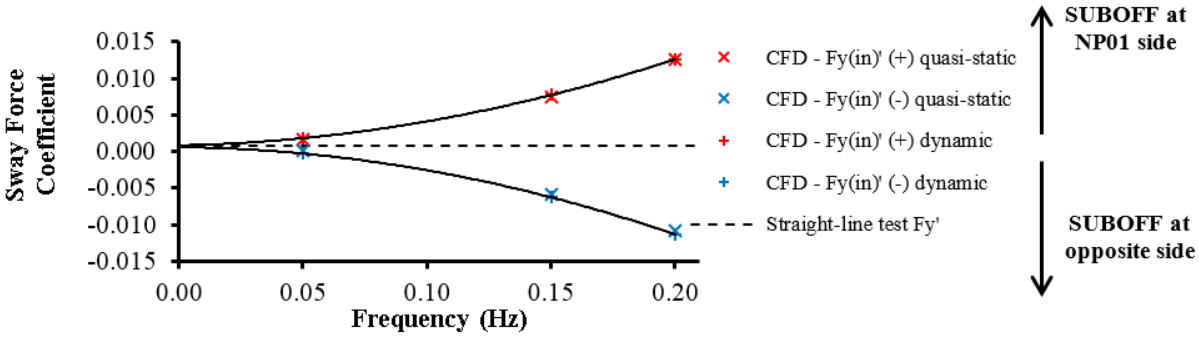

Figure C.16 – Comparison of quasi-static and dynamic $Fy_{(in)}'$

Using this method, the hydrodynamic coefficients of an AUV when operating close to a larger body could be estimated by simply adding the steady-state interaction force coefficients (obtained from Equations (C.3) and (C.4) by substituting Fy_{out} and Fy_{in} with the steady-state force) into the single body hydrodynamic coefficients (i.e., $Y_{\dot{v}}$ and Y_v). Therefore, the variation of hydrodynamic coefficients due to a second body could be estimated by conducting a cost effective steady-state simulation, rather than time intensive dynamic pure sway motion simulations. This method might also be valid for when the AUV is manoeuvring near other types of stationary boundaries such as sea-bed, wall boundaries, and under ice layers, and is worth investigating since the method will save time. However, the proposed method has the following limitations:

- the sway frequency and amplitude of the single body pure sway motion tests should be the same as the sway frequency and amplitude of the required $Fy_{(quasi\text{-}static)}$;
- the lateral body separations of the measured $Fy_{(steady\ state)}$ and $Fy_{(single\ body,\ dynamic)}$ should be equal to the lateral body separation of the required $Fy_{(quasi\text{-}static)}$; and
- the proposed quasi-static approach is validated only for the range shown in Table C.2.

Inverse of the simplified method: obtaining the steady-state interaction sway force

Inverse of the above simplified method is to obtain the two body steady-state interaction force due to straight-line motion using the sway forces obtained from two body pure sway motion tests. The second order polynomial extrapolation of $Fy_{(two\ body,\ dynamic)}$ meets the steady-state interaction force at the sway frequency of 0 Hz (see Figure C.16), with a percentage variation of less than 8%. Similar patterns were observed in all the analysed cases. Therefore, this method could be used to obtain the steady-state interaction sway force due to forward

motion at any lateral separation (within the sway amplitudes) using a set of pure sway motion tests and this method is an efficient way of obtaining the steady-state interaction force at multiple lateral separations. The limitations of this method are as follows:

- validations is limited to the range shown in Table C.2; and
- the steady-state interaction forces obtained from the current study are relatively small due to the small body diameter ratio between the two models, thus, the accuracy of the proposed method needs to be further validated by replicating the study for models having a larger body diameter ratio.

Conclusions

An investigation into the hydrodynamic interaction between an AUV operating in close proximity to a larger moving vehicle such as a submarine was conducted, with the development of a CFD model to replicate the pure sway motion of the AUV under these conditions. The model was validated through physical experimental work conducted using an AUV model fitted to an HPMM and a larger adjacent body moving along the axial direction in AMC's Towing Tank. The percentage difference between the CFD and EFD sway forces were generally below 6% and within the experimental error margins.

The maximum hydrodynamic interaction sway force acting on the smaller body due to the presence of the larger NP01 body was found to be an attraction force when the former is located behind the nose of the latter (i.e., when the longitudinal separation ratio is below zero) and vice versa. This was due to the low pressure field created around the span and the high pressure field created around the nose region of the larger body. The lowest interaction between the two bodies occurred when the smaller body is located around the midship section of the larger body. Furthermore, the interaction sway force coefficient when the SUBOFF is moving towards the NP01 was found to be lower than that when it is moving further apart due to the low pressure field created around the span of the larger body.

The proposed simplified method is able to estimate the hydrodynamic coefficients of an AUV when operating close to a larger underwater body by simply adding the steady-state interaction force coefficient to the single body hydrodynamic coefficient, with a maximum percentage variation of 14%. Therefore, the variation of hydrodynamic coefficients due to a

second body could be estimated by conducting a cost effective steady-state simulation, rather than time intensive dynamic pure sway motion simulations. The inverse of this method is able to provide an approximation of the steady-state interaction force at any lateral separation (within the amplitudes of the pure sway motion tests) using the two body sway force due to pure sway motion with a maximum percentage variation of 8%. This method is an efficient way of obtaining the steady-state interaction force at multiple lateral separations.